

REPORT DOCUMENTATION PAGE				Form Approved OMB NO. 0704-0188	
<p>The public reporting burden for this collection of information is estimated to average 1 hour per response, including the time for reviewing instructions, searching existing data sources, gathering and maintaining the data needed, and completing and reviewing the collection of information. Send comments regarding this burden estimate or any other aspect of this collection of information, including suggestions for reducing this burden, to Washington Headquarters Services, Directorate for Information Operations and Reports, 1215 Jefferson Davis Highway, Suite 1204, Arlington VA, 22202-4302. Respondents should be aware that notwithstanding any other provision of law, no person shall be subject to any penalty for failing to comply with a collection of information if it does not display a currently valid OMB control number.</p> <p>PLEASE DO NOT RETURN YOUR FORM TO THE ABOVE ADDRESS.</p>					
1. REPORT DATE (DD-MM-YYYY) 31-08-2007		2. REPORT TYPE Final Report		3. DATES COVERED (From - To) 1-Aug-2004 - 31-Jan-2007	
4. TITLE AND SUBTITLE Inertial Motion Tracking for Inserting Humans into a Networked Synthetic Environment				5a. CONTRACT NUMBER W911NF-04-1-0301	
				5b. GRANT NUMBER	
				5c. PROGRAM ELEMENT NUMBER 611102	
6. AUTHORS Eric R. Bachmann				5d. PROJECT NUMBER	
				5e. TASK NUMBER	
				5f. WORK UNIT NUMBER	
7. PERFORMING ORGANIZATION NAMES AND ADDRESSES Miami University Roudebush Hall Oxford, OH 45056 -1618				8. PERFORMING ORGANIZATION REPORT NUMBER	
9. SPONSORING/MONITORING AGENCY NAME(S) AND ADDRESS(ES) U.S. Army Research Office P.O. Box 12211 Research Triangle Park, NC 27709-2211				10. SPONSOR/MONITOR'S ACRONYM(S) ARO	
				11. SPONSOR/MONITOR'S REPORT NUMBER(S) 43535-MA.1	
12. DISTRIBUTION AVAILABILITY STATEMENT Distribution authorized to U.S. Government Agencies Only, Contains Proprietary information					
13. SUPPLEMENTARY NOTES The views, opinions and/or findings contained in this report are those of the author(s) and should not be construed as an official Department of the Army position, policy or decision, unless so designated by other documentation.					
14. ABSTRACT Inertial/Magnetic tracking is based on the use of sensors containing three orthogonally mounted angular rate sensors, three orthogonal linear accelerometers and three orthogonal magnetometers to determine independently the orientation of each link of an articulated rigid body. Inertial/magnetic orientation tracking could be applied to a broad range of problems which require real-time tracking of an articulated structure without being continuously dependent upon an artificially generated source. This research focuses on the goal of developing and demonstrating wireless full body tracking using MARG sensor modules.					
15. SUBJECT TERMS inertial/magnetic tracking, MEMS, posture tracking, Virtual Environments (VE), orientation, kalman filter					
16. SECURITY CLASSIFICATION OF:			17. LIMITATION OF ABSTRACT SAR	15. NUMBER OF PAGES	19a. NAME OF RESPONSIBLE PERSON Eric Bachmann
a. REPORT S	b. ABSTRACT U	c. THIS PAGE U			19b. TELEPHONE NUMBER 513-529-1239

Report Title

Final Report Inertial Motion Tracking for Inserting Humans into a Networked Synthetic Environment

ABSTRACT

Inertial/Magnetic tracking is based on the use of sensors containing three orthogonally mounted angular rate sensors, three orthogonal linear accelerometers and three orthogonal magnetometers to determine independently the orientation of each link of an articulated rigid body. Inertial/magnetic orientation tracking could be applied to a broad range of problems which require real-time tracking of an articulated structure without being continuously dependent upon an artificially generated source. This research focuses on the goal of developing and demonstrating wireless full body tracking using MARG sensor modules.

During the period of this report, six manuscripts were submitted for peer-reviewed publication. Of these six, five have been accepted. These include three journal publications and two conference papers. In addition, scientific advances have been made in the following areas:

- Study of the Magnetic Effects on Inertial/Magnetic Sensor Modules
- Development of a singularity free Factored Quaternion Algorithm
- Development of an advanced Kalman Filter for Inertial/Magnetic Body Tracking
- Initial development in using inertial/magnetic sensors for position tracking

List of papers submitted or published that acknowledge ARO support during this reporting period. List the papers, including journal references, in the following categories:

(a) Papers published in peer-reviewed journals (N/A for none)

E. R. Bachmann, X. Yun, A. Brumfield, "An Investigation of the Effects of Magnetic Variations on Inertial/Magnetic Orientation Sensors," in press IEEE Robotics and Automation Magazine.

X. Yun, and E. R. Bachmann, "Design, Implementation, and Experimental Results of a Quaternion-Based Kalman Filter for Human Body Motion Tracking," IEEE Transactions on Robotics, Vol. 22, Issue 6, December 2006.

E. R. Bachmann and X. Yun, "A Single Parameter Tunable Quaternion Based Attitude Estimation Filter," Journal of Navigation, Vol. 53, No. 1, Summer 2006.

Number of Papers published in peer-reviewed journals: 3.00

(b) Papers published in non-peer-reviewed journals or in conference proceedings (N/A for none)

Number of Papers published in non peer-reviewed journals: 0.00

(c) Presentations

Number of Presentations: 0.00

Non Peer-Reviewed Conference Proceeding publications (other than abstracts):

Number of Non Peer-Reviewed Conference Proceeding publications (other than abstracts): 0

Peer-Reviewed Conference Proceeding publications (other than abstracts):

X. Yun, E. R. Bachmann, H. Moore, and J. Calusdian, “Self-contained Position Tracking of Human Movement Using Small Inertial/Magnetic Sensor Modules,” Proceedings of the IEEE International Conference on Robotics and Automation, ICRA 2007, Rome, Italy, April 2007.

X. Yun, C. Aparicio, E. R. Bachmann, R. B. McGhee, “Implementation and Experimental Results of a Quaternion-Based Kalman Filter for Human Body Motion Tracking,” Proceedings of International Conference on Robotics and Automation, ICRA 2005, Barcelona, Spain, April 2005.

X. Yun, E. R. Bachmann, Kavousanos-Kavousanakis, A., Yildiz, F., McGhee, R. B., “Design and Implementation of the MARG Human Body Motion Tracking System,” Proceedings of the International Conference on Intelligent Robots and Systems (IROS 04), Sendai, Japan, September - October 2004.

Number of Peer-Reviewed Conference Proceeding publications (other than abstracts): 3

(d) Manuscripts

X. Yun, E. R. Bachmann, and R. B. McGhee, “A Simplified Quaternion-based Algorithm for Orientation Estimation from Earth Gravity and Magnetic Field Measurements,” submitted to IEEE Transactions on Instrumentation and Measurement, in July 2006.

Number of Manuscripts: 1.00

Number of Inventions:

Graduate Students

<u>NAME</u>	<u>PERCENT SUPPORTED</u>
Bradford Snow	0.00
Nick Adams	0.00
FTE Equivalent:	0.00
Total Number:	2

Names of Post Doctorates

<u>NAME</u>	<u>PERCENT SUPPORTED</u>
FTE Equivalent:	
Total Number:	

Names of Faculty Supported

<u>NAME</u>	<u>PERCENT SUPPORTED</u>	National Academy Member
Eric Bachmann	0.15	No
FTE Equivalent:	0.15	
Total Number:	1	

Names of Under Graduate students supported

<u>NAME</u>	<u>PERCENT SUPPORTED</u>
Meseret (Mez) Redae Gebre	0.00
Justin A. Wilmes	0.25
FTE Equivalent:	0.25
Total Number:	2

Student Metrics

This section only applies to graduating undergraduates supported by this agreement in this reporting period

The number of undergraduates funded by this agreement who graduated during this period: 2.00

The number of undergraduates funded by this agreement who graduated during this period with a degree in science, mathematics, engineering, or technology fields:..... 2.00

The number of undergraduates funded by your agreement who graduated during this period and will continue to pursue a graduate or Ph.D. degree in science, mathematics, engineering, or technology fields:..... 1.00

Number of graduating undergraduates who achieved a 3.5 GPA to 4.0 (4.0 max scale):..... 1.00

Number of graduating undergraduates funded by a DoD funded Center of Excellence grant for Education, Research and Engineering:..... 0.00

The number of undergraduates funded by your agreement who graduated during this period and intend to work for the Department of Defense 0.00

The number of undergraduates funded by your agreement who graduated during this period and will receive scholarships or fellowships for further studies in science, mathematics, engineering or technology fields: 0.00

Names of Personnel receiving masters degrees

NAME

Bradford Snow

Total Number:

1

Names of personnel receiving PhDs

NAME

Total Number:

Names of other research staff

NAME

PERCENT SUPPORTED

FTE Equivalent:

Total Number:

Sub Contractors (DD882)

Inventions (DD882)

5 Method and Apparatus for Motion Tracking of an Articulated Rigid Body

Patent Filed in US? (5d-1) Y

Patent Filed in Foreign Countries? (5d-2) N

Was the assignment forwarded to the contracting officer? (5e) N

Foreign Countries of application (5g-2):

5a: Eric Bachmann

5f-1a: Miami University/NavalPostgraduate School

5f-c:

Oxford Oh 45056

5a: Eric Bachmann

5f-1a: Miami University/NavalPostgraduate School

5f-c:

Oxford OH 45056

AN INVESTIGATION OF THE EFFECTS OF MAGNETIC VARIATIONS ON INERTIAL/MAGNETIC ORIENTATION SENSORS

Eric R. Bachmann¹, Xiaoping Yun², and Anne Brumfield³

¹Department of Computer Science and Systems Analysis, Miami University Oxford, OH 45056

²Department of Electrical and Computer Engineering, Naval Postgraduate School, Monterey, CA 93943

³National Institute of Occupational Safety and Health (NIOSH), 1095 Willowdale Road, Morgantown, WV 26505

bachmaer@muohio.edu, yun@nps.navy.mil, znr1@cdc.gov

1 Introduction

Real-time tracking of the orientation or attitude of rigid bodies has wide applications in robotics [1], helicopters [2], tele-operation, augmented reality, and virtual reality [3]. Limb segment orientation can be estimated through the attachment of an inertial/magnetic sensor module to each segment as depicted in Figure 1. Given the length of each of the segments, their estimated orientation based on sensor module data, and their arrangement relative to one another, the posture of the body can be determined. This method of orientation and posture estimation is desirable since it is not dependent on any artificially generated reference signal and does not suffer from any line of sight restrictions [4].

Inertial/magnetic sensor modules and their associated data filtering algorithms are designed to be capable of estimating three degrees of orientation over a wide area in a variety of unprepared tracking environments. The sensor modules commonly contain three linear accelerometers and three magnetometers. The accelerometers are orthogonally mounted in a triad as are the magnetometers. Sensor modules designed for more dynamic applications may also contain three orthogonally mounted angular rate sensors for use as a high frequency data source. Each of the triads is mounted such that there is an individual sensor aligned with one of the principle axes of the coordinate frame of the sensor module. Thus the total number of sensors contained in modules designed to provide data for estimating orientation in dynamic applications is commonly nine.

In orientation estimation algorithms designed to process inertial/magnetic sensor data, accelerometers are used to measure the gravity vector relative to the coordinate frame of the sensor module. Accelerometers allow accurate determination of pitch and roll, but can not be used to sense rotations about the gravity or vertical axis. Magnetometers are thus commonly used to measure azimuth or rotation in the horizontal plane relative to a “fixed” reference. The data from the incorporated sensors is normally fused using a Kalman or complementary filtering algorithm. Foxlin et al. describes two commercial sensor modules containing accelerometers, magnetometers, and angular rate sensors designed for head tracking applications [5],[6]. Sensor fusion is performed using a complementary separate-bias Kalman filter. Bachman et al. propose a quaternion-based complementary filter for human body tracking [3], [7]. The filter is able to track through all orientations without singularities and continuously correct for bias and drift errors associated with low cost angular rate sensors without a need for stationary periods. Gallagher et al. presents a simpler complementary filter algorithm with lower computational complexity in [8]. Luinge describes a Kalman filter designed for human body tracking applications in [9]. The primary difference between the work presented in this paper and that of Luinge is that Luinge does not use magnetometers. In the absence of magnetometers, drift about the vertical axis is reduced by limiting body segment orientation using a kinematic human body model. The kinematic model incorporates biomechanical constraints on the joints. This method allows calculation of accurate relative orientation between adjacent segments. The proposed Kalman filter is useful for long periods of measurement if only inclination is required. In [10], Zhu and Zhou describe a linear Kalman filter algorithm designed to smooth accelerometer and magnetometer readings. Rather than



Figure 1: Prototype body tracking system based on inertial/magnetic sensors modules.

estimating individual limb segment orientations relative to a fixed reference frame, the system determines joint angles in axis/angle form using data from the two sensor modules mounted on the two segments adjacent to the joint. Kraft describes an “unscented,” quaternion-based Kalman filter for real-time estimation of a rigid body orientation [11]. Simulation results demonstrate the general validity of the described filter. Yan and Yuan describe a single frame orientation tracking algorithm that uses low cost sensor modules to take two axis measurements of gravity and the local magnetic field [12]. Elevation, roll and azimuth angles are sequentially calculated and the method is limited to orientation tracking within a hemisphere. In [13], Gebre-Egziabher et al. describe another single frame attitude determination algorithm for aircraft applications. The algorithm is based on the QUEST (QUaternion ESTimator) algorithm [14] which was originally designed to determine spacecraft attitude given a set of 3-dimensional known reference vectors and their corresponding observation or measurement vectors. In the case of [13], the local magnetic field and gravity vectors are used as reference vectors.

In the above studies with the exception of the work by Luinge [9], both the gravity and local magnetic field vectors are treated as fixed references. In the case of the gravity vector, the assumption that it is fixed leads to no difficulties since this vector does in fact point straight down in any inertial frame located on or near the surface of the earth. Making the same assumption regarding the local magnetic field vector can however lead to problems. In a typical room setting, the direction as well as the magnitude of the local magnetic field vector can be expected to vary due to the presence of ferrous objects or electrical appliances. Relative weighting can be used to reduce the weight applied to magnetometer data in comparison to other sensor information. However, slow drift about the vertical axis in the presence of a sustained change in the direction of the magnetic field vector will still occur. Reducing the weight given to magnetic data does, however, make it possible to reduce orientation errors resulting from transients in the local magnetic field. Such weighting techniques allowing manual adjustment of magnetometer gains are described in [3], [5], and [8].

This paper describes several experiments designed to examine small scale magnetic interference caused by typical objects and how this interference can be expected to affect the accuracy of orientation estimates produced using data from inertial/magnetic sensor modules. The results provide insight into the limitations of inertial/magnetic sensor module orientation tracking. They indicate that while errors due to local variations in a common room environment caused by individual objects can be significant, in most cases they can be avoided by maintaining a separation of approximately one meter from the source of interference. The interference caused by combined sources in a noisy indoor environment can however be quite complex. The results also indicate that inertial/magnetic sensor modules can be used to track link orientation of a mechanical arm relative to an Earth fixed reference frame.

The remainder of this paper provides a brief background and then presents a series of experiments. Section 2 describes the sensors used in the experiments, gives a brief overview of magnetic fields, and magnetometer calibration methods that can be used to deal with various types of magnetic interference. Section 3 presents data from four different experiments in which inertial/magnetic sensor modules are subjected to controlled changes in the magnetic field, exposed at varying distances to sources of magnetic interference, and used to track a robotic arm. The final section of the paper discusses the implications of the experimental results for the use of inertial/magnetic sensor modules and provides a summary.

2 Background

The following paragraphs go deeper into the theory of orientation estimation algorithms designed for inertial/magnetic sensor modules and briefly describe three types of sensor modules. Specifically, the modules discussed are the InterSense InertiaCube, the MicroStrain 3DM-G, and the MARG III. The MARG III was designed by the authors and manufactured by McKinney Technology. Basic background on the ambient magnetic field of the Earth and how it is distorted by ferrous objects and electrically powered devices is then provided. Methods of calibrating magnetic field variations are then discussed.

2.1 Inertial/Magnetic Sensor Modules

Inertial/magnetic sensor modules have been fabricated by both industry and university research laboratories. Filtering algorithms designed for these sensor modules are based on inertial and magnetic quantities directly related to the motion and orientation of a sensor module. Algorithms designed for use with inertial/magnetic sensor modules produce accurate orientation estimates by taking advantage of the complementary nature of the sensed quantities in order to determine orientation.

For a static or slow moving rigid-body, accelerometer triad output can normally be averaged (or low pass filtered) for a short period of time in order to measure the components of the gravity vector in the sensor coordinate frame. Determination of the relationship of the measurement in the sensor coordinate frame to the gravity vector in Earth

coordinate frame allows estimation of orientation relative to the horizontal plane. However, in the event that the sensor module is rotated about the vertical axis, the projection of the gravity vector on each of the principle axes of the accelerometer will not change. Since the accelerometer triad can not be used to sense a rotation about the vertical axis, an orthogonally mounted triad of magnetometers can be used to measure the local magnetic field vector in body coordinates and allow determination of orientation relative to the vertical. Thus, combining magnetometer data with accelerometer data provides a complete method for estimating the orientation.

Alternatively, assuming the initial orientation of the body is known, integration of the output of a triad of orthogonally mounted angular rate sensors provides another method of estimating orientation. If the rate sensors are susceptible to noise or bias effects, as is the case for the small low cost sensors used in inertial/magnetic sensor modules, these estimates become useless after a short period. To avoid lag or overshoot in dynamic applications, many inertial/magnetic sensor filtering algorithms combine high frequency angular rate sensor data with low-frequency accelerometer and magnetometer data in a complementary manner to produce continuously accurate orientation estimates in real-time.

Based on the work of Foxlin, InterSense Inc. developed and marketed a sensor module called the InertiaCube2. The primary application for this module is head tracking. Manufacturer's literature indicates that the InertiaCube2 is capable of measuring angular rates, linear accelerations, and the local magnetic field along three axes. Dimensions for the InertiaCube2 are 29 mm x 24 mm x 34 mm. Orientation estimates are made by a proprietary extended Kalman filter [5],[6]. Manufacturer's literature lists an accuracy of 1.0 degree and an update rate of 180 Hz.

The 3DM-G Gyro Enhanced Orientation Sensor also contains a triad of orthogonally mounted angular rate sensors, a triad of orthogonally mounted accelerometers, and a triad of orthogonally mounted magnetometers. Sensor data is processed by a proprietary filtering algorithm running on an embedded microcontroller. Manufacturer's literature lists an accuracy of +/- 5 degrees for arbitrary orientations. Unlike the InertiaCube2, unscaled as well as scaled raw data output is available from this unit. The update rate is 76.6 Hz. Unit dimensions are 65 mm x 90 mm x 25 mm.

The MARG III sensor module shown in Figure 2 is a research prototype developed by the Modeling, Virtual Environments and Simulation (MOVES) Institute at the Naval Postgraduate School [15]. Primary sensing components for this unit include Tokin CG-L43 ceramic rate gyros, Analog Devices ADXL202E micromachined accelerometers, and Honeywell HMC1051Z and HMC1052 one and two-axis magnetometers. The MARG III sensor module incorporates a Texas Instruments MSP430F149 ultra-low-power, 16-bit RISC architecture microcontroller. Overall, dimensions are approximately 18 mm x 30 mm x 25 mm. The sensor module includes a magnetic set/reset circuit to cancel magnetometer temperature drift and avoid magnetic saturation effects. Various complementary and Kalman filters based on a quaternion representation of orientation have been used to process MARG III sensor data [3], [16]. Estimation accuracy has been measured to be better than one degree.

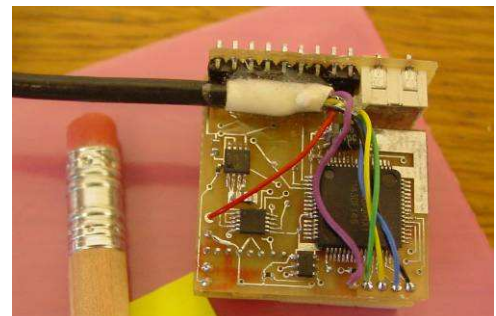


Figure 2: MARG III inertial/magnetic sensor module.

2.2 Magnetic Field Variations

Magnetic fields surround permanent magnets or electrical conductors. They can be visualized as a collection of magnetic flux lines. Flux lines are said to emanate from a 'north' pole and return to a 'south' pole in a magnet. Flux density, or magnetic induction, is a measure of the number of flux lines passing through a given cross sectional area. Magnetic field strength is a measure of force produced by an electric current or a permanent magnet. Magnetic field strength decreases with the cube of the distance from the source. While magnetic field strength and magnetic flux density are not the same, they are equal within a vacuum. Magnetic permeability is a constant of proportionality that exists between magnetic induction, and magnetic field intensity. It can be viewed as a measure of how easily magnetic lines of flux will pass through a given material. In the presence of an object made of a material with a relatively high permeability, magnetic field lines will bend toward or be attracted to the object. Thus distortion can be expected to occur near large ferrous objects [17].

	Distance (15cm)	Distance (30cm)
	Field (Gauss)	Field (Gauss)
Can Opener	1.60	0.27
Electric Saw	1.20	0.25
Vacuum Cleaner	0.75	0.20
Electric Shaver	0.65	0.10
Mixer	0.61	0.11
Hair Dryer	0.50	0.07
Electric Drill	0.20	0.03
Portable Heater	0.15	0.04
Fluorescent Light Fixture	0.13	0.04
Fan (range Hood)	0.09	0.03
Television	0.07	0.02

Table 1: Common magnetic field magnitudes in Gauss at 15 and 30 cm adapted from [18].

The direction and magnitude of ambient magnetic field at a given point is the vector sum of all magnetic fields present at that point. The dominate field in most cases is that of the Earth which varies from approximately 0.23 to 0.61 Gauss. However, additional magnetic fields caused by conductors through which a current is flowing and magnets also contribute to the total field at a given position. All contributing fields will be distorted by objects made of materials with a high magnetic permeability.

In an indoor environment, sources of magnetic interference are constantly present and can include common items such as computer monitors, fluorescent lighting and powered-up electrical wiring inside walls. Table 1 lists the fields generated by some common appliances. In some cases the strength of the generated field exceeds that of the Earth within a short distance of the appliance. If a magnetic sensor is placed in this nearby area the generated field can be expected to have an effect on the direction and magnitude of the field measured by the sensor. Unless the field generated by the appliance happens to be aligned with that of the Earth, the reported direction will not be that of the Earth's magnetic field. In a room size environment such fields would constitute local variations from the average field in the room. It is variations of this type and their effect on the orientation estimates produced by inertial magnetic sensors with which this paper is concerned.

2.3 Magnetic Field Calibration

Magnetic distortions caused by ferrous objects that have a fixed location and orientation relative to the magnetometers being used to determine the direction of the local magnetic field vector can be separated into two categories. These categories are *hard iron* and *soft iron* effects. Hard iron objects are permanently magnetized. Soft iron objects are unmagnetized unless under the influence of a magnetic field.

Hard iron effects add a constant offset to the vector measured by magnetometers making up an orthogonal triad. They can be compensated for in the horizontal plane by rotating the magnetometers together with the involved hard iron objects and sampling at enough points in a circle to determine the offset relative to the horizontal plane. Determination of all components of the offset requires rotation in more than one plane. Unlike hard iron effects, soft iron effects do not produce a constant offset. Soft iron influences are dependent on orientation [19]. Thus correcting for soft iron effects often requires the construction of a heading dependent lookup table [20]. Construction of a three dimensional lookup table is difficult and time consuming. Thus, in a strap-down navigation system, magnetic readings are usually projected onto the horizontal plane using a tilt sensor before corrections are made.

In general, calibration is best approached by removing any soft iron materials and dealing with hard iron effects directly. The magnetic properties of many materials are actually in-between those of soft and hard iron and change over time. During a calibration performed at any given time, the effects of such *sub-permanent* materials will appear to be permanent like hard iron. However, since the effects observed are not truly permanent, calibration procedures must be repeated on a periodic basis [17].

It should be emphasized that the above discussion of calibration focuses only on effects caused by objects that have a fixed position and orientation relative to a magnetic sensor. In a tracking application, moving inertial/magnetic sensor modules can be expected to constantly change position and orientation relative to ferrous objects and other sources of magnetic distortion. These magnetic distortions will not only change from position to position, but can also be expected to change over time as the configuration of the tracking area itself changes. The nature of these distortions and their possible effects on orientation estimation algorithms designed for inertial/magnetic sensor modules is the primary focus of this paper.

3 An Experimental Investigation

Inertial/magnetic sensor module filtering algorithms are dependent on sensing the local magnetic field to eliminate drift in the azimuth portion of orientation estimates. Given that variations in the direction and magnitude of the ambient

magnetic field can be expected to occur as a result of the presence of ferrous materials and electrical appliances operating in the tracking environment, what type of estimation errors can be expected and how large can the estimation errors be expected to be? Knowing the answer to this question provides insight into when inertial/magnetic sensor modules can be expected to work properly with minimal estimation error and what type of algorithm modifications could be expected to improve performance. The experiments described below attempt to answer this question. In the first series of experiments, several types of sensor modules are subjected to controlled changes in the direction and strength of the sensed magnetic field in order to characterize the resulting orientation estimation errors [21]. The second sets of experiments involve exposing a triad of magnetometers to magnetic fields generated by various electrical appliances and ferrous objects in order to examine the magnitude of the errors and the range at which they occur. In the last set of experiments, a robot arm is tracked using inertial/magnetic sensor modules and an optical tracking system.

3.1 Errors Caused by Change in Magnetic Field Direction

In the first series of experiments, magnetic field variations were applied to the three types of sensor modules to measure the deviation in their orientation estimates due to the change in the sensed magnetic field. The change was generated using a Helmholtz coil. The sensors were placed inside the coil to observe how the orientation estimate would change as changes to the local direction of the local magnetic field were applied. The three different sensor modules tested were the MARG III, the MicroStrain 3DM-G, and the InterSense InertiaCube2.

Initial calibration data for the Helmholtz coil was obtained by applying different currents to it and measuring the induced field with a Hall probe. This initial data allowed decisions to be made regarding how much current was necessary to produce the desired magnetic inductions to be applied to the three different inertial/magnetic sensors. The selected magnetic field level was chosen to be on the order of the Earth's Main field. The voltage that was necessary to reach the required magnetic induction was calculated using linear least square fit.

During the experiments, the Helmholtz coil was positioned to attempt to generate a magnetic induction that would be reversed approximately 180° in azimuth from the Earth's magnetic field. In most cases, the actual measured change ranged between 160° and 180° due to imprecise alignment of the coil relative to the local magnetic field vector. Each sensor module was placed in eight different orientations with in the field generated by Helmholtz coil. For each of the orientations the coil was energized to observe the type and magnitude of change that occurred in the orientation estimate produced by the sensor and its associated filtering algorithm [21].

The data plots from these experiments show a period of measuring the Earth's ambient magnetic field, followed by a period in which the Helmholtz coil was energized for 20 to 30 seconds. Following the energized period, the coil was de-energized and the plots reflect the return to sensing only the ambient field of the laboratory. The change in the direction and magnitude of the magnetic field vector is depicted in figure 3. Energizing the coil caused the azimuth direction of the magnetic field vector to change from 0° to 180° . There was no significant change in the y (East) component of the vector. Since the coil was level, the z component of the magnetic field vector also remained unchanged. Prior to energizing of the coil, the magnetic field vector pointed North with a dip angle below the horizontal of 76° . While the coil was energized, the magnetic field vector pointed South with a negative elevation angle of 32° . Thus, in this series of experiments, not only were the sensor modules exposed to a full reversal of the azimuth direction of the magnetic field vector. Depending on their initial orientation relative to the magnetic field, the sensor modules were also exposed to a change in pitch, roll, or some combination of the two totally approximately 44° .

For visualization purposes, all orientation estimates produced by the sensors are displayed in Euler angle form. In the experiments presented here, the sensor modules were oriented in a North-East-Down reference orientation with the x axis of the module pointing towards the local North, the y axis pointing East and the z axis pointing down. At no time was a sensor actually rotated before, during, or after the application of the altered magnetic field.

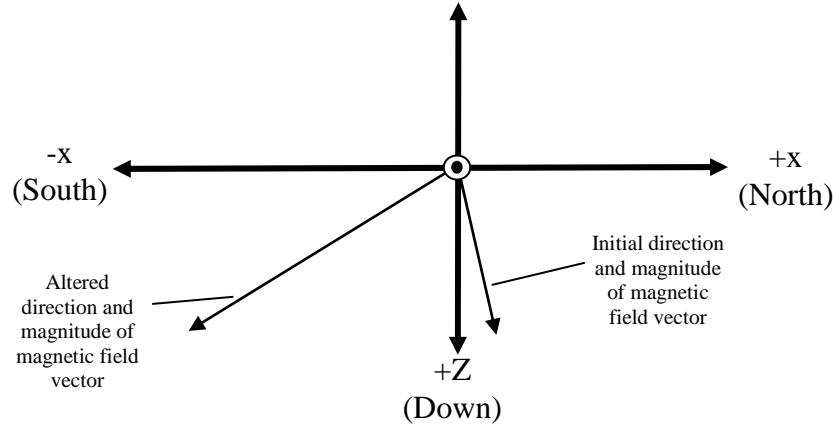


Figure 3: Depiction of total change in the direction and magnitude of the magnetic field vector (East is directly out of the page).

Figure 4 and Figure 5 show the responses for the MARG III and MicroStrain 3DM-G respectively when the magnetic field was altered using the Helmholtz coil. In Figure 4, the MARG III was placed within the Helmholtz coil with an initial orientation of 2° roll, 10° yaw, and 3° pitch. Calibration of the MARG III does not account for non-orthogonality within the magnetometer triad. Thus, small changes and hysteresis can be seen in the roll and pitch estimates and the yaw estimate changes by an amount that is slightly less than the change in azimuth that occurred in the direction of the magnetic field. The smooth response of the MARG III filtering algorithm is due to the particular gain values used in the experiment. In Figure 5, the MicroStrain 3DM-G had an initial orientation of 2° roll, 13° yaw, and 0° pitch. Energizing the coil caused a 165° change in the yaw estimate produced by the sensor module. This change was equal in magnitude to the measured change in azimuth. No significant changes were observed in the roll and pitch estimates. The tuning of the orientation estimation algorithm provides an extremely sharp response to the change in the magnetic field direction. Both the MARG and MicroStrain sensors responded to the change in the sensed magnetic field by altering the yaw portion of their orientation estimates by an amount that was equal to measured azimuth change produced by the Helmholtz coil. Neither showed significant change in their roll and pitch estimates despite the fact that the direction of the magnetic field had changed both pitch angle and azimuth angle as depicted in Figure 3. This was true regardless of the orientation of the sensor modules relative to the coil. This is significant since it indicates the errors due to magnetic variation are restricted only to the horizontal plane. The estimates of pitch and roll are not affected by changes in the magnetic field direction for the sensors and algorithms tested [21]. This is in contrast to some orientation algorithms such as the QUEST [14], where such a change in the direction of the magnetic field will cause an error in both azimuth and pitch.

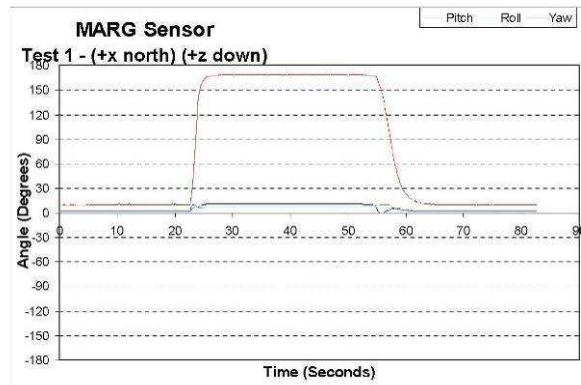


Figure 4: MARG III sensor response to 180° azimuth change in the magnetic field direction.

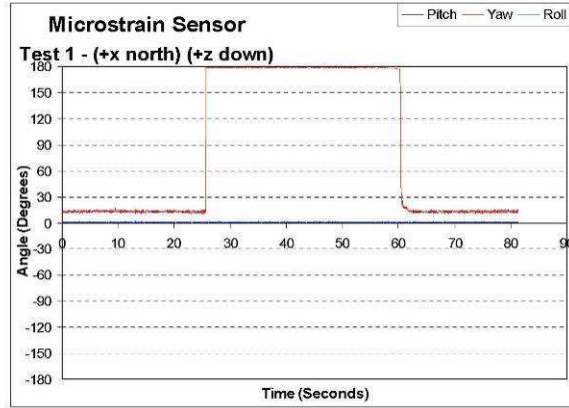


Figure 5: MicroStrain 3DM-G response to 180° azimuth change in the magnetic field direction.

Figure 6 shows the response of the InertiaCube2 to the same magnetic variations as used in the experiments depicted in Figure 4 and Figure 5. Like the other sensors the orientation estimate changes only in azimuth. However, examination of Figure 6 indicates that unlike the other sensors, the estimated orientation produced by the InertiaCube2 algorithm changed by approximately 90° instead of 180°.

In order to investigate the response of the InertiaCube2 further, additional experiments were performed. In Figure 7, the sensor was again left in the same position within the Helmholtz coil. The coil was energized for approximately 30 seconds. Unlike previous experiments, during the time when the magnetic field was changing the sensor was physically tapped. This caused the estimated azimuth to proceed through a change that is similar to that observed with the other two sensor modules. Euler angle azimuth is bounded between 180° and -180°. Though the change is expressed as -180°, it is equivalent to the positive 180° change seen with the other two sensor modules. The knee seen in the trailing edge of Figure 7 is most likely the result of non-zero angular rate readings caused by tapping of the sensor module while the coil was being deenergized. These results indicate that the filtering algorithm of the InertiaCube2 will not accept changes in its orientation estimate without some accompanying non-zero reading from the angular rate sensors.

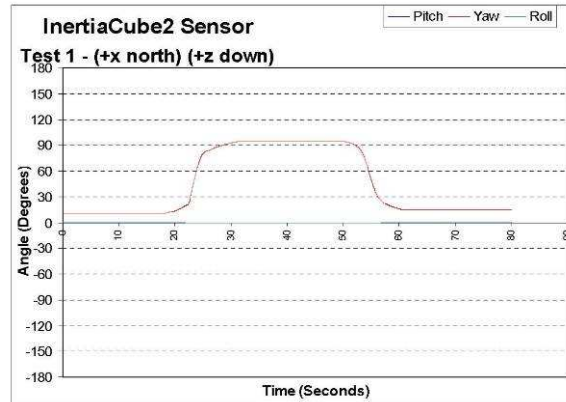


Figure 6: Undisturbed InertiaCube 2 response to 180° change in the magnetic field direction.

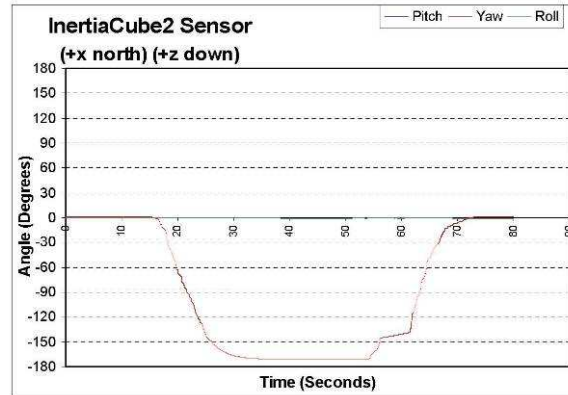


Figure 7: Disturbed InertiaCube 2 response to 180° change in the magnetic field direction.

Based on the results of experiments described above, it appears that unlike active magnetic trackers which suffer estimation errors in all dimensions due to magnetic variations [22], variations in the direction of the local magnetic field only cause estimation errors in azimuth or the horizontal plan. The magnitude of the errors appears to be equal to the amount of deviation of the local magnetic field in the horizontal plane. No significant change was observed in the pitch and roll estimates produced by the three tested algorithms. These experimental results indicate that the dip angle itself or changes in the dip angle of the local magnetic field vector have no bearing on the accuracy or amount of variation seen in orientation estimates produced using inertial/magnetic sensor module data.

3.2 Variations Caused by Common Objects

To determine the magnitude of azimuth errors that can be expected in a typical indoor environment, two types of experiments were performed. Initial experiments measured the magnetic field variation experienced at varying distances from several test objects. Later experiments measured the change in direction of the magnetic field vector at several positions in a magnetically noisy laboratory. The MARG III filtering algorithm utilizes a normalized magnetic field vector of unit length and is thus not affected by changes in the length of the magnetic field vector [3]. Based on manufacturer's literature, the algorithms associated with the InertiaCube and 3DM-G are similar in this regard. Therefore, the experimental results presented here concentrate on the changes in the direction of the local magnetic field and not changes in magnitude. The experiments described above establish that changes in the direction of the magnetic field orientation result only in azimuth errors for the orientation estimation algorithms associated with the tested sensor modules. Therefore, in the experiments described in this section, only magnetic deviation in the horizontal plane is examined.

To measure the magnetic deviation in the horizontal plane caused by test objects, a "track" was constructed using non-ferrous materials and set so that the orientation of an inertial/magnetic sensor module could be held constant as the sensor was moved through successive positions approaching each object. The sensor module was placed at 18 locations with each successive location being 10 cm closer to the test object. In the final position the sensor module was within one centimeter of the test object. This set-up allowed the direction of the magnetic field vector to be measured since the sensor module orientation was kept constant. The test objects included:

- Computer monitor (CRT type), powered and un-powered states
- Simple appliance (small space heater with fan), powered and un-powered states
- Electrical power supply, powered and un-powered states
- Metal filing cabinet
- Mobile robot, un-powered, powered, and motor engaged.

The MicroStrain 3DM-G sensor module is factory calibrated and allows access to scaled sensor output from each of the nine sensors in the module. The magnetometer triad in the 3DM-G sensor was used to measure the magnetic field direction in these experiments.

Prior to examination of the deviations caused by the test objects, a baseline was established by measuring the change in magnetic field direction with no object present. In the baseline case, the direction of the magnetic field in the horizontal plane deviated less the 1.6° as the sensor module was moved a distance of 180 cm down the test track. This deviation is

attributed to noise in the ambient magnetic field of the laboratory. Comparison of these baseline deviations for each sampling position to the deviations that occurred when each of the test objects was present allows a more thorough understanding of the effects each object has on the magnetic field. The baseline was sampled before and after the experiments were conducted. This action helped to insure that no significant changes had occurred in the ambient magnetic field of the laboratory during the course of the experiments.

Figure 8 contains two sub-plots of data from experiments in which a CRT computer monitor was the test object. In each sub-plot, baseline average deviations are displayed along with the average deviations that occurred when the monitor was present. The top sub-plot displays the average deviations that occurred when the monitor was un-powered. The bottom sub-plot displays the average deviations with the monitor turned on and connected to a PC. The error bars represent the standard deviation of the data obtained at each position. The magnetic field showed approximately the same amount of deflection whether the monitor was attached to a PC and powered up or turned off. The standard deviations in both experiments are small and can be attributed to measurement noise, indicating the deviation was a DC effect. Some impact from this appliance can be observed to almost 40 cm of separation distance. In both cases, the computer monitor causes a maximum average deflection of 10.5° in the magnetic field relative to the horizontal plane.

Figure 9 shows two sub-plots of data from experiments in which a portable heater was used as a test object. In the first experiment both the heater fan and heating elements were off. In the second experiment both the fan and the heating elements were on. Examination of the two sub-plots indicates that the average amount of magnetic field deviation is significantly greater when the heater is turned on and increases dramatically as the sensor is brought in close proximity to the appliance. The standard deviations of the data taken at each position also increase significantly as the sensor is brought closer to the running heater. This fluctuation is most likely due to the use of alternating current to power the appliance. With the heater in a powered off state, the largest average deviation is 20.5° . With the heater turned on, the largest average deviation is nearly 90° . In both cases deviation caused by the heater did not begin to occur until the sensor module was within 30 cm of the heater.

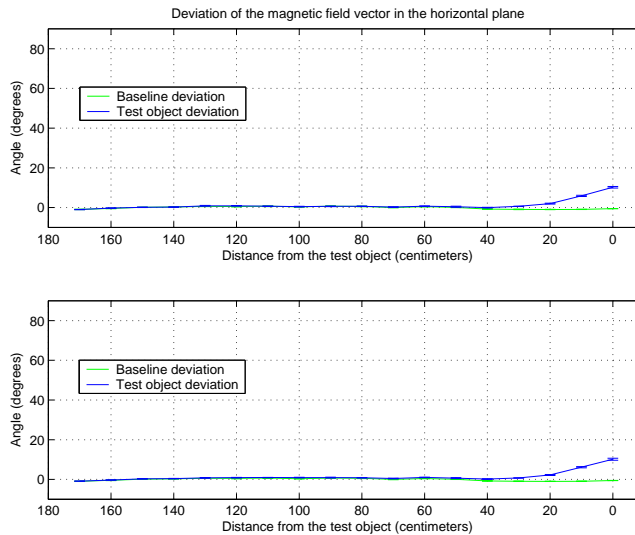


Figure 8: Magnetic field vector deviation in the horizontal plane versus distance from a PC monitor in both un-powered (top) and powered (bottom) states.

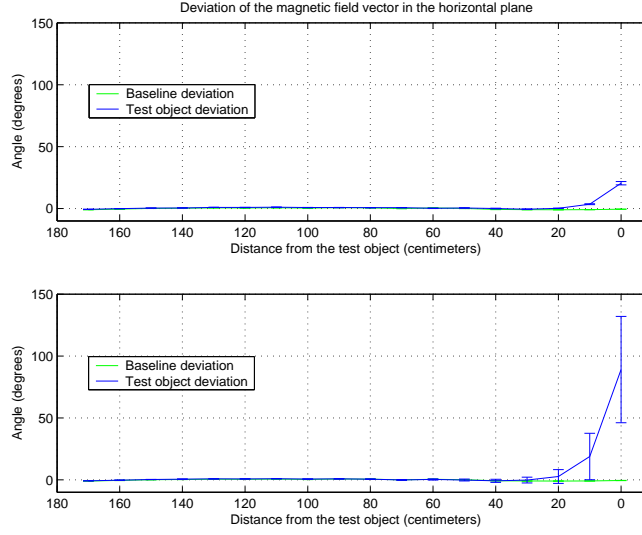


Figure 9: Magnetic field vector deviation versus distance from an appliance (space heater) in both un-powered (top) and powered (bottom) states.

Figure 10 shows two sub-plots of data from experiments in which an electrical power supply was used as a test object. In the first experiment the power supply is off. In the second experiment it is turned on and supplying power. The two sub-plots are very similar. The standard deviations of the data taken at each position are relatively small again indicating the deviation is DC in nature. In both sub-plots, the maximum average deviation is between 60° and 70° . The deviation due to the presence of the power supply begins to occur at a distance of nearly one meter.

Figure 11 presents the deviation in the sensed magnetic field vector as the magnetometer triad of the sensor module approached a large metal filing cabinet. The deviations for this test object are the largest of any observed in the experiments described in this paper. Large standard deviations for the data samples for each of the positions are not observed indicating that the magnetic field deviation was constant in nature. The maximum deflection caused by the filing cabinet is 99.5° and begins at a distance of 1.5 meters.

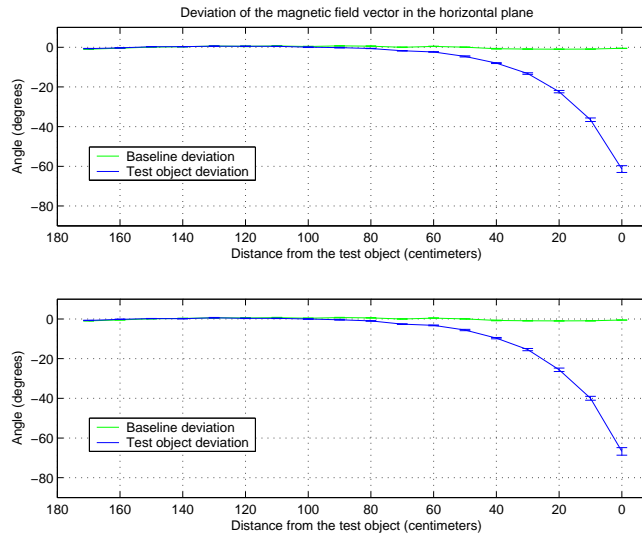


Figure 10: Magnetic field vector deviation versus distance from an electrical power supply in both un-powered (top) and powered (bottom) states.

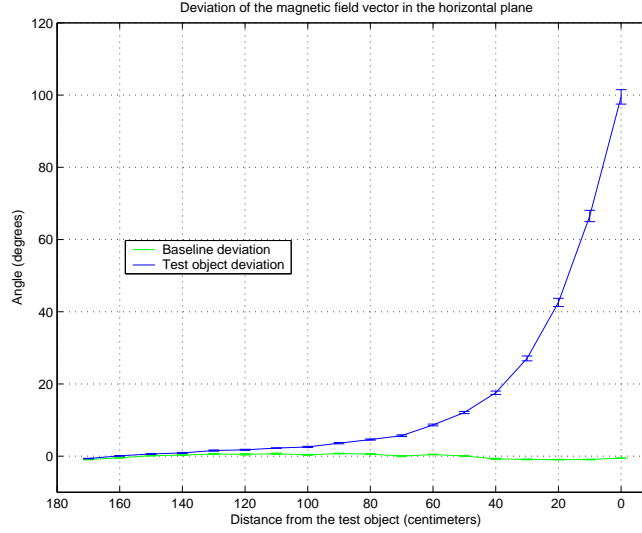


Figure 11: Magnetic field vector deviation versus distance from a metal filing cabinet.

The final test object presented is a Nomad Scout mobile robot. Magnetic deviation due to the presence of the robot was examined with the robot in three different states. These three states correspond to the three sub-plots in Figure 12. The bottom sub-plot displays the deviation induced by the robot when it is in an un-powered state. In the middle sub-plot, all electronic systems of the mobile robot were energized with the exception of the motor used to move the robot. The data displayed in the top sub-plot were collected while all robot systems were powered and the motors were engaged. The robot was placed on a stand so that its wheels could rotate freely. The maximum amount of average deviation observed for the robot is about 9° . This includes the case in which the motors were engaged. The standard deviation of the data for each position is relatively small. No deviation is observed beyond a distance of 40 cm.

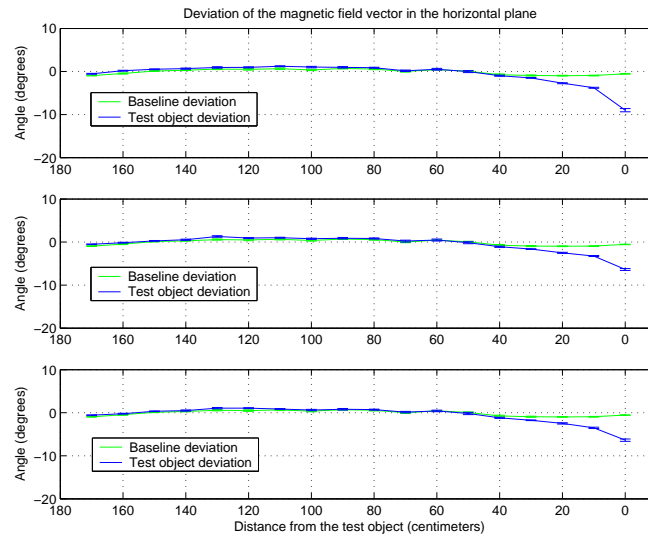


Figure 12: Magnetic field vector deviation versus distance from a mobile robot in a power-off (bottom), systems-on (middle) and motor-engaged (top) states.

Another set of experiments was conducted to examine the amount of variation that can be expected to occur in a laboratory environment in which numerous sources of magnetic noise are present. In these experiments, the azimuth direction of the magnetic field was measured at 25 positions at 10 cm intervals along a straight line with the sensor module orientation being held constant. As the sensor module being used to collect measurement data was moved it came within

close proximity to numerous pieces of lab equipment simultaneously. The equipment included computer monitors, printers, mobile robots, servo control stations, and other miscellaneous lab equipment. Figure 13 contains sub-plots for two straight line samples. In the upper sub-plot, the azimuth direction of the magnetic field varies approximately 16° , with the maximum change between two adjacent positions being 13.1° . In the lower sub-plot, the azimuth direction of the magnetic field varies slightly less than 13° . The average difference from position to position is less than three degrees for both trials. The accruing difference in the magnetic azimuth direction seen in the upper plot indicates the presence of a large scale magnetic disturbance in the lab.

Overall, experiments in which the magnetic field variation caused by individual test objects was examined indicate that when inertial/magnetic sensor modules are separated by a distance of one meter or more from most common appliances and ferrous objects the amount of azimuth error induced by those objects will be negligible. The amount of variation caused by different types of objects can vary significantly. The experimental results demonstrate that while inclination estimates can be expected to remain valid in close proximity to objects causing distortions in the local magnetic field, in some cases the azimuth estimates produced by the implemented algorithms had very little relation to the true orientation of the sensor module and can vary by as much as 100° . In other tests, azimuth estimates varied less than 10° . Experiments in which sensor modules were exposed to multiple sources of distortion simultaneously in a crowded laboratory environment, show that azimuth estimates produced using a sensor module with a constant orientation can be significantly different for closely spaced positions. However, on average, differences in estimated azimuth from one position to another nearby position are much smaller.

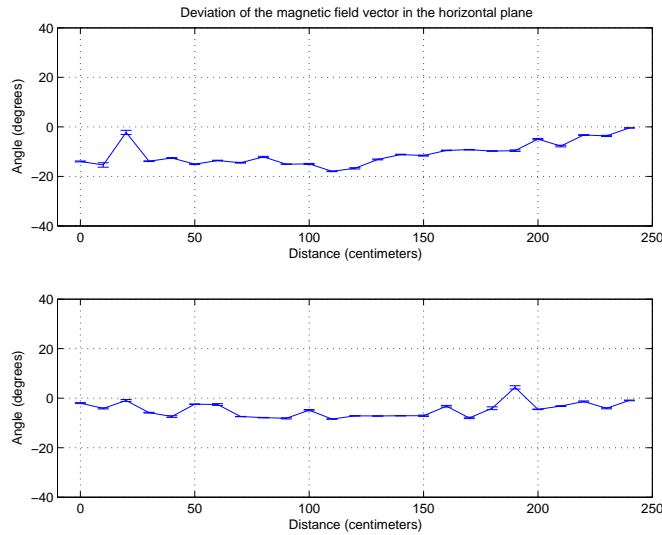


Figure 13: Ambient magnetic field azimuth direction sampled at 10 cm intervals in a laboratory.

3.3 Tracking a Robot Arm

The final set of experiments described in this paper are designed to determine if inertial/magnetic sensor modules can be used to accurately track the orientation of the links of a robot arm made of ferrous materials. In these experiments a SCORBOT-ER III robot arm and three MicroStrain 3DM-G were utilized. The experiments described in section 3.1 established that the response of the three different sensor modules to magnetic variations is essentially the same. In these tracking experiments, one 3DMG-GX1 was securely attached to each link of the arm. While robot encoders provide incremental joint angle readings, use of these angles to obtain orientation estimates relative to an earth fixed reference frame requires forward kinematics and calibration, and the accuracy of the orientation estimates cannot be ascertained for this robot arm. As a result the arm was also tracked using a Qualysis optical tracking system as depicted in Figure 14. The Qualysis system can be used to perform passive optical three degree-of-freedom position tracking and six degree-of-freedom tracking of designated rigid bodies on which four passive markers are mounted. Manufacturer's literature states that position accuracy is 0.1% of the field of view. The robot arm was contained in a one square meter tracking volume. The Qualysis system utilized seven proflex cameras positioned around the tracking volume. In the experiments discussed

here, a total of 17 passive markers were used to track the position of the outboard end of each link and the orientation of the inertial/magnetic sensor module attached to each link. Each link was defined as a rigid body by placing four markers on the surface of the attached inertial/magnetic sensor. The geometric center of these four markers served as the origin of the local coordinate system of each segment. Following calibration, maximum residual error for all cameras was less than 1.127 mm. These calibration results indicate that the system was tracking to 1mm accuracy as would be expected given the size of the tracking volume. Update rate for the optical tracking system was 60 Hz. Given this accuracy, data produced by this system was treated as a reference in these experiments.

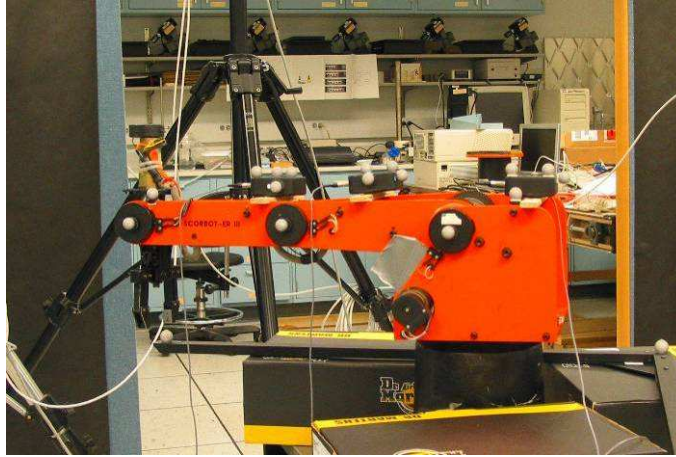


Figure 14: SCORBOT-ER III robot arm instrumented for tracking with both inertial/magnetic sensor modules and an optical tracking system.

Figure 15 shows a comparison of the orientation estimates produced using an inertial/magnetic sensor module and an optical tracking system while simultaneously tracking the robot arm. During the experiment, the robot arm was programmed to repeatedly trace an inclined square pattern with its end effector. Due to a limited number of degrees of freedom in the arm, the programmed pattern did not require any of the tracked arm segments to roll. In Figure 15, yaw and pitch are shown for the most outboard end inertial/magnetic sensor. Examination of the Figure 15 shows that both tracking technologies produced very similar motion plots. Maximum steady state difference between the orientation estimates produced using inertial/magnetic sensors and optical tracking is less than 2.5° in both sub-plots. This accuracy was achieved by the inertial/magnetic sensors despite the largely ferrous nature of the material of which the robot arm was constructed and the presence and operation of several servo motors used to position and move the arm.

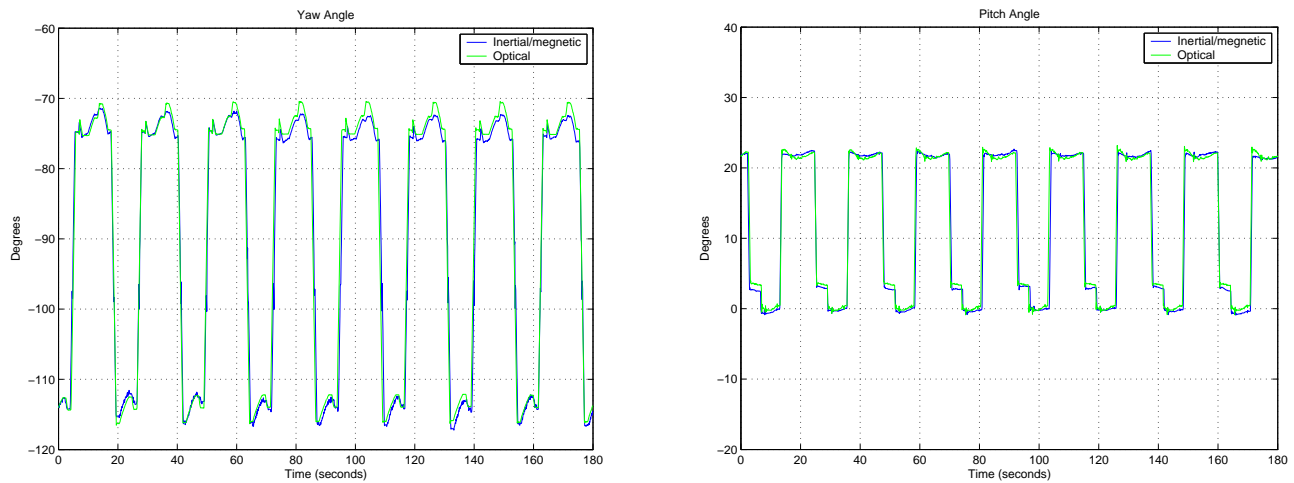


Figure 15: Comparison of yaw and pitch orientation estimates for a robot arm segment produced by an optical tracking system and an inertial/magnetic sensor module.

4 Conclusions and Discussion

The direction of the local magnetic field vector can be altered by the presence of operating electrical appliances or objects made of ferrous materials. The assumption made by orientation estimation algorithms that the direction of the local magnetic field is static makes the algorithms susceptible to errors as the sensor modules are moved from one position to another within a tracking volume. In the algorithms tested, the errors appear only in the azimuth portions of the orientation estimates produced. These errors will be roughly equal in size to the amount the magnetic field deviates in the horizontal plane from the original reference.

The amount of deviation caused by appliances and ferrous objects can range from very small to very large. The horizontal deviation of the magnetic field was measured for several common objects. Maximum deviation ranged from 10.5 degrees to nearly 100 degrees. Experimental data presented here indicates that such deviations can be largely avoided by maintaining a distance of approximately one meter from the source of interference. Only one of the objects caused a horizontal plane deviation at a distance of more than one meter. For this object, horizontal plane deviations did not exceed 4 degrees when at a distance of more than one meter. For many of the objects, no deviation was observed beyond a distance of a half meter. However, in an indoor environment containing numerous sources of interference, it can be difficult to determine which objects are the major contributors to magnetic field deflections and the magnetic field can vary significantly between closely spaced positions.

Despite all the above, the tracking experiments indicate that inertial/magnetic sensor modules can be used to track posture with an accuracy that is comparable to optical tracking. The accuracy of the orientation estimates while tracking a robot arm using data from inertial/magnetic sensor modules indicates that such modules can be used to accurately track orientation in environments and applications in which operating motors and ferrous objects are present. However, given the current state of the art of orientation estimation algorithms designed to process inertial/magnetic sensor module data, they should not be used in an application without first investigating the nature of the magnetic field in the environment in which they will be utilized. While Rotenberg et al. have begun the investigation of modified algorithms designed to alleviate the effects of magnetic variations in [23], further work is needed. This work should include an investigation of the use of arrays of sensor modules placed at slightly different positions and a method of estimating the relative amount of interference to which each individual module is exposed.

The findings and conclusions in this report are those of the authors and do not necessarily represent the views of the National Institute for Occupational Safety and Health.

Acknowledgments

This work was in part supported by the Army Research Office (ARO project number 40410-MA) and the U.S. Navy Modeling and Simulation Office (NMSO). The authors would like to thank the National Institute of Occupational Safety and Health (NIOSH) for allowing the use of their equipment and laboratory facilities for the collection of portions of the experimental data presented.

Keywords

Motion measurement; inertial sensors; orientation estimation; magnetic fields, accelerometers; magnetometers, optical tracking.

References

- [1] G. Dissanayake, S. Sukkarieh, E. Nebot, and H. Durant-Whyte, H., "The Aiding of a Low-Cost Strapdown Inertial Measurement Unit Using Vehicle Model Constraints for Land Vehicle Applications," *IEEE Trans on Robotics and Automation*, Vol. 17, No. 5, pp. 731-747, October 2001.
- [2] S. Sarapalli, J. Roberts, P. Corke, G. Buskey, and G. Sukhatme, "A Tale of Two Helicopters," in *Proceedings of the 2003 IEEE/RSJ Intl. Conf. On Intelligent Robots and Systems*, Las Vegas, NV, October 2003, pp. 805-810.
- [3] E. Bachmann, R. McGhee, X. Yun, and M. Zyda, "Inertial and Magnetic Posture Tracking for Inserting Humans into Networked Virtual Environments," *ACM Symposium on Virtual Reality Software and Technology (VRST) 2001*, Banff, Canada, pp. 9 – 16, November 15-17, 2001.
- [4] K. Meyer, H. Applewhite, and F. Biocca, "A Survey of Position Trackers," *Presence: Teleoperators and Virtual Environments*, Vol. 1, No. 2, pp. 173-200, 1992.

- [5] E. Foxlin, M. Harrington, and Y. Alshuler, "Miniature 6-DOF inertial system for tracking HMDs," in *SPIE vol. 3362, Helmet and Head-Mounted Displays III, AeroSense 98*, Orlando, FL, April 1998.
- [6] E. Foxlin, "Inertial head-tracker fusion by a complementary separate-bias Kalman filter," in *Virtual Reality Annual International Symposium (VRAIS 96)*, Santa Clara, CA, March 1996, pp. 185–194,
- [7] E. Bachmann, *Inertial and magnetic tracking of limb segment orientation for inserting humans into synthetic environments*, Ph.D. dissertation, Naval Postgraduate School, Monterey, CA, 2000.
- [8] A. Gallagher, Y. Matsuoka, and A. Wei-Tech, "An efficient real-time human posture tracking algorithm using low-cost inertial and magnetic sensors," in *Proceedings of 2004 IEEE International Conference on Robotics and Automation*, Sendai, Japan, September 2004, pp. 2967–2972.
- [9] H. J. Luinge, *Inertial sensing of human movement*, Ph.D. dissertation, University of Twente, December 2002.
- [10] R. Zhu and Z. Zhou, "A real-time articulated human motion tracking using tri-axis inertial/magnetic sensors package," *IEEE Transactions on Neural Systems and Rehabilitation Engineering*, vol. 12, no. 2, pp. 295–302, June 2004.
- [11] E. Kraft, "A quaternion-based unscented Kalman filter for orientation tracking," in *Proceedings of the IEEE Sixth International Conference of Information Fusion*, Cairns, Queensland, Australia, 2003, pp. 47–54.
- [12] Z. Yan and K. Yuan, "An orientation tracking algorithm valid in a hemisphere space based on gravity field and earth magnetic field," in *Proceedings of the 2004 IEEE International Conference on Information Acquisition*, Hefei, China, June 2004, pp. 236–239.
- [13] D. Gebre-Egziabher, G. H. Elkaim, J. Powell, and B. W. Parkinson, "A gyro-free quaternion-based attitude determination system suitable for implementation using low cost sensors," in *Proceedings of IEEE 2000 Position Location and Navigation Symposium*, San Diego, CA, March 2000, pp. 185–192.
- [14] M. D. Shuster and S. D. Oh, "Three-axis attitude determination for vector observations," *Journal of Guidance and Control*, vol. 4, no. 1, pp. 70–77, 1981.
- [15] E. Bachmann, X. Yun, D. McKinney, R. McGhee, and M. Zyda, "Design and Implementation of MARG Sensors for 3-DOF Orientation Measurement of Rigid Bodies," *Proceedings of IEEE International Conference on Robotics and Automation (ICRA 2003)*, Taipei, Taiwan, September, 2003.
- [16] X. Yun, C. Aparicio, E. Bachmann, and R. McGhee, "Implementation and Experimental Results of a Quaternion-Based Kalman Filter for Human Body Motion Tracking," *Proceedings of the 2005 IEEE International Conference on Robotics and Automation*, Barcelona, Spain, April 2005.
- [17] W. Denne, *Magnetic compass deviation and correction*, 3rd Edition, Glasgow: Brown and Ferguson, 1979.
- [18] T. S. Tenforde, "Spectrum and Intensity of Environmental Electromagnetic Fields from Natural and Man-Made Sources," *Electromagnetic Fields: Biological Interactions and Mechanisms*, American Chemical Society, Washington, DC, 1995, p. 13-35.
- [19] M. Caruso, "Applications of Magnetic Sensors for Low Cost Compass Systems," *Proceedings of IEEE Symposium on Position Location and Navigation*, San Diego, CA, March, 2000, pp. 177-184.
- [20] B. Hoff, and R. Azuma, "Autocalibration of an Electronic Compass in an Outdoor Reality System," *Proceedings of IEEE Symposium on Augmented Reality (ISAR 2000)*, Munich, Germany, October, 2000, pp. 159-164.
- [21] Peterson, C., *An Investigation of the Effects of Magnetic Variations On Inertial/Magnetic Orientation Sensors*, Master's Thesis, Miami University, Oxford, Oh., 2003.
- [22] M. Nixon, B. McCallum, W. Fright, and N. Price, "The Effects of Metals and Interfering Fields on Electromagnetic Trackers," *Presence: Teleoperators and Virtual Environments*, Vol. 7, No. 2, MIT Press, Cambridge, MA, pp. 204-218, 1998.
- [23] D. Roetenberg, H. J. Luinge, C. T. M. Baten, and P. H. Veltink, "Compensation of Magnetic Disturbances Improves Inertial and Magnetic Sensing of Human Body Segment Orientation," *IEEE Transactions On Neural Systems And Rehabilitation Engineering*, Vol. 13, No. 3, September 2005.

Design, Implementation, and Experimental Results of a Quaternion-Based Kalman Filter for Human Body Motion Tracking

Xiaoping Yun, *Fellow, IEEE*, and Eric R. Bachmann, *Member, IEEE*

Abstract—Real-time tracking of human body motion is an important technology in synthetic environments, robotics, and other human-computer interaction applications. This paper presents an extended Kalman filter designed for real-time estimation of the orientation of human limb segments. The filter processes data from small inertial/magnetic sensor modules containing triaxial angular rate sensors, accelerometers, and magnetometers. The filter represents rotation using quaternions rather than Euler angles or axis/angle pairs. Preprocessing of the acceleration and magnetometer measurements using the Quest algorithm produces a computed quaternion input for the filter. This preprocessing reduces the dimension of the state vector and makes the measurement equations linear. Real-time implementation and testing results of the quaternion-based Kalman filter are presented. Experimental results validate the filter design, and show the feasibility of using inertial/magnetic sensor modules for real-time human body motion tracking.

Index Terms—Inertial sensors, Kalman filtering, magnetic sensors, motion measurement, orientation tracking, pose estimation, quaternions, virtual reality.

I. INTRODUCTION

MOTION tracking is a key technology in synthetic environments, robotics, and other applications that require real-time information about the motion of a human. A number of motion-tracking technologies have been developed for human motion capture in virtual reality and biomedical applications, including mechanical trackers, active magnetic trackers, optical tracking systems, acoustic, and inertial/magnetic tracking systems. Most are dependent on an artificially generated source and are thus range-limited and susceptible to interference and noise.

Mechanical tracking systems can be placed in two separate categories. Body-based systems use an exoskeleton that is attached to the articulated structure to be tracked [1]. Goniometers within the skeletal linkages measure joint angles. Ground-based systems attach one end of a boom or shaft to a tracked object and

typically have six degrees of freedom (DOFs) [2]. Ground-based systems normally only track a single rigid body, but have the advantage of being able to provide haptic feedback.

Practical optical tracking systems can also be separated into two basic categories. Pattern recognition systems sense an artificial pattern of lights and use this information to determine position and/or orientation [3]. Such systems may be “outside-in” when the sensors are fixed and the emitters are mobile, or “inside-out” when sensors are mounted on mobile objects and the emitters are fixed. Image-based systems determine position by using multiple cameras to track predesignated points on moving objects within a working volume. The tracked points may be marked actively or passively [4], [5].

Active magnetic tracking systems determine both position and orientation by using sets of small orthogonally mounted coils to sense a set of sequentially generated magnetic fields. The sequentially emitted fields induce current in each of the sensor coils, allowing measurement of orientation. Changes in total strength across the sensor coils are proportional to the distance from the field transmitter and can be used to measure position [6].

Ultrasonic tracking systems can determine position through either time-of-flight and triangulation or phase-coherence. Phase-coherence trackers determine distance by measuring the difference in phase of a reference signal and an emitted signal detected by sensors.

Body tracking using inertial and magnetic sensors is a relatively new technology. Inertial/magnetic tracking is appealing due to a lack of dependence on an artificially generated source. It thus does not suffer from range limitations and interference problems of sourced technologies. All delay or latency is due to data processing and transmission. The availability of low-cost, small-size micro-electro-mechanical systems (MEMS) sensors has made it possible to build wrist-watch-sized, self-contained inertial/magnetic sensor modules [7], [8]. These modules can be used to accurately track orientation in real time. Attachment of such sensor modules to each of the major limb segments of a human makes it possible to independently determine the orientation of each segment relative to an Earth-fixed reference frame. The human model is constructed from multiple independently oriented limb segments that are constrained by their attachment to each other. Relative orientation between limb segments is not determined or needed.

A naive approach to inertial orientation tracking might involve integration of angular rate data to determine orientation. However, this solution would be prone to drift over time due to

Manuscript received December 22, 2005; revised June 15, 2006. This paper was recommended for publication by Associate Editor J. Tardos and Editor H. Arai upon evaluation of the reviewers' comments. This work was supported in part by the Army Research Office (ARO), and in part by the Navy Modeling and Simulation Management Office (NMSO). This paper was presented in part at the IEEE International Conference on Robotics and Automation, Barcelona, Spain, April 2005.

X. Yun is with the Department of Electrical and Computer Engineering, Naval Postgraduate School, Monterey, CA 93943 USA (e-mail: yun@ieee.org).

E. R. Bachmann is with the Department of Computer Science and System Analysis, Miami University, Oxford, OH 45056 USA.

Digital Object Identifier 10.1109/TRO.2006.886270

the buildup of bias and drift errors. In order to avoid drift, inertial tracking systems make use of additional complementary sensors. Commonly, these sensors include triads of accelerometers and magnetometers for respectively referencing the gravity and magnetic field vectors. Measuring the gravity vector in the sensor coordinate frame using accelerometers allows estimation of orientation relative to the horizontal plane. However, in the event that the sensor module is rotated about the vertical axis, the projection of the gravity vector on each of the principal axes of the accelerometer triad will not change. Since the accelerometer triad can not be used to sense a rotation about the vertical axis, magnetometers are used to measure the local magnetic field vector in sensor coordinates and allows determination of orientation relative to the vertical. The data from the incorporated sensors is normally fused using a Kalman or complementary filtering algorithm. It should be noted that data from low-cost MEMS accelerometers cannot be double-integrated for an extended period of time to determine position, due to a quadratic growth of errors.

This paper describes the design, implementation, and experimental testing of an extended Kalman filter (EKF) for real-time tracking of human body motion. In order to produce 3-D orientation estimates relative to an Earth-fixed reference frame, the filter uses input data from a sensor module containing a triad of orthogonally mounted linear accelerometers, a triad of orthogonally mounted angular rate sensors, and a triad of orthogonally mounted magnetometers. Quaternions are used to represent orientation to improve computational efficiency and avoid singularities. In addition, the use of quaternions eliminates the need for computing trigonometric functions. The filter continuously corrects for drift based on the assumption that human limb acceleration is bounded, and averages to zero over any extended period of time. A first-order linear system is used to model human body limb segment motion. The QUEST algorithm is used to preprocess accelerometer and magnetometer measurements, resulting in a significant simplification of the Kalman filter design. The filter is experimentally validated using actual sensor measurements.

The primary contributions of this paper are:

- analysis that determines that a simple motion model based on a first-order linear system is sufficient for tracking human limb segment orientation;
- an EKF designed for tracking human limb segment orientation that fuses a precalculated quaternion input with angular rate data;
- experimental results validating that filter performance is adequate for human posture tracking applications.

The paper is organized as follows. Section II provides an overview of related work, and contrasts that with the approach described in this paper. Section III gives a brief description of the MARG sensors used to obtain experimental data. Section IV presents the process model of the Kalman filter for human body motion tracking. Section V describes two approaches to Kalman filter design. Section VI describes implementation issues of the Kalman filter with a focus on how the nonlinear process model was first linearized and then discretized. Experimental modeling of the process noise covariance matrix and the measurement noise covariance matrix is also detailed. Section VII reports the

MATLAB simulation and offline testing results of the Kalman filter. Section VIII describes the real-time implementation of the algorithm and testing results. The final section provides a summary and conclusions.

II. RELATED WORK

Many studies of human motion tracking using inertial sensors have been performed. Depending on the type, number, and configuration of sensors used, some studies are limited to tracking two degrees of orientation in a plane, while others track 3-D orientation. Algorithms have also been designed to track limb segment orientations relative to each other or calculate joint angles, as opposed to estimating the orientation of a limb segment relative to an Earth-fixed reference frame.

A study of human motion tracking using accelerometers alone was reported in [9]. During motions involving small linear accelerations, a set of triaxial accelerometers was used to determine joint angles. During motions accompanied by higher accelerations, a technique is described that involves the use of two sets of triaxial accelerometers on a single rigid body to differentiate gravitational acceleration from motion-related linear acceleration. Though the effects of these geometric sensor fusion techniques are depicted, there is no comparison with truth data. The use of magnetometers is mentioned, but not discussed. Rehbindler and Hu [10] describe an attitude estimation algorithm based on the use of angular rate sensors and accelerometers. In this paper, drift in heading estimation was unavoidable due to a lack of additional complementary sensors, such as magnetometers. Thus, only two DOFs of orientation are tracked. Sabatini *et al.* [11] used a single sensor module containing a biaxial accelerometer and one gyroscope to perform gait analysis and measurement. To measure incline, distance, and speed, the method exploits the cyclical features of human gait. Transition from one gait phase to the next is determined using gyroscope data. Acceleration data is double integrated during the swing phase to determine position and used to determine the vertical when the foot is flat on the ground. Since the accelerometers are unable to detect rotations about the vertical plane, all motion is assumed to take place in a nonrotating sagittal plane. Sabatini [12] took this research further by creating a quaternion-based filtering algorithm. A quaternion interpolation technique is used to improve the accuracy of orientation and position estimates by reducing the effects of sensor bias and scale factor drift in both the accelerometers and gyroscope. Unlike the work described in this paper, this gait analysis work does not attempt to measure posture. In similar gait measurement work, Veltink *et al.* [13] use a sensor module containing a three-axis accelerometer and a three-axis angular rate sensor to measure gait characteristics in order to tune an implantable drop-foot simulator.

In a study of dynamic registration in augmented reality applications that require more precise orientation tracking as well as position tracking, Azuma and Bishop [14] use inertial data from linear accelerometers and angular rate sensors to reduce apparent lag in the position and orientation estimates produced by an optoelectronic tracking system. The use of an EKF predictor resulted in errors 5–10 times lower than without predic-

tion. In contrast, the work described in this paper produces only estimates of orientation using inertial and magnetic data.

Full 3-DOF orientation tracking is most commonly performed using nine-axis sensor modules containing three orthogonally mounted triads of angular rate sensors, accelerometers, and magnetometers. Foxlin *et al.* [15], [16] describes two commercial nine-axis sensing systems designed for head tracking applications. Sensor fusion is performed using a complementary separate-bias Kalman filter. Drift correction is described as only being performed during stationary periods when it is assumed accelerometers are sensing only gravitational acceleration. Thus, the described algorithm requires that all motion stop in order to correct inertial drift errors.

Bachmann *et al.* [7], [17] proposed a nonoptimal quaternion-based complementary filter for human body tracking. The filter is able to track through all orientations without singularities, and continuously correct for drift without a need for stationary periods using nine-axis inertial/magnetic sensor module data. Extensions to this work and the development of an optimal filter designed for human posture tracking applications are described in [18]–[20]. Use of a first-order linear system for modeling human body limb motions was first proposed in [18]. A Gauss–Newton iteration method is used to preprocess accelerometer and magnetometer data to produce quaternion input to the EKF. Formulation and simulation testing of a reduced-order implementation of the Gauss–Newton iteration method for this Kalman filter is documented in [19]. Preliminary experimental testing results are presented in [20].

In [21], Gallagher *et al.* present a nonoptimal complementary filter algorithm that has a lower computational complexity and similar accuracy to the work described by Bachmann *et al.* in [7] and [17]. Luongo describes a Kalman filter designed for human body tracking application in [22]–[24]. In the proposed method, inclination is determined without low-pass filtering accelerometer data. The design is based on assumptions concerning the frequency content of the acceleration and the magnitude of gravity. Reduction of drift about the vertical axis is dependent on the use of a kinematic human body model. Magnetometers are not used. More recently, Roetenberg *et al.* [25] extended the Kalman filter described in [23] to include a magnetometer model designed to prevent heading drift and compensate for magnetic disturbances. This compensation allowed a significant estimation accuracy improvement in comparison with no compensation or using angular rate sensors only. In [26], Zhu and Zhou describe a linear Kalman filter algorithm designed to smooth accelerometer and magnetometer readings from a nine-axis sensor module. Rather than estimating individual limb segment orientations relative to a fixed reference frame, as is done in this paper, their system determines joint angles in axis/angle form using the data from the two sensors mounted on the inboard and outboard sides of the joint. The axis/angle pairs are determined analytically using processed measurement data.

Kraft [27] describes an “unscented,” quaternion-based Kalman filter for real-time estimation of rigid-body orientation using nine-axis sensor modules. The described filter approximates the Gaussian probability distribution using a set of sample points instead of linearizing nonlinear process model

equations. Simulation results demonstrate the general validity of the described filter. Tests of the filter with real measurements are mentioned, but not shown or quantified. Haid and Breitenbach [28] also describe a Kalman filter algorithm for use with inertial and magnetic sensors. The primary aim of the filter is the elimination of drift and bias effects observed in low-cost angular rate sensors. The filter works only in the single dimension of the targeted angular-rate sensor. It does not estimate limb segment orientation or joint angles.

Some work has attempted to eliminate the need to include angular rate sensors in inertial/magnetic sensor modules. In [29], Gebre-Egziabher *et al.* describe an attitude determination algorithm for aircraft applications. The algorithm is based on a quaternion formulation of Wahba’s problem [30], where magnetometer and accelerometer measurements are used to determine attitude without the use of angular rate sensors. A Kalman filter implementation of the algorithm is also presented. The algorithm is based on the assumption that the rigid body to which the sensor is attached is stationary or is slow moving, and is thus not applicable to highly dynamic tracking applications. Chin-Woo *et al.* [31] propose a gyroscope free inertial navigation system that uses accelerometers to determine both linear and angular motions of a rigid body. The approach requires a minimum of six accelerometers. Acceptable configurations and basic algorithms are examined through simulation. Use of accelerometers to calculate angular rate results in a faster orientation error growth rate than that associated with conventional angular rate sensors. This result is due to inclusion of the angular acceleration terms which introduce integrated noise and drift. The idea of using accelerometers to measure angular rate is carried further by Ang *et al.* in [32] and [33].

In contrast with the work described above, this paper presents a filter algorithm that is specifically designed for tracking human-limb segment orientation relative to an Earth-fixed frame. The algorithm incorporates a human body motion model. It adopts a two-layer filter architecture, in which the QUEST algorithm preprocesses accelerometer and magnetometer data and an EKF fuses the QUEST output with angular rate data.

III. MARG SENSORS

Experimental data were collected using MARG III inertial/magnetic sensor modules designed by the authors and fabricated by McKinney Technology [8]. The MARG sensor design is based on its primary application, that is, human body motion tracking. Primary sensing components for this unit include Tokin CG-L43 ceramic rate gyros, Analog Devices ADXL202E micromachined accelerometers, and Honeywell HMC1051Z and HMC1052 one- and two-axis magnetometers. The sensor module also incorporates a Texas Instruments MSP430F149 ultra-low-power, 16-bit RISC architecture microcontroller. Overall, dimensions of the MARG III unit are approximately 1.8 cm × 3.0 cm × 2.5 cm.

The manufacturer specified maximum allowable angular rate of the CG-L43 ceramic gyro is $\pm 90^\circ/\text{s}$. This is deemed sufficient to quicken response in human body motion tracking applications, but not accurately measure rates associated with highly dynamic motion. Three of these gyros are orthogonally mounted

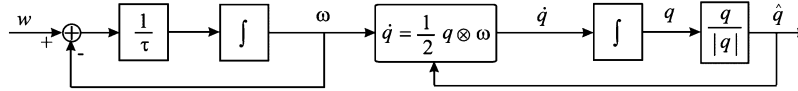


Fig. 1. Kalman filter process model. q is the orientation quaternion, ω is the angular velocity, w is a white noise, and τ is the time constant.

within the MARG unit to form a triad capable of measuring 3-DOF angular rate. In the results presented here, the limitations of the angular rate sensors did not affect the performance or demonstration of the algorithms during typical human motion.

The maximum measurement range of Analog Devices ADXL202E is ± 2 g, which is acceptable for sensing gravitational acceleration. The ADXL202E is a two-axis acceleration sensor on a single chip. As a result, only two of them are required to form a triad for measuring 3-DOF acceleration. The ADXL202E also offers a duty cycle output, which can be directly interfaced to a low-cost microcontroller without analog/digital (A/D) converters. The accelerometers are not used to measure linear accelerations associated with human motion.

In the MARG design, a one-axis HMC1051Z for the z-axis and a two-axis HMC1052 for x-y axes are mounted on the same PCB to form a three-axis magnetometer. The HMC1051Z and HMC1052 are specially designed to be mounted on the same PCB to form an orthogonal triad.

The purpose of the microcontroller is to convert analog sensor outputs to digital data, digitally filter the angular rate sensor data, and perform automatic set/reset of magnetometers to avoid magnetic saturation problems. To prepare angular rate data for processing by the Kalman filter, the data is averaged on start up to establish initial bias values. During run-time, angular rate data is preprocessed using a simple first-order high-pass filter to eliminate drift over time. Static bench tests have established that accelerometer and magnetometer data are relatively stable over time, and they are thus not bias-corrected at run-time. Magnetic interference is a major concern when using magnetometers in environments containing changing or distorted magnetic fields [34]. This is an active area of research by the authors and others [25]. No compensation for external magnetic effects is performed in the work described in this paper. It is noted that the MARG sensor is a prototype constructed using 2 g accelerometers and 90°/s angular rate sensors. These components were chosen for typical human motion, and may not be sufficient for extreme human motion. The algorithm presented in the paper is not limited to these particular sensor parameters.

IV. KALMAN FILTER PROCESS MODEL

As stated above, the objective of this paper is to design a Kalman filter for real-time tracking of human body motion. To do so, it is necessary to establish a process model representing motion dynamics of the human musculoskeletal system. Dynamic models of the human musculoskeletal systems are complex, and have been studied for many years. Such models are ideal for computer simulations of articulated body motions, but remain too computationally demanding for real-time applications such as real-time human motion tracking. Thus, the challenge is to develop a model that is simple yet adequate for motion tracking applications. Based on extensive trial and error

study, a first-order linear system model is adopted to represent the motion of each human body limb segment. Such a model is depicted in the left half of Fig. 1. It is assumed that each limb segment is independent of the others. The input to the linear system is a white noise w , and the output is the angular velocity ω of the limb segment. The most important parameter in this model is the time constant τ , which determines how fast a limb segment (e.g., upper arm) can move in typical human motion conditions. The angular velocity is thus modeled as a colored noise generated by a linear system with a white noise input.

In the filter, quaternions are used to represent the orientation of each body limb segment for two reasons. First, the quaternion representation does not suffer from the singularity problem associated with the Euler angle representation. Second, it avoids trigonometric functions in the filter algorithm, making it more efficient and easier to implement in real time on microcontrollers. In what follows, q will be used to denote the orientation quaternion in Earth coordinates. The angular velocity ω and the quaternion derivative \dot{q} are related by the following well-known identity [35]:

$$\dot{q} = \frac{1}{2} q \otimes \omega \quad (1)$$

where \otimes represents quaternion multiplication. Equation (1) is represented by the center block in Fig. 1. The quaternion derivative \dot{q} is integrated to produce the quaternion q . In order to take advantage of computational simplifications and efficiencies associated with unit quaternions, the resultant quaternion is normalized to unit length in the last step of the process model, as shown in Fig. 1. The quaternion q produced by the integrator may not be exactly unit length, but it is normally very close to a unit quaternion. To avoid the complexity that the normalization introduces into the Kalman filter derivation, it is not included in the process model equations presented in the next section. As a result, although the Kalman filter is an optimal algorithm, this normalization procedure leads to a suboptimal algorithm. In the next section, two Kalman filter designs based on this process model will be presented.

V. KALMAN FILTER DESIGN

Two alternative approaches to the Kalman filter design based on the process model presented in Section IV will be described in this section. The state vector for both approaches is the same. It is a 7-D vector consisting of the three components of angular rate and the four elements of the orientation quaternion. The difference between the two approaches is in the measurement or output equation for the Kalman filter. The first approach uses a standard Kalman filter design, which has a 9-D measurement vector, consisting of 3-D angular rate, 3-D acceleration, and 3-D local magnetic field. This 9-D vector directly corresponds to the measurements provided by inertial/magnetic sensors modules. The first three components of the output equation (angular rate portion) are linearly related to the state vector. However, the

other six components of the output equation are nonlinearly related to the state vector. The nonlinear relationship is quite complicated. As a result, the EKF designed with this output equation is computationally inefficient.

The second approach uses a separate algorithm to find a corresponding quaternion for each set of accelerometer and magnetometer measurements. The computed quaternion is then combined with the angular rate measurements, and presented to the Kalman filter as its measurements. By doing so, the output equations for the Kalman filter become linear, and the overall Kalman filter design is greatly simplified.

A. The First Approach

The first approach is a standard Kalman filter design based on the process model depicted in Fig. 1. The state vector x is 7-D, with the first three components being the angular rate ω , and the last four components being the quaternion q . That is

$$\begin{bmatrix} x_1 \\ x_2 \\ x_3 \end{bmatrix} = \begin{bmatrix} \omega_1 \\ \omega_2 \\ \omega_3 \end{bmatrix} = \omega, \quad \begin{bmatrix} x_4 \\ x_5 \\ x_6 \\ x_7 \end{bmatrix} = \begin{bmatrix} q_1 \\ q_2 \\ q_3 \\ q_4 \end{bmatrix} = q.$$

Based on Fig. 1, the state equations are given by

$$\begin{bmatrix} \dot{x}_1 \\ \dot{x}_2 \\ \dot{x}_3 \end{bmatrix} = \frac{1}{\tau} \left(- \begin{bmatrix} x_1 \\ x_2 \\ x_3 \end{bmatrix} + \begin{bmatrix} w_1 \\ w_2 \\ w_3 \end{bmatrix} \right) \quad (2)$$

$$\begin{bmatrix} \dot{x}_4 \\ \dot{x}_5 \\ \dot{x}_6 \\ \dot{x}_7 \end{bmatrix} = \frac{1}{2} \begin{bmatrix} x_4 \\ x_5 \\ x_6 \\ x_7 \end{bmatrix} \otimes \begin{bmatrix} 0 \\ x_1 \\ x_2 \\ x_3 \end{bmatrix}. \quad (3)$$

It is noted that quaternion normalization is not modeled in these state equations, but is carried out in the real-time implementation.

Since measurement data to the filter are provided by MARG sensors, it is natural to choose the following as the measurements of the Kalman filter:

$$\begin{bmatrix} z_1 \\ z_2 \\ z_3 \end{bmatrix} = \begin{bmatrix} x \text{ component of angular rate} \\ y \text{ component of angular rate} \\ z \text{ component of angular rate} \end{bmatrix} \\ \begin{bmatrix} z_4 \\ z_5 \\ z_6 \end{bmatrix} = \begin{bmatrix} x \text{ component of acceleration} \\ y \text{ component of acceleration} \\ z \text{ component of acceleration} \end{bmatrix} \\ \begin{bmatrix} z_7 \\ z_8 \\ z_9 \end{bmatrix} = \begin{bmatrix} x \text{ component of local magnetic field} \\ y \text{ component of local magnetic field} \\ z \text{ component of local magnetic field} \end{bmatrix}.$$

Since angular rates are part of the state, the first three measurement equations are simply given by the following:

$$z_1 = x_1 + v_1 \quad (4)$$

$$z_2 = x_2 + v_2 \quad (5)$$

$$z_3 = x_3 + v_3 \quad (6)$$

where v_i is the measurement noise that is assumed to be white. As for the remaining six measurement equations, they turn out to

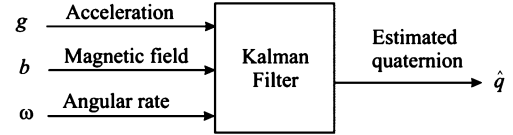


Fig. 2. Block diagram of the first approach to Kalman filter design.

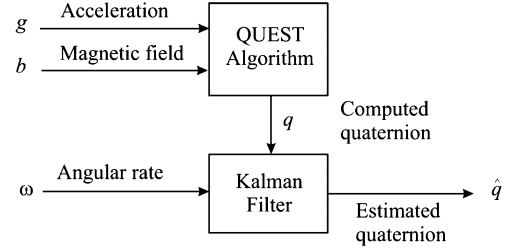


Fig. 3. Block diagram of the second approach to Kalman filter design.

be quite complicated. As an example, the seventh measurement equation is given by

$$z_7 = ((x_4^2 + x_7^2 - x_5^2 - x_6^2)/h_1 + 2(x_4x_5 - x_6x_7)/h_2 + 2(x_4x_6 + x_5x_7)/h_3) / (x_4^2 + x_5^2 + x_6^2 + x_7^2) + v_4 \quad (7)$$

where h_1, h_2 , and h_3 are values of the Earth magnetic field measured in the Earth coordinates, which are constant for a given location. It is not difficult to design an EKF, as shown in Fig. 2, based on state (2) and (3), and the nine measurement equations, which was indeed carried out in [36]. The problem is that computational requirements for implementing such a filter are extremely high, making it unfeasible for real-time motion tracking. An alternative approach to the Kalman filter design is thus presented in the next subsection.

B. The Second Approach

Fig. 3 shows a block diagram of an alternative approach to filter design. Acceleration and local magnetic field measurements are used as input to the QUEST algorithm [37] to produce what will be called *the computed quaternion*. The computed quaternion together with angular rate measurements is then presented to a Kalman filter as measurements. It will be seen below that the Kalman filter in this case is significantly simpler, owing to the fact that the measurement equations are linear. It is true that there is an additional computational cost to implement the QUEST algorithm in this approach. Still, the overall computational requirements for this approach are much less than what is needed for the first approach.

The QUEST (quaternion estimator) algorithm is a popular algorithm for a single-frame estimation of an attitude quaternion [37]. The algorithm was created to solve Wahba's problem [30] that involved determination of the attitude of a rigid body in reference to a fixed coordinate system based on a set of measurement or observation vectors using a closed form solution. The minimum number of measurement vectors required to compute orientation is two. Early solutions to Wahba's problem directly compute a rotation matrix capable of rotating the measurement (assuming no errors) vectors to match the reference vectors. The

QUEST algorithm solves Wahba's problem by calculating the four elements of the corresponding optimal quaternion [37].

This alternative approach to filter design as shown in Fig. 3 is not without reasons. If the limb segment to which an inertial/magnetic sensor module is attached is stationary, acceleration (gravity) and local magnetic field measurements are sufficient to determine the orientation of the body. While stationary, accelerometers measure the local gravity vector in the body frame. The 3-D gravity measurements can be used to determine roll and pitch angles of the body relative to the fixed Earth frame. The yaw angle of the body is determined from the local magnetic field measurements. In this application, the QUEST algorithm takes gravity and magnetic field measurement vectors with equal weight and computes the optimal quaternion that will rotate these vectors to match their corresponding reference vectors.

While the rigid body is in motion, the computed quaternions from this algorithm do not represent the actual real-time orientation of the body, because accelerometers measure the sum of gravity and motion induced acceleration. This is where angular rate measurements come to help estimate the orientation of the rigid body. While angular rate measurements can be integrated to yield an orientation estimate, they are prone to drift over an extended period of time. Acceleration and magnetic field measurements do not drift over time. The Kalman filter in this approach is designed to optimally fuse the complementary information provided by the angular rate measurements and the computed quaternion.

It should be pointed out that this filtering architecture has been previously proposed and successfully applied in other areas such as attitude heading and reference systems (AHRS) [38]. In [38], an inertial navigation system for autonomous underwater vehicles was developed, in which a complementary filter first combines measurement data from accelerometers, angular rate sensors, and magnetic sensors. An EKF then fuses the output of the complementary filter with the GPS/DGPS measurements.

The state equations in the second approach are the same as those in the first approach, that is, equations (2) and (3). The measurement equations in this case are much simpler, and they are

$$z_i = x_i + v_i, \quad i = 1, \dots, 7 \quad (8)$$

where v_i is the white noise measurement. Although the measurement equations are linear, an EKF is still required since the second part of the state (3) is nonlinear. Nevertheless, linearity in the measurement equations significantly simplifies the filter design and reduces computational requirements for real-time implementation.

C. Discussion

The first-order process model and an early version of the second approach to the Kalman filter design was first reported in [18]. Rather than using the QUEST algorithm, a Gauss–Newton iteration method was used to preprocess accelerometer and magnetometer data to produce quaternion input to the EKF. A

reduced-order implementation of the Gauss–Newton iteration method was described in [19]. This reduced order implementation requires computing the inverse of a 3×3 matrix rather than that of a 4×4 matrix. The Gauss–Newton iteration method was replaced by the factored quaternion algorithm in [20]. While more efficient, the factored quaternion algorithm provides a suboptimal solution. The QUEST algorithm provides an optimal solution for noisy measurement data. Preliminary experimental results were also reported in [20]. In this paper, the QUEST algorithm is adopted to preprocess the acceleration and magnetic field measurement data. The QUEST algorithm requires computing the inverse of a 4×4 matrix, but it is a single-frame or noniterative algorithm. The QUEST algorithm needs to be executed once for each sampling step of the Kalman filter. The Gauss–Newton method needs to be iteratively evaluated several times until it converges for each sampling step of the Kalman filter.

VI. KALMAN FILTER IMPLEMENTATION

In this section, the implementation of the second approach Kalman filter design will be described. First, the state equations are linearized and discretized to yield a discrete process model. Second, modeling of the process noises and measurement noises is presented.

The state equations (2) and (3) can be written together in the following form:

$$\dot{x} = f(x) + w(t). \quad (9)$$

This nonlinear process model can be linearized along the currently estimated trajectory \hat{x}

$$\Delta \dot{x} = \frac{\partial f(x)}{\partial x} \Big|_{x=\hat{x}} \Delta x + w(t). \quad (10)$$

The actual trajectory x is the sum of the estimated trajectory \hat{x} and the small increment Δx

$$x = \hat{x} + \Delta x. \quad (11)$$

The next step is to convert the continuous-time model (10) into a discrete-time model. Let $\delta = \Delta t$ be the sampling interval. Then the difference equation corresponding to the differential (10) is given by

$$\Delta x_{k+1} = \Phi_k \Delta x_k + w_k \quad (12)$$

where the discrete state transition matrix is

$$\Phi_k = \begin{bmatrix} e^{-\frac{\delta}{\tau_1}} & 0 & 0 & 0 & 0 & 0 & 0 \\ 0 & e^{-\frac{\delta}{\tau_2}} & 0 & 0 & 0 & 0 & 0 \\ 0 & 0 & e^{-\frac{\delta}{\tau_3}} & 0 & 0 & 0 & 0 \\ -\frac{\hat{x}_5 \delta}{2} & -\frac{\hat{x}_6 \delta}{2} & -\frac{\hat{x}_7 \delta}{2} & 1 & -\frac{\hat{x}_1 \delta}{2} & -\frac{\hat{x}_2 \delta}{2} & -\frac{\hat{x}_3 \delta}{2} \\ \frac{\hat{x}_4 \delta}{2} & -\frac{\hat{x}_7 \delta}{2} & \frac{\hat{x}_6 \delta}{2} & \frac{\hat{x}_1 \delta}{2} & 1 & \frac{\hat{x}_3 \delta}{2} & -\frac{\hat{x}_2 \delta}{2} \\ \frac{\hat{x}_7 \delta}{2} & \frac{\hat{x}_4 \delta}{2} & -\frac{\hat{x}_5 \delta}{2} & \frac{\hat{x}_2 \delta}{2} & -\frac{\hat{x}_3 \delta}{2} & 1 & \frac{\hat{x}_1 \delta}{2} \\ -\frac{\hat{x}_6 \delta}{2} & \frac{\hat{x}_5 \delta}{2} & \frac{\hat{x}_4 \delta}{2} & \frac{\hat{x}_3 \delta}{2} & \frac{\hat{x}_2 \delta}{2} & -\frac{\hat{x}_1 \delta}{2} & 1 \end{bmatrix} \quad (13)$$

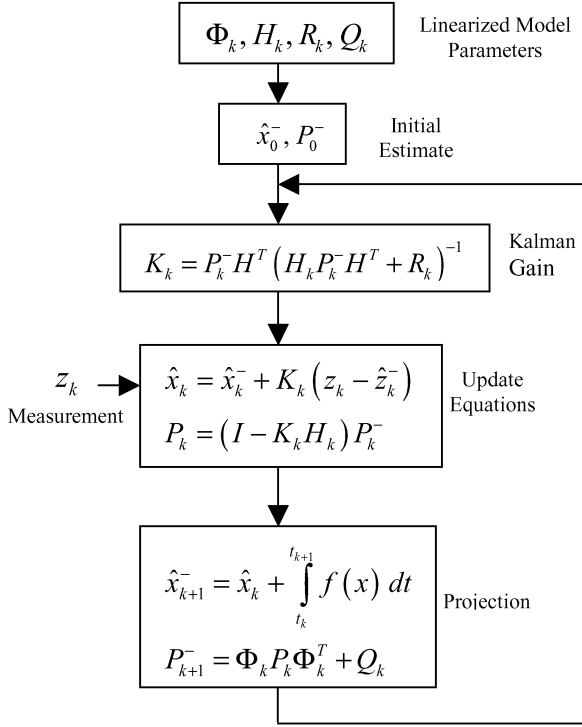


Fig. 4. Block diagram of the EKF.

and w_k is a vector of discrete white process noise and its elements are given by

$$w_{ik} = \begin{cases} \int_{t_k}^{t_{k+1}} e^{-\frac{t_{k+1}-\gamma}{\tau_i}} w_i(\gamma) d\gamma, & i = 1, 2, 3 \\ 0, & i = 4, 5, 6, 7. \end{cases} \quad (14)$$

The measurement (8) are linear and thus linearization is not required. The corresponding discrete measurement equation is given by

$$z_k = H_k x_k + v_k \quad (15)$$

where H_k is the 7×7 identity matrix. An EKF can now be designed for the discrete process (12) and the discrete measurement (15). A complete diagram of the filter is depicted in Fig. 4. It is seen from Fig. 4 that the model parameters Φ_k , H_k , R_k , and Q_k need to be provided to start the filter. Φ_k is the discrete state transition matrix given by (13). H_k is the identity measurement equation matrix of (15). The determination of the covariance matrix Q_k of the process noises and the covariance matrix R_k of the measurement noises is discussed below.

The process noise covariance matrix Q_k is defined by

$$Q_k = E[w_k w_k^T] \quad (16)$$

where E is the expectation operator, and w_k is the discrete process white noise vector of (12), whose components are given by (14). Before computing Q_k , it should be noted that the continuous process noises $w(t) = [w_1(t), w_2(t), w_3(t)]^T$ of the state (2) are independent white noises with zero mean and variance D_i . As such, the covariance is given by

$$E[w_i(t) w_j(s)] = \begin{cases} D_i \delta(t - s), & i = j \\ 0, & i \neq j. \end{cases} \quad (17)$$

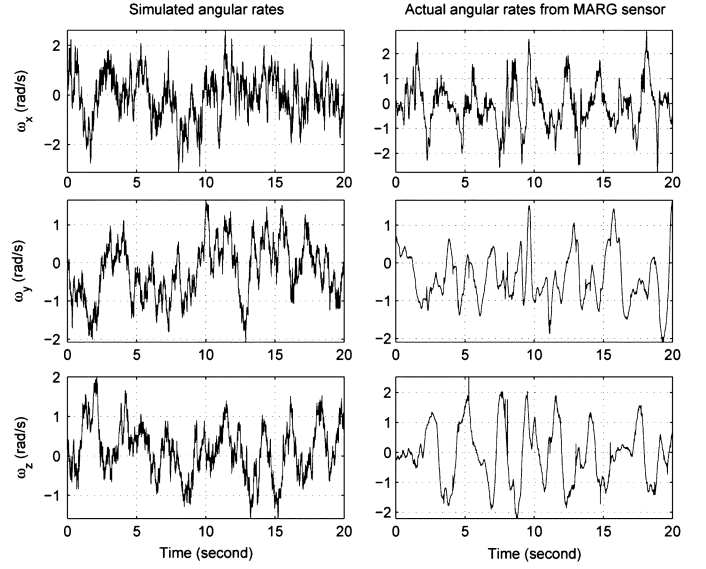


Fig. 5. Comparison of the simulated angular rate (left) and actual angular rate measurements (right).

Using (17) and (14), the process noise covariance matrix Q_k of (16) is evaluated to be

$$Q_k = \begin{bmatrix} q_{11} & 0 & 0 & 0 & 0 & 0 & 0 \\ 0 & q_{22} & 0 & 0 & 0 & 0 & 0 \\ 0 & 0 & q_{33} & 0 & 0 & 0 & 0 \\ 0 & 0 & 0 & 0 & 0 & 0 & 0 \\ 0 & 0 & 0 & 0 & 0 & 0 & 0 \\ 0 & 0 & 0 & 0 & 0 & 0 & 0 \\ 0 & 0 & 0 & 0 & 0 & 0 & 0 \end{bmatrix} \quad (18)$$

where q_{11} , q_{22} , and q_{33} are given by

$$q_{11} = E[w_{1k} w_{1k}] = \frac{D_1}{2\tau_1} \left(1 - e^{-\frac{2\Delta t}{\tau_1}}\right) \quad (19)$$

$$q_{22} = E[w_{2k} w_{2k}] = \frac{D_2}{2\tau_2} \left(1 - e^{-\frac{2\Delta t}{\tau_2}}\right) \quad (20)$$

$$q_{33} = E[w_{3k} w_{3k}] = \frac{D_3}{2\tau_3} \left(1 - e^{-\frac{2\Delta t}{\tau_3}}\right). \quad (21)$$

What remains to be determined are the variance D_i of the continuous white noise processes and the time constant τ_i of the process model. They are determined using actual measurement data from the MARG sensors and a Matlab simulation implementing the angular rate process model (2). The variance and time constant in the simulation are adjusted until the output of the simulation closely matches the actual measurement data. For this purpose, a MARG sensor was attached to the right lower arm of a user and typical arm motion data were collected. It was experimentally determined that $\tau_i = 0.5$ s, $D_i = 0.4$ rad²/s².

Fig. 5 shows a comparison between the simulated angular rates and the actual angular rates obtained from a MARG III sensor for typical arm motions. The graphs to the left represent the angular rates generated by the simulation model. The graphs to the right are the angular rates measured by a MARG sensor. It can be observed that the two sets of data exhibit similar characteristics. Autocorrelations of the simulated and actual x-axis angular rate data are plotted in Fig. 6. The autocorrelation of the actual angular rate data obtained from the MARG sensor was

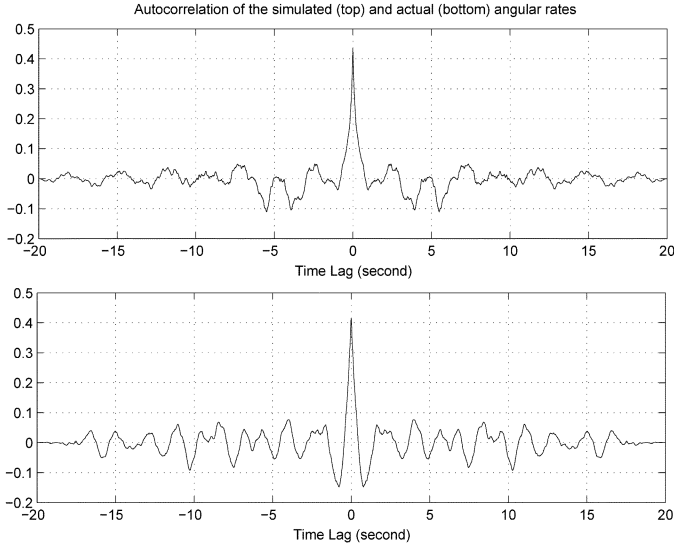


Fig. 6. Autocorrelations of the simulated x-axis angular rate (top plot) and the actual x-axis angular rate (bottom plot).

first computed. The parameters of the process model were then adjusted so that the autocorrelation of the simulated angular rate closely matches that of the actual data. It is seen that they are not exactly the same, but closely resemble each other.

The measurement noise covariance matrix R_k represents the level of confidence placed in the accuracy of the measurements, and is given by

$$R_k = E[v_k v_k^T]. \quad (22)$$

In principle, R_k is not necessarily diagonal. For practical purposes, only diagonal elements are experimentally determined based on actual measurements. A MARG sensor was placed in various static configurations, and data were collected. The variances of the first three measurement components are determined directly from angular rate measurements, and the variances of the other four components (quaternion components) are determined using computed quaternions. The experimentally determined values are $R_{11} = R_{22} = R_{33} = 0.01 \text{ rad}^2/\text{s}^{-2}$, and $R_{44} = R_{55} = R_{66} = R_{77} = 0.0001$.

VII. OFFLINE MATLAB TESTING RESULTS

After deriving all the required parameters to initialize the Kalman filter, it was implemented using MATLAB to test the performance and accuracy of the quaternion orientation estimates. Real world data recorded using a MARG sensor was used in these tests.

Since the Kalman gain was determined such that the sum of squared errors is minimized, one way to measure the convergence of the Kalman filter is through examination of the trace of the error covariance matrix P_k . Fig. 7 shows the trace of P_k for the first 200 samples of data obtained with the sensor in its reference position (x-axis pointing north, y-axis pointing east, and z-axis point down). It is noted that the sum of squared errors reaches a steady state after approximately 0.6 s.

Table I shows the elements of the quaternion for the first five samples. The initial estimate was chosen to be the unit quaternion

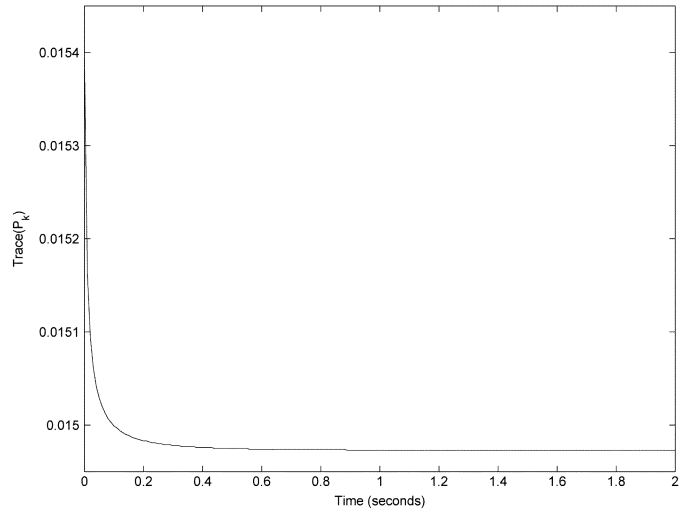


Fig. 7. Trace of the error covariance matrix.

TABLE I
CONVERGENCE OF THE QUATERNION ESTIMATES

Sample	\hat{q}_0	\hat{q}_1	\hat{q}_2	\hat{q}_3
1	0.99985	0.0082135	0.0066032	0.013570
2	0.99991	0.0057585	0.0049037	0.011901
3	0.99990	0.0055983	0.0048826	0.011882
4	0.99990	0.005288	0.0046884	0.011784
5	0.99990	0.0052297	0.0046353	0.011506

nion (0.5, 0.5, 0.5, 0.5). The actual position of the sensor in the reference position is represented by the quaternion (1, 0, 0, 0). The data shown in Table I indicates that the Kalman filter estimate converged to the actual position in a single iteration.

While the QUEST algorithm works well for static orientation and slow movements, the objective of the Kalman filter is to blend angular rate measurements with the estimates produced using magnetometer and accelerometer data during periods in which the sensor module is subjected to motions involving high angular rates and large linear accelerations. To verify the estimation accuracy during such periods, the orientation estimates of the Kalman filter were compared with the estimates produced using only the QUEST algorithm with no rate measurement and with the reference motion of a precision tilt table. Two kinds of experiments were conducted for this test. The first used controlled rotations produced by a HAAS precision tilt table. The table has two DOFs and is capable of positioning to an accuracy of 0.001° at rates ranging from 0.001 to $80^\circ/\text{s}$. In order to mitigate any possible magnetic effects generated by the steel construction of the tilt table, the sensor package was mounted on a nonferrous extension above the table as shown in Fig. 8. The extension is made of a piece of PVC pipe and is approximately 1 m in length. The second experiment used a random motion pattern produced while the sensor was attached to the arm of a person.

In the first set of experiments, the sensor was initially placed with its xyz axes aligned with north-east-down directions. The sensor was rotated -90° about the x-axis at a rate of $60^\circ/\text{s}$ and then rotated 90° at the same rate (in the reverse direction) for

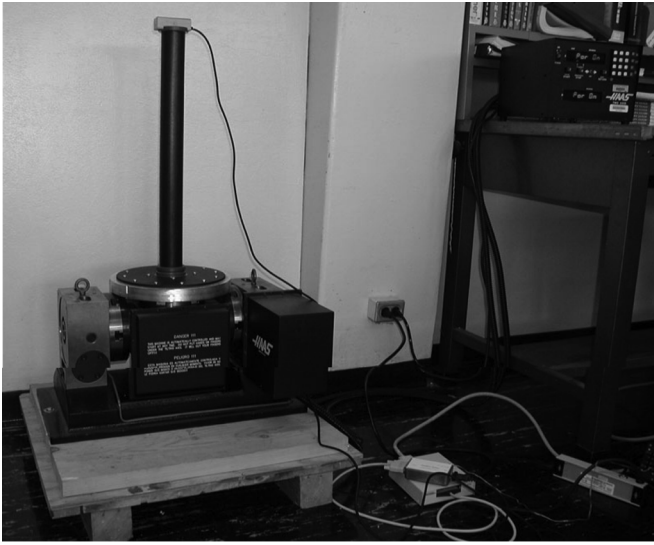


Fig. 8. Experimental setup using a HAAS precision tilt table.

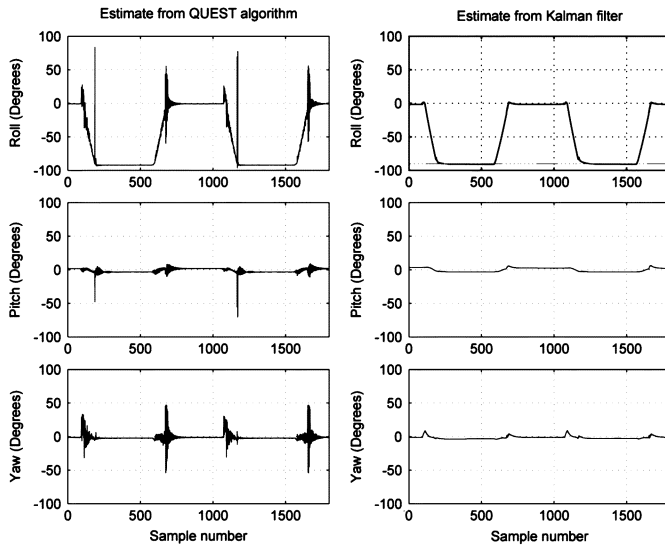


Fig. 9. Orientation estimate produced by the QUEST algorithm (left) and the Kalman filter (right) with a 90° rotation in roll axis.

two cycles. Fig. 9 shows the performance of the Kalman filter in estimating the orientation of the sensor. The graphs to the left show the orientation estimated by the QUEST algorithm, and the graphs to the right show the orientation estimated by the Kalman filter. It can be seen that the QUEST algorithm was able to correctly estimate the roll angle before the first (negative) rotation, between the first and second (positive) rotations, and after the second rotation, but it is not able to correctly estimate orientation during the rotational motions. During the rotational motions, the accelerometers measure the sum of gravity and motion induced acceleration. Without rate sensors, the QUEST algorithm is not able to differentiate gravity from the motion acceleration. Relatively large errors in pitch and yaw were also produced by the QUEST algorithm. On the other hand, it can be seen from the top-right plot that the Kalman filter was able to correctly estimate the roll angle throughout the duration of the experiment. The small pitch and yaw motions seen in the center-right and bottom-right plots are due to misalignment of

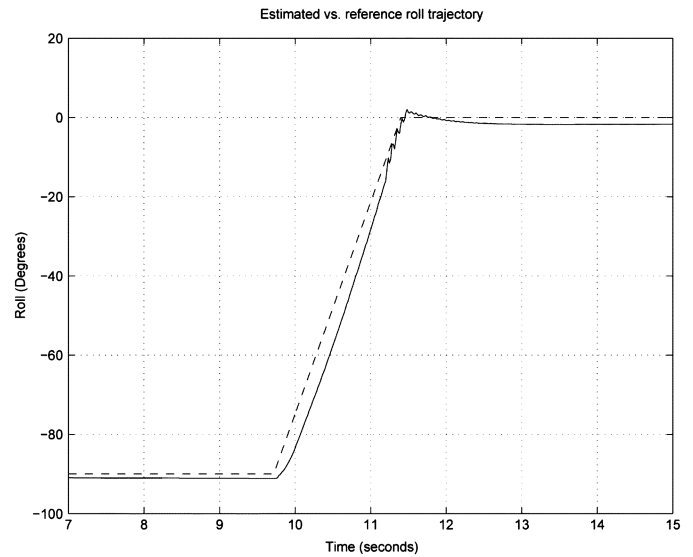


Fig. 10. Zoom-in view of the roll estimate (solid curve) from the Kalman filter and the tilt table reference motion (dashed curve) with a 90° rotation in roll.

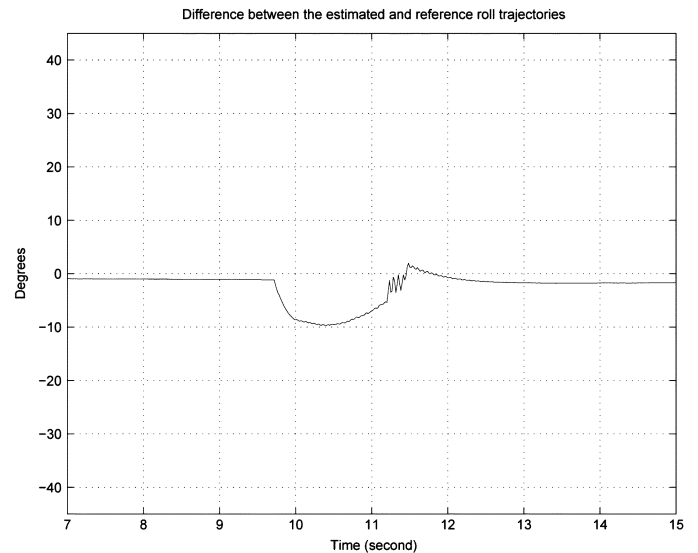


Fig. 11. Difference between the roll estimate and the tilt table reference motion.

the sensor module with the motion axes of the experimental tilt table. The misalignments were corrected manually, but could not be completely removed without the use of equipment not available to the authors. To confirm that the errors were due to misalignments, the algorithm was tested using synthetically generated, noise-free data with rotation in only one axis. These results demonstrated that the algorithm does not produce any observable cross-coupling responses in other axes.

To illustrate the accuracy of the Kalman filter, the estimates produced by the Kalman filter can be compared with the motion of the tilt table. Since the tilt table used in the experiments is much more accurate than the tracking system under evaluation, its motion can be treated as a truth reference. In Fig. 10, the top-right plot of Fig. 9 is replotted in a zoom-in view for the time period of 7–15 s. The solid curve represents the roll estimate from the Kalman filter, and the dashed curve is the reference trajectory of the tilt table. The difference between these two curves is shown in Fig. 11. It is observed from Figs. 10 and 11 that the static accuracy of the filter is better than 2° for the time

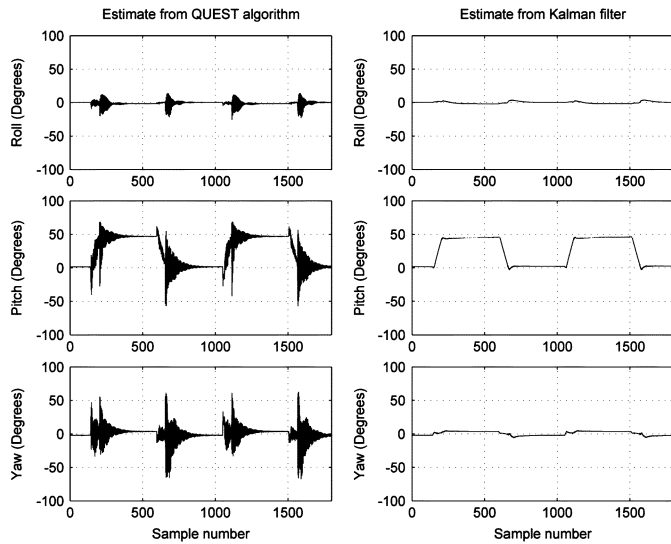


Fig. 12. Orientation estimate produced by the QUEST algorithm (left) and the Kalman filter (right) with a 45° rotation in pitch axis.

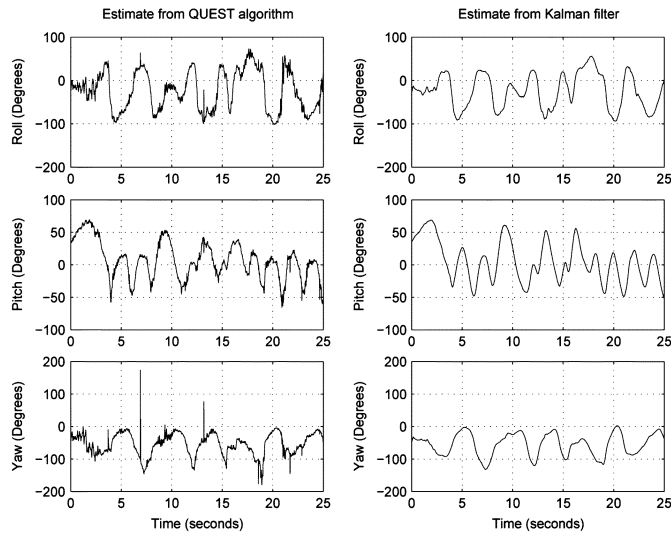


Fig. 13. Orientation estimate produced by the QUEST algorithm (left) and the Kalman filter (right) with random arm movements.

periods of about 7–9.8 s and 11.3–15 s. During the time period of 9.8–11.3 s, the tilt table and the MARG sensor are in the dynamic state moving from -90.0° to 0.0° at the rate of $60^\circ/\text{s}$. It can be observed from Fig. 11 that the maximum error is about 9° . This large dynamic error is mainly due to the lag of the tracking system. The lag is on the order of 100 ms, as depicted by the horizontal gap between the blue curve and green curve during the time period of 10–11 s. The sampling rate is 100 Hz, which yields a lag of 10 ms. The computational time required to execute the filter algorithm is about 1.6 ms. The additional lag is caused by data transmission. In human body tracking applications, this lag-induced error is only observable during highly dynamic motion, and is not of great enough magnitude to impair user interaction with a virtual environment.

Fig. 12 shows plots of rotating the sensor about the y-axis first by 45° and then by -45° at a rate of $45^\circ/\text{s}$. Similar results are observed in this experiment.

Fig. 13 shows the results of an experiment in which the sensor was rotated randomly while attached to the arm of a person. Al-

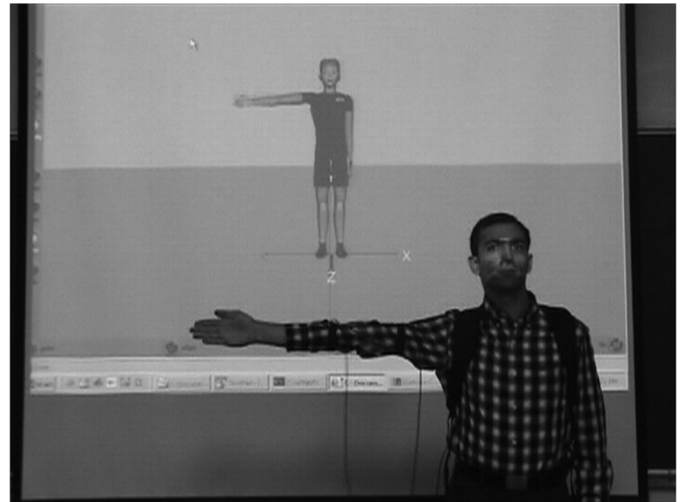


Fig. 14. Snapshot of real-time testing. The user with two MARG sensors attached to the right arm is the foreground and the human avatar projected on a screen is in background.

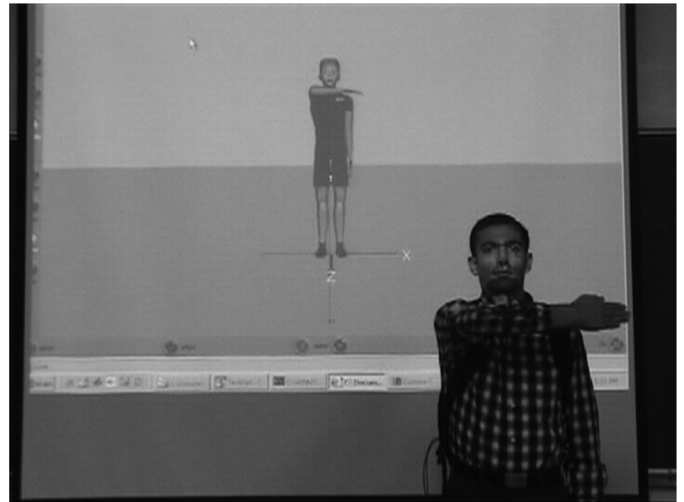


Fig. 15. Another snapshot of real-time testing.

though there is no true reference in this case, it can be seen that the Kalman filter eliminated the jittering and spiking contained in the orientation estimates produced by using the QUEST algorithm alone.

VIII. REAL-TIME TESTING RESULTS

After initial testing of the EKF with the MATLAB implementation, the QUEST algorithm and EKF algorithm were implemented in Java for real-time testing and evaluation. Computation time required to perform a single update is 1.6 ms. Memory management in the Java implementation is carefully performed to avoid the requirement for garbage collection and possible interruption of filter processing. The real-time quaternion produced by the Kalman filter was visualized using a human-like avatar as seen in Figs. 14 and 15. Two MARG sensors were used to track the motion of a human arm, one sensor being attached to the upper arm and the other attached to the lower arm. A video clip demonstrating real-tracking of human arm motions is available at <http://ieeexplore.ieee.org>.

The QUEST algorithm was able to track the motion of the human arm under slow-moving conditions where linear acceleration was not significant. However, when the arm motion became faster, the algorithm was not able to follow the arm motion, resulting in observable lag as well as overshoots.

When the EKF was integrated with the QUEST algorithm, the avatar was able to successfully track the human arm motion in real time under all conditions. Furthermore, the filtering process did not produce any noticeable lag. Movement of the human arm and the avatar was synchronized.

IX. CONCLUSION

This paper presents the design, implementation, and experimental results of a quaternion-based Kalman filter for real-time human body motion tracking using inertial/magnetic sensor modules containing orthogonally mounted triads of accelerometers, angular rate sensors, and magnetometers. This subject filter is not applicable to applications in which accelerations due to forces other than gravity are present for indefinite periods. The filter was designed with the goal of being able to produce highly accurate orientation estimates in real time. This real-time requirement precluded the use of complex models of human motion. Instead the filter design makes use of a simple first-order linear system model. Output of the model is angular velocity modeled as colored noise generated from white noise input. The Kalman filter design is further simplified by preprocessing accelerometer and magnetometer data using the single-frame QUEST algorithm. The quaternion produced by QUEST is provided as input to the Kalman filter along with angular rate data. In comparison to more traditional approaches, this preprocessing step significantly reduces the complexity of filter design by allowing the use of linear measurement equations. Prior to testing of the filter algorithm, values for variances and time constants were determined by comparing simulation results to actual measurement data obtained during typical arm motions. This process was considered complete when the autocorrelation of the simulation data closely matched that of the actual data. In experiments designed to validate filter performance, this approach was shown to work well. In these experiments, filter orientation estimates were compared with truth data obtained from a rotary tilt table. Filter response very closely matched tilt table motion with a static accuracy better than 2° and a dynamic accuracy of better than 9° . This larger error during motion was largely caused by data communication delays. Even with this delay, qualitative experiments in which the algorithm was used demonstrate that these dynamic errors were not of great enough magnitude to impair user interaction with a virtual environment.

The Kalman filter design presented in this paper is the result of several years of effort. With refinement of this design and others mentioned in the related work section, orientation estimation algorithms have reached a limit given the accuracy and noise characteristics of the MEMs sensors employed in the application. The angular rate sensors and accelerometers are truly "sourceless" and do not depend on any outside reference. However, though it is not artificially generated, the magnetometers must sense a homogenous ambient magnetic field in order for these systems to deliver orientation estimates that are stable in

azimuth. Thus the ultimate accuracy of these algorithms can not be determined by considering only the sensors and the implemented algorithms.

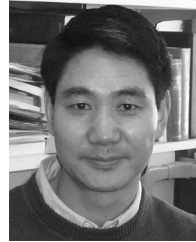
ACKNOWLEDGMENT

The authors would like to thank Dr. R. McGhee for insightful advice and guidance throughout this project, J. Calusdian for technical support, C. Aparicio for implementing the Kalman filter and conducting experimental testing, and D. McKinney for collaboration on the MARG sensors.

REFERENCES

- [1] Gypsy4 Mechanical Motion Capture 2004 [Online]. Available: <http://www.animazoo.com/products/gypsy4.htm>.
- [2] Products: Phantom 1.5/6DOF and 3.0/6DOF 2005 [Online]. Available: http://www.sensable.com/products/phantom_ghost/premium6DOF.asp
- [3] G. Welch, G. Bishop, L. Vicci, S. Brumback, K. Keller, and D. Colucci, "The HiBall tracker: High-performance wide-area tracking for virtual and augmented environments," in *Proc. ACM Symp. Virtual Reality Softw. Technol.*, London, U.K., Dec. 1999, pp. 1–11.
- [4] Motion Capture Systems From Vicon Peak 2005 [Online]. Available: <http://www.vicon.com/>
- [5] Qualisys Motion Capture Analysis System of Kinematics Data 2005 [Online]. Available: <http://www.qualisys.com/>
- [6] F. Raab, E. Blood, O. Steiner, and H. Jones, "Magnetic position and orientation tracking system," *IEEE Trans. Aerosp. Electron. Syst.*, vol. AES-15, no. 5, pp. 709–717, May 1977.
- [7] E. R. Bachmann, R. B. McGhee, X. Yun, and M. J. Zyda, "Inertial and magnetic posture tracking for inserting humans into networked virtual environments," in *Proc. ACM Symp. Virtual Reality Softw. Technol.*, Banff, AB, Canada, Nov. 2001, pp. 9–16.
- [8] E. R. Bachmann, X. Yun, D. McKinney, R. B. McGhee, and M. J. Zyda, "Design and implementation of MARG sensors for 3-DOF orientation measurement of rigid bodies," in *Proc. IEEE Int. Conf. Robot. Autom.*, Taipei, Taiwan, May 2003, vol. 1, pp. 1171–1178.
- [9] J. Lee and I. Ha, "Sensor fusion and calibration for motion captures using accelerometers," in *Proc. IEEE Int. Conf. Robot. Autom.*, Detroit, MI, May 1999, pp. 1954–1959.
- [10] H. Rehlinger and X. Hu, "Drift-free attitude estimation for accelerated rigid bodies," in *Proc. IEEE Int. Conf. Robot. Autom.*, Seoul, Korea, May 2001, pp. 4244–4249.
- [11] A. M. Sabatini, C. Martelloni, S. Scapellato, and F. Cavallo, "Assessment of walking features from foot inertial sensing," *IEEE Trans. Aerosp. Electron. Syst.*, vol. 52, no. 3, pp. 486–494, Mar. 2005.
- [12] A. M. Sabatini, "Quaternion-based strap-down integration method for applications of inertial sensing to gait analysis," *Med. Biol. Eng. Comput.*, vol. 43, no. 1, pp. 94–101, Jan. 2005.
- [13] P. H. Veltink, P. Slycke, J. Hemssens, T. Buschman, G. Bulstra, and H. Hermens, "Three dimensional inertial sensing of foot movements for automatic tuning of a two-channel implantable drop-foot stimulator," *Med. Eng. Phys.*, vol. 25, no. 1, pp. 21–28, Jan. 2003.
- [14] R. Azuma and G. Bishop, "Improving static and dynamic registration in an optical see-through HMD," in *Proc. 21st Annu. Conf. Comput. Graph. Interactive Techniques*, Orlando, FL, Jul. 1994, pp. 197–204.
- [15] E. Foxlin, M. Harrington, and Y. Alshuler, "Miniature 6DOF inertial for track HMDs," in *Proc. SPIE Helmet, Head-Mounted Displays III.*, Orlando, FL, Apr. 1998, vol. 3362, pp. 214–228.
- [16] E. Foxlin, "Inertial head-tracker fusion by a complementary separate-bias Kalman filter," in *Proc. Virtual Reality Annu. Int. Symp.*, Santa Clara, CA, Mar. 1996, pp. 185–194.
- [17] E. R. Bachmann, "Inertial and magnetic tracking of limb segment orientation for inserting humans into synthetic environments," Ph.D. dissertation, Naval Postgraduate School, Monterey, CA, 2000.
- [18] J. L. Marins, X. Yun, E. R. Bachmann, R. B. McGhee, and M. J. Zyda, "An extended Kalman filter for quaternion-based orientation estimation using MARG sensors," in *Proc. IEEE/RSJ Int. Conf. Intell. Robots Syst.*, Maui, HI, Oct. 2001, pp. 2003–2011.
- [19] X. Yun, M. Lizaraga, E. Bachmann, and R. McGhee, "An improved quaternion-based kalman filter for real-time tracking of rigid body orientation," in *Proc. IEEE/RSJ Int. Conf. Intell. Robots Syst.*, Las Vegas, NV, Oct. 2003, vol. 2, pp. 27–31.

- [20] X. Yun, C. Aparicio, E. R. Bachmann, and R. B. McGhee, "Implementation and experimental results of a quaternion-based Kalman filter for human body motion tracking," in *Proc. IEEE Int. Conf. Robot. Autom.*, Barcelona, Spain, Apr. 2005, pp. 317–322.
- [21] A. Gallagher, Y. Matsuoka, and W.-T. Ang, "An efficient real-time human posture tracking algorithm using low-cost inertial and magnetic sensors," in *Proc. IEEE Int. Conf. Robot. Autom.*, Sendai, Japan, Sep. 28–Oct. 2, 2004, pp. 2967–2972.
- [22] H. J. Luinge, P. H. Veltink, and C. T. Baten, "Estimating orientation with gyroscopes and accelerometers," *Technol. Health Care*, vol. 7, no. 6, pp. 455–459, Jan. 1999.
- [23] H. J. Luinge, "Inertial sensing of human movement," Ph.D. dissertation, Univ. Twente, Enschede, The Netherlands, Dec. 2002.
- [24] H. J. Luinge and P. H. Veltink, "Inclination measurement of human movement using a 3-D accelerometer with autocalibration," *IEEE Trans. Neural Syst. Rehab. Eng.*, vol. 12, no. 1, pp. 112–121, Mar. 2004.
- [25] D. Roetenberg, H. J. Luinge, T. M. Baten, and P. H. Veltink, "Compensation of magnetic disturbances improves inertial and magnetic sensing of human body segment orientation," *IEEE Trans. Neural Syst. Rehab. Eng.*, vol. 13, no. 3, pp. 395–405, Sep. 2005.
- [26] R. Zhu and Z. Zhou, "A real-time articulated human motion tracking using tri-axis inertial/magnetic sensors package," *IEEE Trans. Neural Syst. Rehab. Eng.*, vol. 12, no. 2, pp. 295–302, Jun. 2004.
- [27] E. Kraft, "A quaternion-based unscented Kalman filter for orientation tracking," in *Proc. IEEE 6th Int. Conf. Inf. Fusion*, Cairns, Queensland, Australia, 2003, pp. 47–54.
- [28] M. Haid and J. Breitenbach, "Low cost inertial orientation tracking with Kalman filter," *Appl. Math. Comput.*, vol. 153, pp. 567–575, 2004.
- [29] D. Gebre-Egziabher, G. H. Kikaim, J. Powell, and B. W. Parkinson, "A gyro-free quaternion-based attitude determination system suitable for implementation using low cost sensors," in *Proc. IEEE Position Location, Navig. Symp.*, San Diego, CA, Mar. 2000, pp. 185–192.
- [30] G. Wahba, "Problem 65-1: A least squares estimate of satellite attitude," *SIAM Rev.*, vol. 7, no. 3, p. 409, Jul. 1965.
- [31] T. Chin-Woo, S. Park, K. Mostov, and P. Varaiya, "Design of gyroscope-free navigation systems," in *Proc. IEEE Intell. Transport. Syst.*, Oakland, CA, Aug. 2001, pp. 286–291.
- [32] W. T. Ang, P. K. Khosla, and C. Riviere, "Kalman filtering for real-time orientation tracking of handheld microsurgical instrument," in *Proc. IEEE Int. Conf. Intell. Robots Syst.*, Sendai, Japan, Sep. 2004, pp. 2574–2580.
- [33] —, "Design of all-accelerometer inertial measurement unit for tremor sensing in hand-held microsurgical instrument," in *Proc. IEEE Int. Conf. Robot. Autom.*, Taipei, Taiwan, Sep. 2003, vol. 2, pp. 1781–1786.
- [34] E. Bachmann and X. Yun, "An investigation of the effects of magnetic variations on inertial/magnetic orientation sensors," *IEEE Robot. Autom. Mag.*, to be published.
- [35] J. B. Kuipers, *Quaternions and Rotation Sequences*. Princeton, NJ: Princeton Univ. Press, 1999.
- [36] J. L. Marins, "An extended Kalman filter for quaternion-based attitude estimation," Master's thesis, Naval Postgraduate School, Monterey, CA, Sep. 2000.
- [37] M. D. Shuster and S. D. Oh, "Three-axis attitude determination for vector observations," *J. Guid. Control*, vol. 4, no. 1, pp. 70–77, 1981.
- [38] G. Grenon, P. E. An, S. M. Smith, and A. J. Healey, "Enhancement of the inertial navigation system for the morpheus autonomous underwater vehicles," *IEEE J. Ocean. Eng.*, vol. 26, no. 4, pp. 548–560, Oct. 2001.



Xiaoping Yun (S'86–M'87–SM'96–F'05) received the B.S. degree from Northeastern University, Shenyang, China in 1982, and the M.S. and D.Sc. degrees from Washington University, St. Louis, MO, in 1984 and 1987, respectively.

He is currently a Professor of Electrical and Computer Engineering at the Naval Postgraduate School, Monterey, CA. His research interests include coordinated control of multiple robotic manipulators, mobile manipulators, mobile robots, control of nonholonomic systems, MEMS sensors, carbon nanotubes-

based sensors, and human body motion tracking using inertial/magnetic sensors.

Dr. Yun was an Associate Editor of the IEEE TRANSACTIONS ON ROBOTICS AND AUTOMATION from 1993 to 1996, and a Co-Editor of the Special Issue on "Mobile Robots" of the IEEE Robotics and Automation Society (RAS) Magazine in 1995. He was Co-Chair of the RAS Technical Committee on Mobile Robots in 1992–2003, a member of the RAS Conference Board in 1999–2003, a member of the Program Committee of the IEEE International Conference on Robotics and Automation in 1990, 1991, 1997, 1999, 2000, 2003, and 2004, a member of the Program Committee of the IEEE/RSJ International Conference on Intelligent Robots and Systems in 1998, 2001, 2003, and 2004, General Co-Chair of the 1999 IEEE International Symposium on Computational Intelligence in Robotics and Automation, Finance Chair of the IEEE International Conference on Robotics and Automation in 2002 and 2004, Finance Chair of the IEEE/RSJ International Conference on Intelligent Robots and Systems in 2001, 2004, 2005, and 2006, and Finance Chair of the IEEE International Conference on Nanotechnology in 2001. He is Treasurer of IEEE Robotics and Automation Society for 2004–2009, and was Vice President for Finance of the IEEE Nanotechnology Council in 2004–2006.



Eric R. Bachmann (M'01) received the Bachelors degree from the University of Cincinnati, Cincinnati, OH, and the M.S. and Ph.D. degrees from the Naval Postgraduate School, Monterey, CA.

He holds positions as an Associate Professor at Miami University, Oxford, OH, and as a Research Assistant Professor at the Naval Postgraduate School. Prior to this he served as an officer and an unrestricted naval aviator in the United States Navy. His research interests include inertial/magnetic human motion tracking, virtual environments,

computer graphics, and visualization.

NAVIGATION

JOURNAL OF THE INSTITUTE OF NAVIGATION

SUMMER 2006



VOL. 53, No. 2

LONGITUDE FROM LUNAR ALTITUDES SIMPLIFIED	69
<i>George G. Bennett</i>	
PRECISE ROBUST POSITIONING WITH INERTIALLY AIDED RTK	73
<i>Bruno M. Scherzinger</i>	
EFFECT OF SAMPLING FREQUENCY ON GNSS RECEIVER PERFORMANCE	85
<i>Dennis M. Akos and Marco Pini</i>	
PERFORMANCE AND AVAILABILITY ANALYSIS OF A SIMPLE LOCAL AIRPORT POSITION DOMAIN MONITOR FOR WAAS	97
<i>Curtis A. Shively, Rick Niles, and Thomas T. Hsiao</i>	
A SINGLE PARAMETER TUNABLE QUATERNION BASED ATTITUDE ESTIMATION FILTER	109
<i>Eric R. Bachmann and Xiaoping Yun</i>	
ATTITUDE DETERMINATION METHODS USING PSEUDOLITE SIGNAL PHASE MEASUREMENTS	121
<i>Keun Joo Park and John L. Crassidis</i>	

A Single Parameter Tunable Quaternion Based Attitude Estimation Filter

ERIC R. BACHMANN

Department of Computer Science and Systems Analysis
Miami University, Oxford, Ohio

XIAOPING YUN

Department of Electrical and Computer Engineering
Naval Postgraduate School, Monterey, Ca

Received March 2005; Revised July 2006.

ABSTRACT: *In human posture tracking applications, limb segment attitude can be estimated without the aid of a generated source using small inexpensive inertial/magnetic sensor modules. In the absence of an adequate process model and process noise characteristics or in an application in which the dynamic and measurement relations are non-linear, a simple complementary filter represents a computationally inexpensive solution that produces accurate attitude estimates superior to those of an improperly tuned Kalman filter. This paper presents the theory and experimental results for a single parameter tunable quaternion based attitude estimation filter. The described sub-optimal constant gain complementary filter is the first filter designed for inertial/magnetic sensor modules capable of estimating orientation in all attitudes without singularities while continuously correcting for drift without the need for still periods. Experimental results qualitatively and quantitatively demonstrate the accuracy and stability of the filtering algorithm.*

INTRODUCTION

Accurate real-time tracking of the orientation or attitude of rigid bodies has wide application in navigation, robotics [1], helicopters [2], tele-operation, augmented reality, and virtual reality [3]. Advances in the field of miniature sensors have made possible inertial/magnetic tracking of the three degrees of orientation using sensor modules containing three orthogonal angular rate sensors, three orthogonal linear accelerometers and three orthogonal magnetometers. The orientation estimates are based on the passive measurement of physical quantities that are directly related to the rate of rotation and the orientation of the tracked rigid-body. The estimates are expressed relative to an Earth fixed reference frame.

The purpose of the human body tracking system is to estimate the orientation of multiple human limb segments and use the resulting estimates to set the posture of the human body model that is visually displayed. Figure 1 depicts experiments designed to qualitatively evaluate and demonstrate this capability. In these experiments three inertial/magnetic sensor modules attached to the limb seg-

ments to be tracked. Video recordings of the system in normal operation indicate that posture estimation was accurate and showed very little lag. A quicktime movie of these experiments may be downloaded at <http://www.users.muohio.edu/bachmaer/research.htm>. This video qualitatively demonstrates the dynamic accuracy of the quaternion attitude estimation filter which is the subject of this article.

A naive approach to inertial orientation tracking might simply involve integration of angular rate data to determine orientation. However, this solution is prone to drift over time due to the buildup of small bias and drift errors. In order to avoid drift, inertial tracking systems make use of complementary sensors to continuously correct the orientation estimate. Accelerometers are used for low frequency measurement of the gravity vector relative to the coordinate frame of the sensor module. Since accelerometers actually sense the sum of gravity and linear acceleration due to motion, low pass filtering is generally required to discriminate against the latter. Magnetometers serve a similar function for the local magnetic field vector. Taken together, the use of accelerometers and magnetometers and the use of angular rate sensors, respectively, represent complementary low and high frequency methods of attitude estimation. When combined, these two types can also be used for continuously

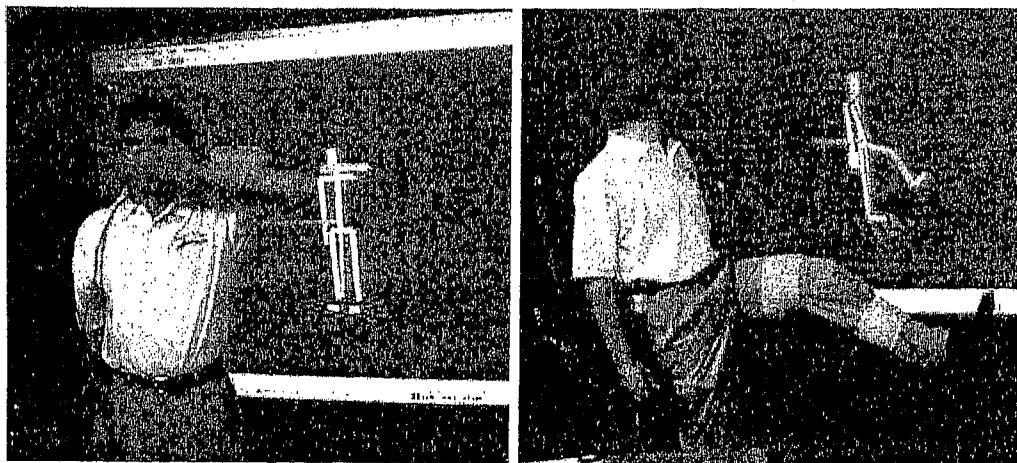


Fig. 1—Inertial/Magnetic Tracking of the Arm and Leg Using Three Sensor Modules [4]

accurate attitude estimation in dynamic applications without latency.

In recent years, this type of problem has most commonly been solved by designing a Kalman filter to integrate the data from the complementary sensor types. In applications such as spacecraft attitude estimation where the dynamics of the tracked body are well defined and an accurate process model is available, the ideal solution to the tracking problem would be an extended Kalman filter [5]. In the work described here, the targeted application is real-time human posture tracking. Dynamic models for the musculoskeletal system have been studied for many years [6]. Such models are ideal for computer simulations of articulated body motions, but remain too computationally demanding for real-time applications such as human motion tracking. Thus, the challenge would be to develop a model that is adequate, but not overwhelmingly complex for motion tracking applications. In the end, however, it may be the case that a properly tuned complementary filter will provide attitude estimates with an accuracy that is comparable to those made by an extended Kalman filter without the associated complexity and development time. Thus, the prototype research described here makes use of a complementary filter based upon a quaternion representation of orientation.

The remainder of this paper will describe a prototype attitude estimation filter designed for an inertial/magnetic human body tracking system. The filter processes sensor data and produces orientation estimates expressed in quaternion form [7] without singularities. Estimation error is minimized using Gauss-Newton iteration. Unlike filters previously designed for the targeted application, drift is corrected continuously without any requirement for still periods. Experimental results qualitatively and quantitatively demonstrate the performance of the

filter showing that the produced attitude estimates are stable and accurate. The work described here laid the foundation for numerous attitude estimation filters designed for inertial/magnetic sensor modules [8, 9].

Background and Related Work

Use of angular rate sensors and accelerometers, or inertial measurement units (IMU) in land and/or underwater robots has been well documented [1][10–12]. A study of human motion tracking using accelerometers alone was reported in [11]. For motion involving small linear accelerations, a set of tri-axial accelerometers was used to determine two degree of freedom (DOF) rotation angles. During motions accompanied by higher accelerations, a technique is described that involves the use of two sets of tri-axial accelerometers on a single rigid-body to differentiate gravitational acceleration from motion related linear acceleration. Reference [14] described an attitude estimation algorithm based on the use of angular rate sensors and accelerometers. In this case, drift in heading estimation was unavoidable due to a lack of additional complementary sensors such as magnetometers.

Reference [15] presents an attitude tracking system with GPS and inertial sensors used for aircraft. Differences between the GPS signals received by three antennas are used to estimate attitude. Reference [16] replaces the antenna information with celestial observation data. Reference [17] describes an attitude package, which combines the outputs of inclinometers, gyros, and compasses to obtain attitude estimation. All three examples utilize Euler angles to represent orientation and a Kalman filtering algorithm to integrate the information.

Reference [18] presented the first inertial/magnetic system for head tracking applications.

This system utilized a fluid pendulum and three solid-state piezoelectric angular rate sensors. The initial system did not include a compass or magnetometers and thus drifted about the vertical axis. Subsequent systems include three orthogonal solid-state rate sensors, a two-axis fluid inclinometer and a two-axis fluxgate compass [19]. InterSense, Inc. was started as a result of this research and continues to produce inertial tracking devices designed for head tracking applications. Sensor data is processed by a complementary separate-bias Kalman filter which required periods of "still time" to correct for rate sensor drift [19].

The fact that inertial data lends itself to prediction through the use of motion derivatives has resulted in the use of inertial sensors in numerous efforts to combat latency problems. Reference [20] demonstrates that predicting future head location using three angular rate sensors and three linear accelerometers is an effective approach for significantly reducing dynamic errors in an augmented reality head tracking system. In this study, prediction caused the head tracking dynamic accuracy to increase by factors of 5 to 10. Linear Kalman filters are used to estimate and predict translation terms and an Extended Kalman Filter (EKF) is used to estimate and predict orientation terms.

Estimating Orientation

This section describes how angular rate, gravitational acceleration, and the local magnetic field sensed in the coordinate frame of a moving rigid body can be used to estimate the orientation of the body relative to an Earth fixed reference frame. For illustrative purposes, the discussion begins with a static situation in which the body is not in motion and later describes how the same techniques are used in a dynamic tracking situation. All rotations are expressed using quaternions. The use of quaternions reduces the number of required scalar operations, and eliminates calculations involving trigonometric functions. In addition, using quaternions allows the avoidance of singularities associated with Euler angle descriptions of orientation.

Estimation Using Accelerometers and Magnetometers

Accelerometers measure the combination of forced linear acceleration and the reaction force due to gravity. Thus, the output of an accelerometer triad is given by

$$a_{\text{measured}} = a - g \quad (1)$$

For bodies that are not in motion, forced linear acceleration is zero ($a = 0$). In this case accelerometers sense only gravity. Gravity in Earth coordinates

is always down and can be expressed as the down unit vector in quaternion form as

$${}^E m = [0 \ 0 \ 0 \ -1] \quad (2)$$

where the superscript, E, indicates the vector is described relative to an Earth fixed reference frame. Three orthogonally mounted accelerometers sense the same vector relative to their own coordinate frame. This vector quantity can also be expressed as a pure vector quaternion

$${}^S h = [0 \ h_1 \ h_2 \ h_3] \quad (3)$$

where the superscript, S, indicates that the vector is described relative to the moving coordinate frame of the sensor module. Both m and h describe the same vector. If it is assumed that there is no measurement error in the accelerometers, all differences can be attributed to rotation of the frame of reference of the module. This rotation can be expressed using quaternion multiplication involving a quaternion, q , as:

$${}^S h = q^{-1} \otimes {}^E m \otimes q \quad (4)$$

Solving for q based on the known m and the measured h produces an expression for the orientation of the sensor relative to the Earth fixed reference frame. Unfortunately, the quaternion, q , will remain constant if the body is rotated about a vertical axis aligned with the gravity vector. To eliminate this ambiguity, another vector that is assumed to remain constant over a given working volume is used as a reference.

Like gravity, the direction of the local magnetic field is a known quantity. It can be expressed relative to the Earth fixed reference frame as the pure vector quaternion

$${}^E n = [0 \ n_1 \ n_2 \ n_3] \quad (5)$$

Three orthogonally mounted magnetometers can sense the same local magnetic field relative to their own coordinate frame. The pure vector quaternion, b , is used to express this sensor based quantity.

$${}^S b = [0 \ b_1 \ b_2 \ b_3] \quad (6)$$

if it is assumed that the axes of the accelerometer triad are aligned with those of the three axis magnetometer. Both the gravity and magnetic field vectors are measured relative to the same sensor coordinate frame. If the magnetometers perfectly measure the three components of the local magnetic field vector, the quaternion, q , from Eq. (4) that relates the rotated frame of the accelerometers to the Earth fixed reference frame also relates the rotated frame of the magnetometers to the Earth fixed reference frame. That is,

$${}^S b = q^{-1} \otimes {}^E n \otimes q \quad (7)$$

Applying the rationale of Eq. (4), Eq. (7) will remain constant if the tracked body is rotated about an axis aligned with the local magnetic field vector. However, under the assumption that the magnetic and gravity vectors are not parallel, both equations can be used together to determine orientation. Any axis-aligned rotations that allow one equation to remain constant will result in a change in the measured quantities involved in the other. As shown later in this paper, this circumstance can be used to obtain a unique estimated orientation quaternion, \hat{q} . Solving for \hat{q} based on measurements of the gravity and magnetic field reference vectors is essentially a quaternion version of the *Wahba problem* [21, 22].

In order to track the orientation of moving bodies using the above methods, the following assumption is made. For all moving bodies, linear acceleration will average to zero given a period of sufficient length. Otherwise, the bodies would soon reach excessive velocities. Therefore, when averaged over time, an accelerometer triad returns only the components of the gravity vector or the local vertical. This averaging allows accelerometers combined with magnetometers to be used as a low frequency source of orientation estimates. The length of the period over which acceleration must be averaged is dependent upon the type and frequency of motion being tracked. These estimates would not be useful in applications involving feedback control since they would tend to lag behind the true orientation of an object undergoing rapid changes in orientation. However, in experiments they have been found to still be useful by themselves in applications where some lag is acceptable and it is desirable to keep the cost of individual sensor modules to a minimum.

Estimation Using Angular Rate Sensors

Three orthogonally mounted angular rate sensors can be used to determine the rotational velocity of a body in three dimensions. In the same way a car speedometer can be used to determine travel distance given a known starting point, angular rate sensors can be used to determine attitude. The three-axis angular rate sensor outputs measure the rotational rates about the body x, y, and z axes. The measurements can be used to construct a rate vector that can be expressed as the pure quaternion

$$s_\omega = [0 \quad p \quad q \quad r] \quad (8)$$

where p, q, and r, respectively, represent the rates of rotation about the body x, y, and z axes. The pure quaternion, s_ω , is used to obtain a rate quaternion [23],

$$\dot{q} = \frac{1}{2} q \otimes s_\omega \quad (9)$$

where q is a quaternion representing the current orientation, the indicated product is a quaternion product, and \hat{q} is expressed relative to the Earth fixed reference frame.

If the sensor data is noiseless and unbiased, the rate quaternion derived in Eq. (9) can be integrated for an unlimited amount of time to determine the orientation of the rigid-body to which the sensors are attached. In reality, low-cost miniature rate sensors can be assumed to operate under some bias and noise effects. In the same way distance estimates made using a poorly calibrated speedometer would steadily become more and more inaccurate, so too will orientation estimates based on the use of miniature angular rate sensors. Thus, the angular rate sensors can only be considered a high frequency source of orientation estimates that must be periodically or continuously corrected using a low frequency source.

Quaternion Based Complementary Attitude Filter

The two previous sections establish the complementary nature of orientation estimates derived using accelerometers and magnetometers and those derived using angular rate sensors. An efficient quaternion based complementary attitude filter has been devised that combines the data from all three types of sensors to produce an estimate that is continuously accurate through all orientations. Figure 2 is a block diagram of a simple complementary quaternion-based attitude estimation filter. The filter inputs are a three-axis angular rate sensor, a three-axis accelerometer, and a three-axis magnetometer. Its output is a quaternion representation of the orientation of the sensor module relative to an Earth fixed reference frame.

Parameter Optimization

Combining the complementary sensor inputs is regarded as a parameter optimization problem. The

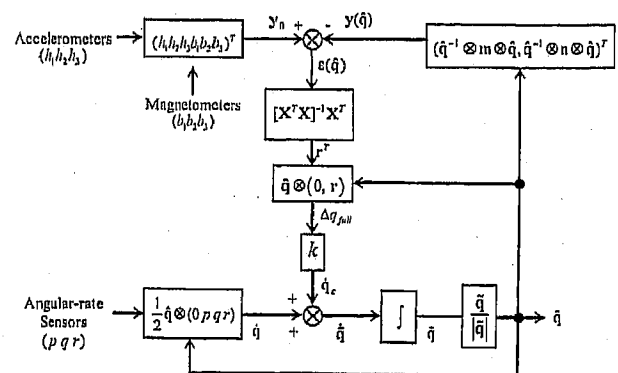


Fig. 2-Quaternion Based Attitude Estimation Filter [4]

goal of this optimization problem is to minimize a modeling error that is based on the difference between what the accelerometers and magnetometers measure and what they are expected to measure given the last estimated orientation. The rate sensors serve to quicken the overall response of the system.

The three orthogonally mounted accelerometers return an approximation to the local vertical relative to the sensor coordinate frame, the unit vector \mathbf{h} . The magnetometer returns the direction of the local magnetic field relative to the sensor coordinate frame, the unit vector \mathbf{b} . We combine the vector parts of the quaternions defined by Eq. (3) and Eq. (6) to produce a 6×1 measurement vector

$$\mathbf{y}_0 = [h_1 \ h_2 \ h_3 \ b_1 \ b_2 \ b_3]^T \quad (10)$$

In order to compare the expected measurement with what is contained in the measurement vector, all vectors must be expressed relative to the same coordinate frame. The vectors defined by Eq. (2) and Eq. (5) are mapped from the Earth fixed frame to the sensor frame through quaternion multiplications as follows [1]

$${}^s\mathbf{h} = \mathbf{q}^{-1} \otimes \mathbf{E}\mathbf{h} \otimes \mathbf{q}, \quad {}^s\mathbf{b} = \mathbf{q}^{-1} \otimes \mathbf{E}\mathbf{b} \otimes \mathbf{q} \quad (11)$$

Combining the vector parts of Eq. (11) into a single 6×1 computed measurement vector produces

$$\mathbf{y}(\mathbf{q}) = [y_1 \ y_2 \ y_3 \ y_4 \ y_5 \ y_6]^T \quad (12)$$

where y_1, y_2 , and y_3 , are the elements of the vector part of ${}^s\mathbf{h}$ and y_4, y_5 , and y_6 , are the elements of the vector part of ${}^s\mathbf{b}$. The difference between the actual measurements and the computed measurements is the 6×1 modeling error vector

$$\boldsymbol{\varepsilon}(\mathbf{q}) = \mathbf{y}_0 - \mathbf{y}(\mathbf{q}) \quad (13)$$

In viewing Eq. (13), note that if there is no measurement noise (perfect sensors), the difference between the measured and computed values will equal the zero vector. However, when real sensors are used, this can no longer be expected. Instead, a value for the estimated orientation quaternion, $\hat{\mathbf{q}}$, can be obtained by minimizing the squared error criterion function:

$$\varphi(\mathbf{q}) = \boldsymbol{\varepsilon}^T(\mathbf{q})\boldsymbol{\varepsilon}(\mathbf{q}) \quad (14)$$

In the current version of the filter, the criterion function is minimized using Gauss-Newton iteration [24]. This method is based on linearized least squares regression analysis where \mathbf{y}_0 is considered a vector of data points and $\mathbf{y}(\mathbf{q})$ is a vector to be fitted to those points. The full correction step is [24]

$$\Delta\mathbf{q}_{\text{full}} = [\mathbf{X}^T\mathbf{X}]^{-1}\mathbf{X}^T\boldsymbol{\varepsilon}(\hat{\mathbf{q}}) \quad (15)$$

where $\hat{\mathbf{q}}$ is the previous estimate for \mathbf{q} and the individual elements of the measurement linearization matrix, \mathbf{X} , are defined as [25]

$$\mathbf{X}_{ij} = \left[\frac{\partial y_i}{\partial q_j} \right] \quad (16)$$

Since we are dealing with data corrupted by noise, the correction step is scaled by a value α producing

$$\Delta\mathbf{q}_{\text{partial}} = \alpha[\mathbf{X}^T\mathbf{X}]^{-1}\mathbf{X}^T\boldsymbol{\varepsilon}(\hat{\mathbf{q}}) \quad (17)$$

where

$$\alpha = k\Delta t \quad (18)$$

and k represents the filter gain value. Thus, for discrete time step integration, each successive estimate of orientation would be calculated as

$$\begin{aligned} \hat{\mathbf{q}}_{n+1} &= \hat{\mathbf{q}}_n + \frac{1}{2}\hat{\mathbf{q}}_n^s\omega\Delta t + \alpha[\mathbf{X}^T\mathbf{X}]^{-1}\mathbf{X}^T\boldsymbol{\varepsilon}(\hat{\mathbf{q}}_n) \\ &= \hat{\mathbf{q}}_n + \dot{\mathbf{q}}\Delta t + k\Delta\mathbf{q}_{\text{full}} \end{aligned} \quad (19)$$

If $\hat{\mathbf{q}}$ is constrained to unit length as depicted in Figure 2, a unique solution to the optimization problem will exist and the regression matrix

$$\mathbf{S} = \mathbf{X}^T\mathbf{X} \quad (20)$$

can be inverted [25]. A more efficient computation of $\Delta\hat{\mathbf{q}}$ results from noting that if

$$\hat{\mathbf{q}}_{\text{new}} = \hat{\mathbf{q}}_{\text{old}} + \Delta\mathbf{q}_{\text{full}} \quad (21)$$

and if both $\hat{\mathbf{q}}_{\text{old}}$ and $\hat{\mathbf{q}}_{\text{new}}$ are unit quaternions, then any small $\Delta\hat{\mathbf{q}}_{\text{full}}$ must be orthogonal to $\hat{\mathbf{q}}$. If \mathbf{p} and \mathbf{q} are any two quaternions, then \mathbf{p} is orthogonal to \mathbf{q} if and only if \mathbf{p} is the quaternion product of \mathbf{q} and a unique vector \mathbf{v} (real part equal to zero) where \mathbf{v} is given by

$$\mathbf{v} = \mathbf{q}^{-1} \otimes \mathbf{p} \quad (22)$$

Accordingly, $\Delta\mathbf{q}$ can be written in the form

$$\Delta\mathbf{q} = \mathbf{q} \otimes \mathbf{v} = \mathbf{q} \otimes [0 \ v_1 \ v_2 \ v_3] \quad (23)$$

With this constraint, linearization of the computed measurement vector, $\mathbf{y}(\mathbf{q})$, in Figure 2, yields

$$\begin{aligned} \mathbf{y}(\mathbf{q} + \Delta\mathbf{q}) &= \mathbf{y}(\mathbf{q}) + \mathbf{X}\Delta\mathbf{q} \\ &= \mathbf{y}(\mathbf{q}) + \mathbf{X}(\mathbf{q} \otimes [0 \ v_1 \ v_2 \ v_3]) \end{aligned} \quad (24)$$

and consequently:

$$\frac{\partial \mathbf{y}}{\partial v_1} = \mathbf{X}(\mathbf{q} \otimes [0 \ 1 \ 0 \ 0]) = \mathbf{X}(\mathbf{q} \otimes \mathbf{i})^T \quad (25)$$

$$\frac{\partial \mathbf{y}}{\partial v_2} = \mathbf{X}(\mathbf{q} \otimes [0 \ 0 \ 1 \ 0]) = \mathbf{X}(\mathbf{q} \otimes \mathbf{j})^T \quad (26)$$

$$\frac{\partial \mathbf{y}}{\partial v_3} = \mathbf{X}(\mathbf{q} \otimes [0 \ 0 \ 0 \ 1]) = \mathbf{X}(\mathbf{q} \otimes \mathbf{k})^T \quad (27)$$

where \mathbf{i} , \mathbf{j} , and \mathbf{k} are quaternion forms of unit vectors pointing in the directions of the positive x , y , and z axes, respectively. Thus, when Gauss-Newton iteration is applied to unit quaternions, it is sufficient to solve for only three unknowns rather than

four as in the methods for estimation of $\Delta \mathbf{q}_{full}$ in Eq. (15). That is, if \mathbf{X} is the 6×3 matrix

$$\mathbf{X}_v = \begin{bmatrix} \frac{\partial y}{\partial v_1} & \frac{\partial y}{\partial v_2} & \frac{\partial y}{\partial v_3} \end{bmatrix} \quad (28)$$

then,

$$\Delta \mathbf{v}_{full} = [\mathbf{X}_v^T \mathbf{X}_v]^{-1} \mathbf{X}_v^T \mathbf{e}(\hat{\mathbf{q}}) \quad (29)$$

and

$$\Delta \mathbf{q}_{full} = \hat{\mathbf{q}} \otimes [0, \Delta \mathbf{v}_{full}] \quad (30)$$

Incorporation of the above into the Gauss-Newton algorithm notably simplifies the computation of the $\Delta \mathbf{q}$ quaternion since it requires only a 3×3 matrix inversion rather than the 4×4 matrix inversion of the basic algorithm. This is important since best algorithms for matrix inversion are of $O(n^3)$ complexity [26].

The above dimension reduction also leads to an efficient approach to the 3×3 problem formulation. Specifically, let \mathbf{q}_r be the *incremental rotation quaternion* given by:

$$\mathbf{q}_r = [1 \quad r_1 \quad r_2 \quad r_3] = [0, \mathbf{r}] \quad (31)$$

Evidently, as the *rotation vector*, \mathbf{r} , approaches the zero vector, then \mathbf{q}_r approaches a unit quaternion. Thus, if a value is found for \mathbf{q}_r that reduces the squared error criterion function, $\phi(\mathbf{q})$, it follows that

$$\hat{\mathbf{q}}_{new} = \mathbf{q}_{old} \otimes \mathbf{q}_r \quad (32)$$

and that, in the limit, as \mathbf{r} approaches zero, $\hat{\mathbf{q}}_{new}$ will also be a unit quaternion. More practically, the results of Eq. (32) should be normalized to a unit quaternion after every iterative application of this equation [24], thereby removing any limitations on the magnitude of \mathbf{r} .

Eq. (21) can be rewritten in additive form by noting that

$$\Delta \hat{\mathbf{q}} = \hat{\mathbf{q}}_{new} - \hat{\mathbf{q}}_{old} = \hat{\mathbf{q}}_{old} \otimes [1 \quad r_1 \quad r_2 \quad r_3] - \hat{\mathbf{q}}_{old} \otimes [1 \quad 0 \quad 0 \quad 0] \quad (33)$$

$$= \hat{\mathbf{q}}_{old} \otimes [1 \quad r_1 \quad r_2 \quad r_3] = \hat{\mathbf{q}}_{old} \otimes [0, \mathbf{r}] \quad (34)$$

where

$$\mathbf{r}^T = [\mathbf{X}_v^T \mathbf{X}_v]^{-1} \mathbf{X}_v^T \mathbf{e}(\hat{\mathbf{q}}_{old}) \quad (35)$$

and, the measurement linearization matrix, \mathbf{X} , is the 6×3 *reduced order* matrix:

$$\mathbf{X} = 2 \begin{bmatrix} 0 & -y_3 & y_2 \\ y_3 & 0 & -y_1 \\ -y_2 & y_1 & 0 \\ 0 & -y_6 & y_5 \\ y_6 & 0 & -y_4 \\ -y_5 & y_4 & 0 \end{bmatrix} \quad (36)$$

To understand the importance of these results, it must be recognized that the elements of the linearization matrix are directly related to the components of the computed measurement vector, $\mathbf{y}(\mathbf{q})$, given by Eq. (12). Since this vector is needed in every cycle of Gauss-Newton iteration to compute the modeling error vector, $\mathbf{e}(\hat{\mathbf{q}}_{old})$, given by Eq. (13), it follows that the above value for \mathbf{X}_v is "free" since all terms are known once $\mathbf{e}(\hat{\mathbf{q}}_{old})$ has been computed. Eq. (36) provides an order of magnitude reduction in the amount of computation needed to obtain \mathbf{X}_v [24, 25]. This has significant importance when applying Gauss-Newton iteration in practical real-time orientation tracking systems.

Linearization 1.1.1

Figure 3 is a block diagram of the linearized quaternion attitude estimation filter. The inputs n_1 and n_2 are maneuver induced noise and rate sensor noise, respectively. The basis for linearization is the assumption that in the absence of measurement noise the computation of $\Delta \mathbf{q}_{full}$ is exact and therefore

$$\Delta \mathbf{q}_{full} = \mathbf{q}_{true} - \hat{\mathbf{q}} \quad (38)$$

This assumption would be exact only if \mathbf{y} depended linearly on \mathbf{q} , which it does not.

Application of Mason's formula to Figure 3 produces:

$$\frac{\hat{\mathbf{q}}}{\mathbf{q}_{true}} = \frac{\frac{k}{s^2} + \frac{1}{s}}{1 + \frac{k}{s}} = \frac{1}{s} \quad (39)$$

Thus, with correct initial conditions, in the absence of noise,

$$\hat{\mathbf{q}} = \frac{1}{s} \dot{\mathbf{q}}_{true} \quad (40)$$

regardless of the value of k . This means that, under the linearization assumptions, Figure 3 is a complementary filter [3] since, for all k , if n_1 and n_2 are zero, then $\hat{\mathbf{q}} = \mathbf{q}_{true}$.

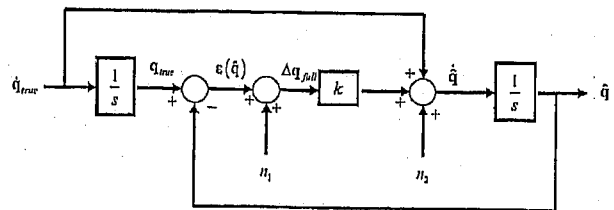


Fig. 3-Block Diagram of Linearized System

Noise Response

Applying Mason's formula to noise disturbances n_1 and n_2 in Figure 3, produces the following low pass filter transfer functions.

$$\frac{\hat{q}}{n_1} = \frac{k \frac{1}{s}}{1 + k \frac{1}{s}} = \frac{k}{s + k} \quad (41)$$

$$\frac{\hat{q}}{n_2} = \frac{\frac{1}{s}}{1 + k \frac{1}{s}} = \frac{1}{s + k} \quad (42)$$

Eq. (41) and Eq. (42) can be used to find an optimal k value in Eq. (18) based upon power spectral density functions for both the noise signals and actual maneuvering behavior of the tracked object. Unfortunately, this information will rarely be available, so ad hoc "tuning" of k is more likely to succeed in practical circumstances [27].

Response to Initial Condition Errors

Eq. (40) assumes that \hat{q} has been correctly initialized. In order to understand how an erroneous initialization approaches q_{true} over time, consider the following static sensor scenario. Suppose the sensor module is mounted in a static reference position and

$$q_{true} = [1 \ 0 \ 0 \ 0] \quad (43)$$

Assume that the unit quaternion, \hat{q} , is incorrect and is represented by

$$q_{true} = [1 \ \delta_x \ \delta_y \ \delta_z] \quad (44)$$

where all δ are small quantities. In the absence of motion and noise, $\dot{q} = 0$ and both n_1 and n_2 equal zero. Based on Figure 3, the initial value for epsilon of $s(\hat{q}_0)$ is

$$s(\hat{q}_0) = \hat{q}_{true} - \hat{q}_0 = [0 \ -\delta_x \ -\delta_y \ -\delta_z] \quad (45)$$

Since the first component of \hat{q}_1 in Eq. (45) will always be zero, it can be assumed that the first component of Eq. (43) will remain unchanged and \hat{q} will take on the form

$$\hat{q} = (1 \ \hat{x} \ \hat{y} \ \hat{z}) \quad (46)$$

The transfer function to the scalar \hat{x} from δ_x is given by:

$$\frac{\hat{X}(s)}{\delta_x} = \frac{s^{-1}}{1 + ks^{-1}} = \frac{1}{s + k} \quad (47)$$

Employing the inverse Laplace transform produces the result

$$\hat{x}(t) = \delta_x e^{-kt} \quad (48)$$

Equivalent results apply for $\hat{y}(t)$ and $\hat{z}(t)$. This implies that any transient errors in \hat{q} resulting from erroneous initialization will persist for a time inversely proportional to k . Specifically

$$\tau_{\Delta q} = \frac{1}{k} \quad (49)$$

and for any disturbance, δ_x , the resulting errors in the x component of s will be

$$s_x(t) = \delta_x e^{-t/\tau_{\Delta q}} \quad (50)$$

Thus, it can be predicted that any error will be reduced to 37 percent of the initial value by the time $t = \tau_{\Delta q}$. Similar results apply to δ_y and δ_z .

Since the nonlinear simulation results shown by the lower line in Figure 4 have the characteristics of a typical first order linear system, the value of linearization is established. This theory provides a framework under which to choose filter gains. Broadband noise simulation shows noise reduces accuracy, but the filter still works well [4].

Bias Effects

Integration of a biased angular rate signal will cause a steady state error in a complementary filter. To reduce this effect, following the approach described in [28], an initial estimate for bias can be calculated by averaging rate sensor output prior to maneuvering and then tracking the time-varying bias with a very long time constant, low pass filter.

From Figure 5,

$$\frac{\dot{q}_{measured}}{\dot{q}_{true}} = \frac{1}{1 + k_{bias} \frac{1}{s}} = \frac{s}{s + k_{bias}} \quad (51)$$

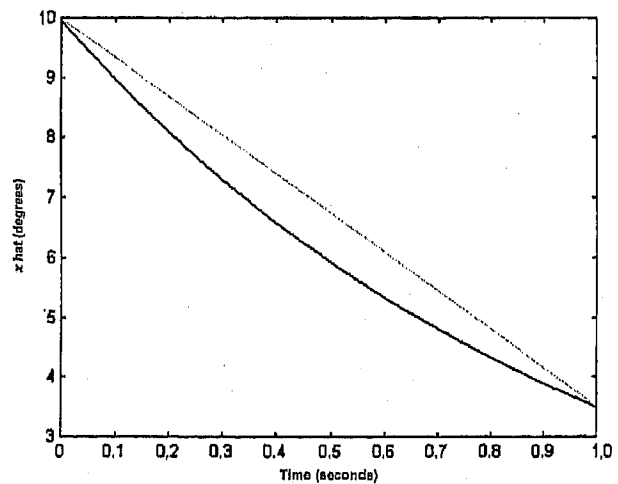


Fig. 4—Simulated Nonlinear Filter Response, 10 Degree Offset, $\alpha = 0.1$, $\Delta t = 0.1$

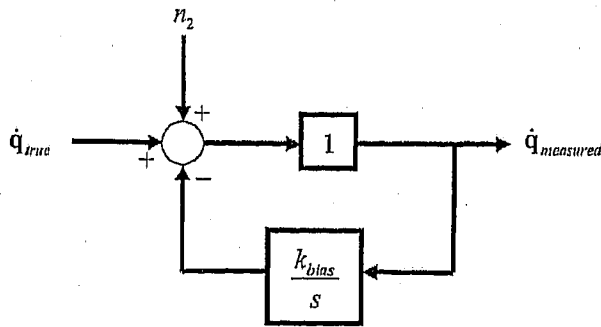


Fig. 5-Block Diagram of Bias Estimation Filter

which is the equation for a highpass filter with a 3 db cutoff at

$$\omega_c = k_{bias} \quad (52)$$

Based on the high-pass nature of Eq. (51), it can be seen that the addition of bias estimation to the quaternion filter means it will no longer be complementary [3]. This is evident since constant rotation rates will over time be eliminated from \dot{q}_{true} . Thus, k must be greater than zero in Eq. (18) in order to detect these rates. In [28] it is shown that this effect can be minimized by applying the constraint

$$k \gg k_{bias} \quad (53)$$

Note, however, that if k is too large, the filter may become unstable or too much maneuver induced error will appear in \hat{q} . Thus, for a given k_{bias} , it can be expected there will be an optimal k value.

From Eq. (49), it can be seen that k should not be too small if the filter is to converge in a reasonable time period. On the other hand, $\tau_{\Delta q}$ must be larger than the maneuver time constant, $\tau_{maneuver}$, in order to adequately suppress maneuver noise. Combining this result with Eq. (53) leads to the qualitative requirement

$$\tau_{maneuver} \ll \tau_{\Delta q} \ll \tau_{bias} \quad (54)$$

or

$$1/\tau_{maneuver} \gg k \gg 1/\tau_{bias} \quad (55)$$

This result in addition to Eq. (38) provides guidelines for the selection of "reasonable" values for k and Δt . With power spectral density functions for \dot{q}_{true} , n_1 , and n_2 , a Kalman filtering approach [3] could be used for this problem. In the absence of such statistical information, gain values may be selected through experimental "tweaking" of the scalar gain, k , in laboratory studies.

A Simple Prototype System and Experimental Results

The quaternion filter was tested in a prototype inertial/magnetic posture tracking system. The system was designed with several goals in mind. Among these was validation of the quaternion filter algorithm in a physical system and a demonstration of the practicality and robustness of real-time inertial and magnetic posture tracking.

Figure 6 is a diagram of the prototype system hardware. Depicted are three body-mounted inertial/magnetic sensor modules outputting analog signals to three I/O connection boards. The output from each connection board was digitized by an associated A/D converter card. The cards themselves are mounted in a standard Wintel desktop computer. All data processing and rendering calculations are performed by software running on this single processor machine. In order to ensure sufficient dynamic response to capture fast human body motion, the system update rate was maintained at 100 Hz.

The prototype tracking system was capable of simultaneously estimating the attitude of three

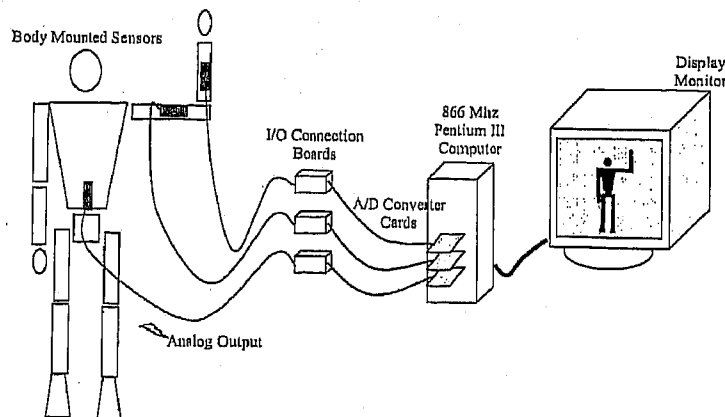


Fig. 6-Prototype Inertial/Magnetic Body Tracking System

rigid-bodies. To track the posture of the entire human body, approximately fifteen sensor modules would be required. One sensor would be attached to each limb segment to be tracked. The exact number of sensors needed would depend upon the desired motion tracking detail to be captured.

The body tracking experiments discussed in the following text were conducted using a MARG-0-2 sensor fabricated by McKinney Technology [33]. The primary sensing components are a Crossbow CXL04M3 triaxial accelerometer [30], a Honeywell HMC2003 3-axis magnetometer [31] and three Tokin CG-16D series miniature angular rate sensors mounted in an orthogonal configuration [32]. The MARG-0-2 incorporates a capacitive coupling rate bias compensation circuit. [34] describes the use of a digital filter designed to replace the capacitive coupling circuit. Sensor module calibration for null values and scale factors was accomplished without the use of any specialized equipment using a simple algorithm. Possible non-orthogonalities within each sensor triad and misalignments between the triads were ignored [36].

Quantitative and qualitative experiments to obtain data related to the accuracy and robustness of the system under various dynamic and static conditions have been performed. The static experiments are related to the stability, convergence properties, and accuracy of the orientation estimates produced by the quaternion attitude filter algorithm when processing sensor data. The qualitative experiments examine the performance of the system as a whole in relationship to the goal of robust posture estimation. The performance of the system while using differential weighting of sensor data, increased drift correction intervals, and the effects of magnetic field variations have also been investigated [4, 37].

Static Stability

The drift characteristics of the quaternion filter algorithm over extended periods have been evaluated using static tests. Figure 7 graphically depicts the drift of each of the four components of the quaternion estimate produced by the filter when processing sensor data as well as the *rms* drift from the initial orientation quaternion estimate. The maximum possible difference between two quaternions of unit length is 2.0 or 180 deg. It can thus be observed through examination of Figure 7 that average total drift is about 0.25 percent. During the experiment shown, the filter gain, k (Eq. (18)), was set to 4.0. Reducing the gain to 1.0 increases the error to 1.0 percent. Further experiments [4] indicated that nearly all drift was due to slowly varying bias errors in the rate sensors.

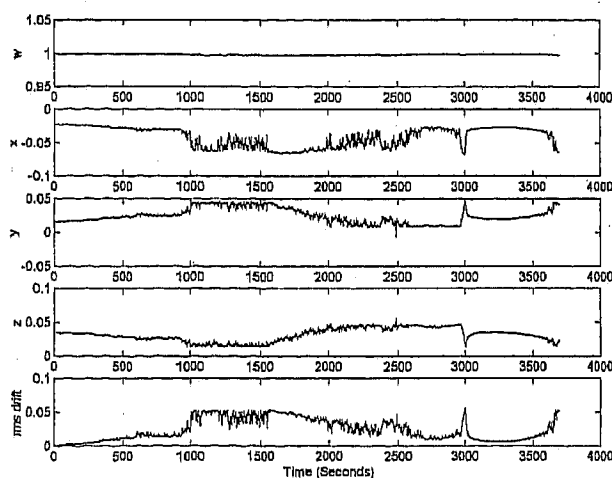


Fig. 7—Quaternion Real And Vector Parts and RMS Drift During One Hour Static Test of Orientation Estimate Stability While Processing MARG-0-2 Sensor Module Data, $k = 4.0$

Dynamic Response and Accuracy

Experiments to establish the accuracy of the orientation estimates and the dynamic response of the system were conducted. These experiments were completed by mounting a MARG sensor on a Hass rotary tilt table. The test procedure consisted of repeatedly cycling a sensor through various angles of roll, pitch, and yaw at rates ranging from 10 to 60 deg/s.

Figure 8 is a typical result of the dynamic accuracy experiments. The estimates produced by the tracking system are presented in Euler angle form. Accuracy is measured to be better than one degree. The overall smoothness of the plot shows excellent dynamic response. The small impulses observed each time motion is initiated are due to linear acceleration effects exaggerated by the "whipping" motion of the non-magnetic extension on which the sensor module was mounted during the experiments.

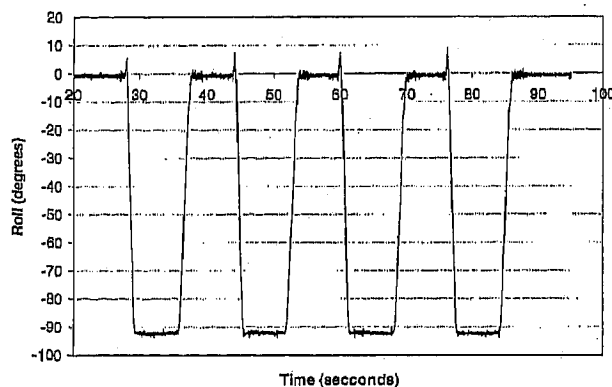


Fig. 8—Quaternion Filter Attitude Estimates During Negative 90 deg Roll Excursions at 60 Deg/s, $k = 1.0$

The maximum value for k can be quantitatively established through a geometric series [4]. The maximum value for which the filter can be expected to be stable is

$$k_{\max} = \frac{2}{\Delta t} \quad (37)$$

When working with perfect noiseless data, values for k greater than $1/\Delta t$ can be expected to cause correction "overshoots" and oscillations in the attitude estimate. The effects of varying the filter gain value, k , are depicted in Figure 9. The same exaggeration due to the whipping motion of the non-magnetic extension can be seen. The top sub-plot in which the filter gain was set to 2.0 shows a smooth plot which

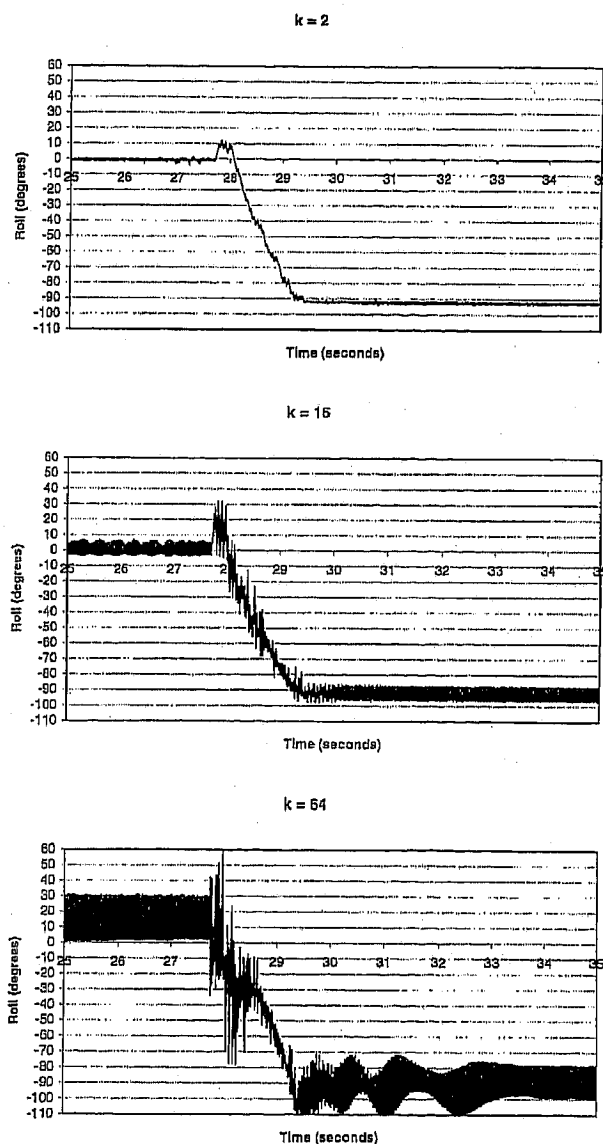


Fig. 9—Exploded Quaternion Filter Attitude Estimates During Negative 90 deg Roll Excursions at 60 Deg/s, with $k = 2.0$, $k = 16.0$, and $k = 64.0$

closely follows the actual motion of the sensor module. The middle sub-plot shows that the filter is less able to discriminate against sensor noise with a gain of 16.0. It is, however, still able to track the actual motion of the module. In the bottom sub-plot with a gain of 64.0, the filter estimate overshoots the rotation significantly following the end of motion. The overshoot is followed by oscillations for a period of several seconds.

In the absence of statistical information, gain values are selected through experimental "tweaking" of the scalar gain, k , in laboratory studies. During posture tracking the filter gain is normally set through qualitative observation of the system performance. For normal human motion, a filter gain of $k = 4.0$ was found to produce stable and accurate performance with no observable under-shoots or overshoots.

Summary and Conclusions

This research has demonstrated an alternative technology for tracking the posture of an articulated rigid body. The technology is based on the use of inertial/magnetic sensors to independently determine the orientation of each link in the rigid body. At the core of the system is an efficient complementary filter that uses a quaternion representation of orientation. The filter can continuously track the orientation of human body limb segments through all attitudes without singularities. Drift corrections are made continuously with no requirement for still periods. Experimental results indicate that the filter is both accurate and efficient.

Current technology has permitted the construction of sensors that are much smaller than the prototype modules described here [36]. An optimal inertial sensor would have the same size and form factor as a wristwatch. It would include an embedded microprocessor on which the filter algorithm is implemented as well as an analog to digital converter. The sensor would have a self-contained power source and would wirelessly transmit orientation data. Efforts are currently being made to untether the user of the sensor system by feeding sensor data to a wearable computer. Filter research has continued with the development of an extended Kalman Filter for real-time estimation of rigid body orientation [34, 39]. Quantitative comparisons of the dynamic and static performance of the algorithms are currently underway.

Acknowledgements

The authors wish to acknowledge the support of the U. S. Army Research Office (ARO) and the U. S. Navy Modeling and Simulation Management Office

(N6M) for making this work possible. The authors also wish to thank Robert B. McGhee for his instrumental contributions to this work.

REFERENCES

1. Dissanayake, G., Sukkariéh, S., Nebot, E., and Durrant-Whyte, H., *The Aiding of a Low-Cost Strapdown Inertial Measurement Unit Using Vehicle Model Constraints for Land Vehicle Applications*, IEEE Transactions on Robotics and Automation, Vol. 17, No. 5, October 2001, pp. 731–747.
2. Sarapalli, S., Roberts, J., Corke, P., Buskey, G., and Sukhatme, G., *A Tale of Two Helicopters*, Proceedings of the 2003 IEEE/RSJ International Conference On Intelligent Robots and Systems, Las Vegas, NV, October 2003, pp. 805–810.
3. Bachmann, E., McGhee, R., Yun, X., and Zyda, M., *Inertial and Magnetic Posture Tracking for Inserting Humans into Networked Virtual Environments*, ACM Symposium on Virtual Reality Software and Technology (VRST 2001), Banff, Canada, November 15–17, 2001, pp. 9–16.
4. Bachmann, E., *Inertial and Magnetic Angle Tracking of Limb Segments for Inserting Humans into Synthetic Environments*, Ph.D. dissertation, Naval Postgraduate School, Monterey, CA, 2000.
5. Lefferts, E., Markley, F., and Shuster, M., *Kalman Filtering for Spacecraft Attitude Estimation*, Journal of Guidance, Control, and Dynamics, Vol. 5, No. 5, September–October 1982, pp. 417–429.
6. Featherstone, R., and Orin, D., *Robot Dynamics: Equations and Algorithms*, Proceedings of the 2000 IEEE International Conference on Robotics and Automation, San Francisco, CA, 2000.
7. Shuster, M., *A Survey of Attitude Representations*, Journal of Astronautical Sciences, Vol. 41, No. 4, October–December 1993, pp. 439–517.
8. Luinge, H., *Inertial Sensing of Human Movement*, Twente University Press, P.O. Box 217, 7500 AE Enschede, the Netherlands, 2002.
9. MicroStrain 3DM-GX1, MicroStrain Inc., <http://www.microstrain.com/3dm-gx1.aspx>
10. Barshan, B., and Durrant-Whyte, H., *Inertial Navigation Systems for Mobile Robots*, IEEE Transactions on Robotics and Automation, Vol. 11, No. 3, June 1995, pp. 328–342.
11. Lee, J., and Ha, I., *Sensor Fusion and Calibration for Motion Captures Using Accelerometers*, Proceedings of the 1999 IEEE International Conference on Robotics and Automation, Detroit, MI, May 1999, pp. 1954–1959.
12. Sykkariéh, S., Nebot, E., and Durrant-Whyte, H., *A High Integrity IMU/GPS Navigation Loop for Autonomous Land Vehicle Applications*, IEEE Transactions on Robotics and Automation, Vol. 15, June 1999, pp. 572–578.
13. Yun, X., Bachmann, E., Arslan, S., Akyol, K., and McGhee, R., *An Inertial Navigation System for Small Autonomous Underwater Vehicles*, Advanced Robotics, Vol. 15, No. 5, 2001, pp. 521–532.
14. Hehbinder, H., and Hu, X., *Drift-Free Attitude Estimation for Accelerated Rigid Bodies*, Proceedings of the 2001 IEEE International Conference on Robotics and Automation, Seoul, Korea, May 2001, pp. 4244–4249.
15. Hayward, R., Gebre-Egziabher, D., and Powell, J., *GPS-Based Attitude for Aircraft*, http://www.metavr.com/technology/papers/3691_07.html (15 April 2000).
16. Quine, B., *Attitude Determination Subsystem*, http://www.yorku.ca/bquine/pages/attitude_determination_subsystem.htm (03 June 2000).
17. Leader, D., *Kalman Filter Estimation of Underwater Vehicle Position and Attitude Using a Doppler Velocity Aided Inertial Motion Unit*, Engineer Degree Thesis, Massachusetts Institute of Technology and Woods Hole Oceanographic Institution, Massachusetts, September 1994.
18. Fuchs, E., *Inertial Head-Tracking*, Master's Thesis, Massachusetts Institute of Technology, Cambridge MA, 1993.
19. Foxlin, E., *Inertial Head-Tracker Sensor Fusion by a Complementary Separate-Bias Kalman Filter*, Proceedings of Virtual Reality Annual International Symposium, VRAIS '96, IEEE, 1996, pp. 185–194.
20. Azuma, R., *Predictive Tracking for Augmented Reality*, Ph.D. Dissertation, University of North Carolina at Chapel Hill, Computer Science Technical Report TR#95–007, Chapel Hill, NC, 1995.
21. Wahba, G., *Problem 65–1: A least square estimate of spacecraft attitude*, SIAM Review, 7(3):409, July 1965.
22. Markley, L. F., and Mortari, D., *Quaternion attitude estimation using vector observations*, The Journal of the Astronautical Sciences, Vol. 48, No. 2/3, April–September 2000, pp. 359–380.
23. Kuipers, J., *Quaternions and Rotation Sequences*, Princeton University Press, Inc., Princeton, NJ, 1998.
24. McGhee, R., *Some Parameter-Optimization Techniques*, Digital Computer User's Handbook, McGraw-Hill, 1967, pp. 234–253.
25. McGhee, R., Bachmann, E., Yun X. and Zyda, M., *Real-Time Tracking and Display of Human Limb Segment Motions Using Sourceless Sensors and a Quaternion-Based Filtering Algorithm—Part I: Theory*, MOVES Academic Group Technical Report NPS-MV-01-001, Naval Postgraduate School, Monterey, CA, 2000.
26. Cormen, T., Leiserson, C., and Rivest, R., *Introduction to Algorithms*, McGraw-Hill, New York, 1994.
27. Yun, X., et. al., *Testing and Evaluation of an Integrated GPS/INS System for Small AUV Navigation*, IEEE Journal of Oceanic Engineering, Vol. 24, No. 3, July 1999, pp. 396–404.
28. Bachmann, E., Duman I., Usta, U., McGhee R., Yun, X., and Zyda, M., *Orientation tracking for Humans and Robots Using Inertial Sensors*, International Symposium on Computational Intelligence in Robotics & Automation (CIRA 99), Monterey, CA, 1999, pp. 187–194.
29. Brown, R. and Hwang, P., *Introduction to Random Signals and Applied Kalman Filtering, Second Edition*, John Wiley and Sons, Inc., New York, NY, 1992.
30. Crossbow Inc., *Crossbow CXLO4M3 Data Sheet*, 1998.
31. Honeywell Inc., *Honeywell Three-Axis Magnetic Sensor Hybrid, HMC2003*, 1998.

32. Tokin American Inc., *Tokin CG16D Solid State Rate Sensor Data Sheet*, http://www.tokin.com/Tokin_America_Products/46/p46c/p46c.html, 1998.
33. McKinney, D., McKinney Technology, 4890 S. Hudson Place, Chandler, AZ. 85249, doug@mt.to.
34. Yun, X., Aparicio, C., Bachmann, E., and McGhee, R., *Implementation and Experimental Results of a Quaternion-Based Kalman Filter for Human Body Motion Tracking*, Proceedings of the 2005 International Conference on Robotics and Automation (ICRA 2005), April 18–22, 2005 Barcelona, Spain.
35. Caruso, M., *Set/Reset Pulse Circuits for Magnetic Sensors*, Honeywell, Inc., AN-201, 1995.
36. Bachmann, E., Yun, X., McKinney, D., McGhee, R., and Zyda, M., *Design and Implementation of MARG Sensors for 3-DOF Orientation Measurement of Rigid Bodies*, Proceedings of the 2003 IEEE International Conference on Robotics and Automation (ICRA 2003), September 14–19, Taipei, Taiwan, 2003.
37. Bachmann, E., Yun, X., and Peterson, C., *An Investigation of the Effects of Magnetic Variations on Inertial/Magnetic Orientation Sensors*, Proceedings of the IEEE International Conference on Robotics and Automation, ICRA 2004, New Orleans, Louisiana, April–May, 2004.
38. McGhee, R., Nakano, E., Koyachi, N., and Adachi, H., *An Approach to Computer Coordination of Motion for Energy-Efficient Walking Machines*, Bulletin of Mechanical Engineering Laboratory, Japan, No. 43, 1986.
39. Marins, João Luís, Yun, Xiaoping, Bachmann, E. R., McGhee, R. B., and Zyda, M. J., *An Extended Kalman Filter for Quaternion-Based Orientation Estimation Using MARG Sensors*, Proceedings of 2001 IEEE/RSJ International Conference on Intelligent Robots and Systems (IROS), October 29–November 3, Maui, Hawaii, 2001.

Factored Quaternion Algorithm for Orientation Estimation from Earth Gravity and Magnetic Field Measurements

Xiaoping Yun, Fellow, IEEE, Eric R. Bachmann, Member, IEEE, and Robert B. McGhee, Fellow, IEEE

Abstract—Orientation of a rigid body can be determined from measured gravity and local magnetic field vectors. In human body tracking applications, where it is assumed linear acceleration will average to zero over any extended period, triads of accelerometers and magnetometers can be used to measure gravity and local magnetic field vectors in sensor coordinates. Pitch and roll can be determined using only accelerometer data. Due to deviations of the direction of magnetic field vector between locations, it is desirable to use magnetic data only in calculations related to the azimuth. The TRIAD algorithm can be used to algebraically solve this problem. Alternatively, some formulation of the QUEST algorithm can be used to find an optimal solution based on a given set of measurements. This paper presents an intuitive geometric 3-DOF orientation estimation algorithm with physical meaning, called the factored quaternion algorithm. Through a derivation based on half-angle formulas, the algorithm sequentially calculates three angles and produces a quaternion output to represent orientation. The use of magnetic data is restricted to determination of rotation about the vertical. Thus, magnetic variations cause only azimuth errors. A singularity avoidance method is introduced that allows the algorithm to track through all orientations. Experimental results demonstrate that the proposed algorithm has an overall accuracy that is essentially identical to that of the TRIAD and QUEST algorithms, and has a computational efficiency that is comparable to the TRIAD and better than the QUEST.

Index Terms—Motion measurement; inertial sensors; magnetic sensors; accelerometers; orientation estimation; QUEST algorithm; quaternions; factored quaternion algorithm.

I. Introduction

ACCURATE real-time tracking of the orientation or attitude of rigid bodies has applications in robotics, aerospace, underwater vehicles, synthetic reality, and others. For synthetic reality applications, the human body can be viewed as an articulated rigid-body consisting of approximately fifteen links. If the orientation relative to a fixed reference frame can be determined for each of the links, then the overall posture of the human subject can be accurately rendered and communicated in real-time. The orientation of an individual limb segment can be measured through the attachment of an inertial/magnetic

sensor module. Such sensor modules typically contain a triad of orthogonally mounted accelerometers and a triad of orthogonally mounted magnetometers. Under the assumption that human limb acceleration is bounded and averages to zero over any extended period of time, the accelerometers are used to measure the gravity vector relative to the coordinate frame of the sensor module. The magnetometers serve a similar function for the local magnetic field vector. In dynamic applications, a triad of angular rate sensors can be added as a high frequency source of orientation information. The availability, low-cost, and small-size Micro-Electro-Mechanical Systems (MEMS) sensors has made it possible to build wrist watch sized, self-contained inertial/magnetic sensor modules [4], [15]. These modules can be used to accurately track orientation in real-time. This technique of orientation estimation is dependent only on passive measurement of physical quantities that are directly related to the rate of rotation and orientation of a rigid body. Since no generated signals are involved, there are no restrictions on the range of operation. All latency in such a system is due to the computational demands of the data processing algorithms.

In body tracking applications based on the use of small inertial/magnetic sensors [4], the gravity and local magnetic field vectors are often measured and compared to reference vectors in order to determine orientation. In the case of the gravity vector, the assumption that it is fixed leads to no difficulties since this vector points straight down in any inertial frame located on or near the surface of the earth. Making the same assumption regarding the local magnetic field vector can lead to problems. In a typical room setting the direction of the local magnetic field vector can be expected to vary due to the presence of ferrous objects or electrical appliances. In inertial/magnetic tracking algorithms, the local magnetic field vector is commonly treated as a fixed reference. It is assumed that this reference will remain constant. If it does not, algorithms may be prone to errors not only in azimuth, but also in pitch and roll as well.

The TRIAD algorithm [11] is a single frame deterministic method for calculating the attitude of a rigid body relative to a Earth fixed reference frame. The algorithm requires normalized measurements of two nonparallel reference vectors as input. Since the problem is overspecified, the TRIAD algorithm works by throwing away some components of these measurement vectors. It is used to

Xiaoping Yun is with Department of Electrical and Computer Engineering, Naval Postgraduate School, Monterey, CA 93943, USA. All correspondence should be addressed to this author.

Eric R. Bachmann is with Department of Computer Science and System Analysis, Miami University, Oxford, OH 45056, USA.

Robert B. McGhee is with Department of Computer Science and MOVES Institute, Naval Postgraduate School, Monterey, CA 93943, USA.

algebraically solve for the 3×3 orthogonal orientation matrix A , such that

$${}^b v = A {}^E v \quad (1)$$

where ${}^E v$ and ${}^b v$ are representations of a vector v in Earth and body coordinates respectively. The algorithm constructs two triads of orthonormal unit vectors. The two triads are the components of an inertial frame expressed in both the body and Earth fixed reference frames. Let ${}^b a$ and ${}^b m$ be accelerometer and magnetometer measurements relative to the body frame of the the gravity and magnetic field reference vectors, ${}^E g$ and ${}^E m$. The reference vectors are expressed relative to an Earth fixed frame. The first triad is given by

$$\hat{s}_1 = {}^E g \quad (2)$$

$$\hat{s}_2 = \frac{({}^E g \times {}^E m)}{|{}^E g \times {}^E m|} \quad (3)$$

$$\hat{s}_3 = \frac{({}^E g \times ({}^E g \times {}^E m))}{|{}^E g \times {}^E m|} \quad (4)$$

The second triad is given by

$$\hat{r}_1 = {}^b a \quad (5)$$

$$\hat{r}_2 = \frac{({}^b a \times {}^b m)}{|{}^b a \times {}^b m|} \quad (6)$$

$$\hat{r}_3 = \frac{({}^b a \times ({}^b a \times {}^b m))}{|{}^b a \times {}^b m|} \quad (7)$$

The triads are then used to create measurement and reference matrices such that

$$M_{mea} = [\hat{r}_1 \ \hat{r}_2 \ \hat{r}_3] \quad M_{ref} = [\hat{s}_1 \ \hat{s}_2 \ \hat{s}_3] \quad (8)$$

The orientation matrix, A , representing the attitude of a rigid body is then simply

$$A = M_{mea} M_{ref}^T \quad (9)$$

It should be noted that if the measurements of the gravity and the magnetic field are ordered as described above the cross-products used to calculate \hat{s}_2 and \hat{r}_2 eliminate any contribution of the magnetic measurements relative to the vertical. Thus, pitch and roll components of orientation are determined using only accelerometer measurements.

The QUEST (QUaternion ESTimator) algorithm is an optimal algorithm for single-frame estimation of a quaternion that represents the attitude of a rigid body relative to a fixed coordinate system. The algorithm was created to solve Wahba's problem [10] in the context of spacecraft attitude determination. Given a set of 3-dimensional known reference unit vectors V_1, V_2, \dots, V_n , and a set of the corresponding observation or measurement unit vectors W_1, W_2, \dots, W_n (which could be the direction of the sun or a star observed from a spacecraft measured in the spacecraft's body frame), Wahba's problem is to find the least squares estimate of spacecraft attitude by minimizing the following loss function

$$L(A) = \frac{1}{2} \sum_{i=1}^n a_i (W_i - AV_i)^T (W_i - AV_i) \quad (10)$$

with respect to the 3×3 orthogonal orientation matrix A , where a_1, a_2, \dots, a_n are nonnegative weighting coefficients. The minimum number of measurement and reference vector pairs is two. Early solutions to Wahba's problem directly computed the orientation matrix A [12]. Davenport [13] introduced a method of parameterizing the orientation matrix by a unit quaternion q , and proved that the loss function (10) can be transformed into a quadratic gain function of the unit quaternion in the form of

$$G(A(q)) = \sum_{i=1}^n a_i - L(A(q)) = q^T K q \quad (11)$$

where K is a 4×4 matrix constructed from the reference vectors V_i , measurement vectors W_i , and weighting coefficients a_i , $i = 1, 2, \dots, n$. Based on Davenport's work, Shuster and Oh derived the QUEST algorithm [11], and showed that the optimal quaternion q that maximizes the gain function (11) while satisfying the unit quaternion (unit norm) constraint is the eigenvector of the K matrix corresponding to the largest eigenvalue of K . Thus, the problem is reduced to finding the eigenvalues and eigenvectors of a 4×4 matrix.

Extensive research has been conducted to investigate the use of inertial/magnetic sensor modules for posture estimation in human body tracking applications. Foxlin et al. describes two commercial systems based on the use of sensor modules containing accelerometers, magnetometers, and angular rate sensors [1], [2]. The described algorithm is designed for head tracking applications and requires still periods to correct for inertial drift. Bachman et al. proposed a quaternion-based complementary filter for human body motion tracking [3], [4]. The filter is able to track through all orientations without singularities and continuously correct for drift without a need for stationary periods using data from inertial/magnetic sensor module containing nine sensors. Gallagher et al. presents a simpler complementary filter algorithm with lower computational complexity in [5]. Luinge describes a Kalman filter designed for human body tracking applications. The filter is based on the use of only accelerometers and rate sensors. Drift about the vertical axis is reduced by limiting body segment orientation using a kinematic human body model [6]. Rather than estimating individual limb segment orientations relative to an Earth fixed reference frame, Zhu and Zhou determine joint angles in axis/angle form using the data from the two nine-axis sensors mounted on the inboard and outboard sides of the joint [7]. Yan and Yuan describe an orientation tracking algorithm that uses low cost sensor modules to take two axis measurements of gravity and the local magnetic field [8]. In a manner similar to the method described in this paper, elevation, roll and azimuth angles are sequentially calculated. The angles are used to construct rotation matrices and the use of trigonometric functions is required. The method is limited to orientation tracking within a hemisphere. In [9], Gebre-Egziabher et al. describe an attitude determination algorithm for aircraft applications. The algorithm is based on a quaternion formulation of Wahba's problem [10],

where magnetometer and accelerometer measurements are used to determine attitude.

This paper presents an alternative algorithm for estimating orientation based on a set of measurements from triads of orthogonally mounted magnetometers and accelerometers. It is called the factored quaternion algorithm (FQA). It is a intuitive alternative to the TRIAD and QUEST algorithms. Local magnetic field data is used only in azimuth angle calculations. This decoupling of accelerometer and magnetometer data eliminates the influence of magnetic variations on calculations that determine pitch and roll. Through a derivation based on half-angle formulas, the computational cost of computing trigonometric functions is avoided. The algorithm produces a quaternion output. It is able to track through all orientations without singularities. Experimental results in which the factored quaternion algorithm is compared with the TRIAD and QUEST algorithms indicate that it has nearly identical accuracy at a comparable or lower computational expense.

The primary contributions of this work are:

- Derivation of a new geometrically intuitive algorithm for determining orientation relative to an Earth fixed reference frame based on a set of accelerometer and magnetometer measurements.
- A singularity avoidance method that allows the algorithm to track through all orientations.
- Experimental results which validate the performance of the algorithm and compare it to more established methods.

The rest of this paper is organized as follows. Section II presents a derivation of the factored quaternion algorithm. Section III describes experiments in which the factored algorithm is compared to the QUEST algorithm for efficiency and accuracy. The ability of the algorithm to track through all orientations without singularities is demonstrated as is it's decoupling property. The final section discusses the experimental results and provides a summary.

II. Factored Quaternion Algorithm

The factored quaternion algorithm presented in this section is for estimating the orientation of a rigid body based on Earth gravity and magnetic field measurements [14]. Sensor modules such as the MARG III described in [15] contain a triad of accelerometers and a triad of magnetometers, and can be used to provide measurement data for the factored quaternion algorithm.

In a typical application, a sensor module is employed as a strap down inertial measurement unit (IMU) attached to a rigid body whose orientation is to be determined. To facilitate the analysis, it is convenient to define three coordinate systems. An Earth-fixed coordinate system $x_e y_e z_e$ is defined to follow the North-East-Down (NED) convention, that is, x_e points to north, y_e points to east, and z_e points down. A body coordinate system $x_b y_b z_b$ is attached to the rigid body whose orientation is to

be measured. The sensor module has its own coordinate system $x_s y_s z_s$ corresponding to the axes of three orthogonally mounted accelerometers/magnetometers. Since the sensor module is rigidly attached to the rigid body, the body coordinate system $x_b y_b z_b$ differs from the sensor coordinate system $x_s y_s z_s$ by a constant offset. For the convenience of discussions, in what follows, the body coordinate system is assumed to coincide with the sensor coordinate system.

A. Quaternion Rotation Operator

Unit quaternions can be used to perform rotation operations in the 3-D space [16]. In this paper, the following notation will be used to represent a quaternion q :

$$q = (q_0 \ q_1 \ q_2 \ q_3) \quad (12)$$

where q_0 is the scalar (or real) part and $[q_1 \ q_2 \ q_3]^T$ is the vector part. Let

$$u = \begin{bmatrix} u_1 \\ u_2 \\ u_3 \end{bmatrix} \quad (13)$$

be a unit vector in the 3-D space. The following unit quaternion

$$q = \cos \frac{\beta}{2} (1 \ 0 \ 0 \ 0) + \sin \frac{\beta}{2} (0 \ u_1 \ u_2 \ u_3) \quad (14)$$

is commonly utilized to perform rotation operations. Specifically, for any vector $v = [v_1 \ v_2 \ v_3]^T$ in the 3-dimensional space, the following operation

$$v' = q v q^{-1} \quad (15)$$

produces a vector v' by rotating the vector v about the axis defined by u by an angle θ . In the above, all multiplications are quaternion multiplications, and v and v' are treated as a pure quaternion whose real part is zero. q^{-1} is the inverse quaternion of q [16].

B. Elevation Quaternion

A rigid body is said to be in its reference orientation when its $x_b y_b z_b$ -axes are aligned with those of the Earth coordinate system. It is known that a rigid body can be placed in an arbitrary orientation by first rotating it about its z -axis by an angle ψ (azimuth or yaw rotation), then about its y -axis by angle θ (elevation or pitch rotation), and finally about its x -axis by angle ϕ (bank or roll rotation).

In order to derive a quaternion describing only elevation, it is useful to note that when a rigid body is moving at a constant velocity and is in a fixed orientation, then an accelerometer measures only gravity. Furthermore, the x -axis accelerometer senses only the component of gravity along the x -axis, and this component in turn depends only on elevation angle. This can be seen from the following argument. Starting with the rigid body in its reference orientation, the x -axis accelerometer is perpendicular to gravity and thus registers zero acceleration. The y -axis

accelerometer also reads zero while the z-accelerometer reads -g. If it is then rotated in azimuth about its z-axis, the x-axis accelerometer still reads zero, regardless of the azimuth angle. If the rigid body is next pitched up through an angle θ , the x-axis accelerometer will read:

$$a_x = g \sin \theta \quad (16)$$

and the z-axis accelerometer will read:

$$a_z = -g \cos \theta \quad (17)$$

where $g = 9.81 \text{ m/s}^2$ is the gravitational acceleration, and

$$a = \begin{bmatrix} a_x \\ a_y \\ a_z \end{bmatrix} \quad (18)$$

is the acceleration vector in the body coordinate system. For convenience, the accelerometer and magnetometer output from a sensor module is normalized to a unit vector. Let \bar{a} denote the normalized vector of the acceleration measurements:

$$\bar{a} = \frac{a}{|a|} = \begin{bmatrix} \bar{a}_x \\ \bar{a}_y \\ \bar{a}_z \end{bmatrix} \quad (19)$$

where $|a|$ is the norm of the acceleration vector a . It follows from equation (16) that the value for $\sin \theta$ can be expressed as:

$$\sin \theta = \bar{a}_x. \quad (20)$$

The value for $\cos \theta$ can be computed from

$$\cos \theta = \sqrt{1 - \sin^2 \theta}. \quad (21)$$

It should be noted that a positive value for $\cos \theta$ is assumed in the above equation. This is because the elevation angle θ is by convention restricted to the range of $-\pi/2 \leq \theta \leq \pi/2$. It is noted that if the rigid body is rolled about its x-axis, equation (17) will change, but equation (16) will remain the same. This means that equation (16) holds for any orientation of the rigid body.

In order to obtain an elevation quaternion using equation (14), a value is needed for $\sin(\theta/2)$ and $\cos(\theta/2)$. From trigonometric half-angle formulas, half-angle values are given by

$$\sin \frac{\theta}{2} = \text{sign}(\sin \theta) \sqrt{(1 - \cos \theta)/2} \quad (22)$$

$$\cos \frac{\theta}{2} = \sqrt{(1 + \cos \theta)/2} \quad (23)$$

where $\text{sign}()$ is the sign function that returns +1 for positive arguments and -1 for negative arguments. The sign function is not needed in equation (23) since $\cos(\theta/2)$ is always positive within the elevation angle range.

Elevation is a rotation about y-axis. The unit quaternion representing elevation motion can now be computed using equation (14) and values for the half angle trigonometric functions as follows:

$$q_e = \cos \frac{\theta}{2} (1 \ 0 \ 0 \ 0) + \sin \frac{\theta}{2} (0 \ 0 \ 1 \ 0). \quad (24)$$

C. Roll Quaternion

The acceleration measured by the z-axis accelerometer with roll angle $\phi = 0$ is given by equation (17). Changing azimuth does not alter this measurement, but changing roll does. A more general formula for y-axis accelerometer reading is:

$$a_y = -g \cos \theta \sin \phi. \quad (25)$$

Likewise, the z-axis accelerometer will read:

$$a_z = -g \cos \theta \cos \phi. \quad (26)$$

In terms of the normalized acceleration measurement, the two equations above can be written as:

$$\bar{a}_y = -\cos \theta \sin \phi \quad (27)$$

$$\bar{a}_z = -\cos \theta \cos \phi \quad (28)$$

where the value for $\cos \theta$ was determined in equation (21). If $\cos \theta$ is not equal to zero, the values of $\sin \phi$ and $\cos \phi$ can be easily determined by:

$$\sin \phi = -\bar{a}_y / \cos \theta \quad (29)$$

$$\cos \phi = -\bar{a}_z / \cos \theta. \quad (30)$$

If $\cos \theta$ is equal to zero, it means that x-axis of the body coordinates is vertically oriented. In such cases, the roll angle is undefined and it can be assumed to have a value equal to zero. The range of the roll angle ϕ is by convention restricted to $-\pi \leq \phi \leq \pi$. The half angle values for ϕ can be computed in a manner similar to equations (22) and (23) with one exception. When $\cos \phi = -1$ and $\sin \phi = 0$, the use of equations (22) and (23) will result in a value of zero for both $\sin(\phi/2)$ and $\cos(\phi/2)$. This case can be treated in implementation by assigning a value of one to the sign function when its argument is zero. Having obtained the half angle values for the roll angle ϕ , the roll quaternion is computed as follows:

$$q_r = \cos \frac{\phi}{2} (1 \ 0 \ 0 \ 0) + \sin \frac{\phi}{2} (0 \ 1 \ 0 \ 0). \quad (31)$$

D. Azimuth Quaternion

Since azimuth rotation has no effect on the estimation of roll or elevation quaternions from accelerometer data, the strategy to be employed in this paper for azimuth quaternion estimation is to first solve for the elevation and roll quaternions. These can then be used to rotate the normalized magnetic field measurement vector in the body coordinate system

$${}^b m = \begin{bmatrix} {}^b m_x \\ {}^b m_y \\ {}^b m_z \end{bmatrix} \quad (32)$$

into the Earth coordinate system by the quaternion rotation operation:

$${}^e m = q_e q_r {}^b m q_r^{-1} q_e^{-1}. \quad (33)$$

In the above, ${}^b m$ stands for the pure quaternion of the 3-dimensional vector itself, i.e., ${}^b m = (0 \ {}^b m_x \ {}^b m_y \ {}^b m_z)$. The same convention is used for ${}^e m$. In the absence of

measurement error, ${}^e m$ should agree with the known local normalized magnetic field vector $n = [n_x \ n_y \ n_z]^T$, except for the effects of azimuth rotation on the sensor magnetometer readings. In such a case, $n_z = {}^e m_z$ and

$$\begin{bmatrix} n_x \\ n_y \end{bmatrix} = \begin{bmatrix} \cos \psi & -\sin \psi \\ \sin \psi & \cos \psi \end{bmatrix} \begin{bmatrix} {}^e m_x \\ {}^e m_y \end{bmatrix} \quad (34)$$

where ψ is the azimuth angle. Before proceeding further, it should be noted that equation (34) implies that the two 2-dimensional vectors differ only in orientation. In fact, experimental data show that, in the presence of measurement noise, they may also differ in length. To compensate for this effect, the vectors on both sides of equation (34) can be normalized. Specifically, let the normalized local magnetic field reference vector in the horizontal plane be:

$$N = \begin{bmatrix} N_x \\ N_y \end{bmatrix} = \frac{1}{\sqrt{n_x^2 + n_y^2}} \begin{bmatrix} n_x \\ n_y \end{bmatrix} \quad (35)$$

and the corresponding quantity measured by the magnetometer be:

$$M = \begin{bmatrix} M_x \\ M_y \end{bmatrix} = \frac{1}{\sqrt{{}^e m_x^2 + {}^e m_y^2}} \begin{bmatrix} {}^e m_x \\ {}^e m_y \end{bmatrix}. \quad (36)$$

With these definitions, equation (34) becomes:

$$\begin{bmatrix} N_x \\ N_y \end{bmatrix} = \begin{bmatrix} \cos \psi & -\sin \psi \\ \sin \psi & \cos \psi \end{bmatrix} \begin{bmatrix} M_x \\ M_y \end{bmatrix} \quad (37)$$

from which the value of $\cos \psi$ and $\sin \psi$ can be solved as:

$$\begin{bmatrix} \cos \psi \\ \sin \psi \end{bmatrix} = \begin{bmatrix} M_x & M_y \\ -M_y & M_x \end{bmatrix} \begin{bmatrix} N_x \\ N_y \end{bmatrix}. \quad (38)$$

The azimuth angle ψ is restricted to the range $-\pi < \psi \leq \pi$. The half angle formulas given by equations (22) and (23) can again be used to compute the half angle values of ψ . The azimuth quaternion is then given by:

$$q_a = \cos \frac{\psi}{2} (1 \ 0 \ 0 \ 0) + \sin \frac{\psi}{2} (0 \ 0 \ 0 \ 1). \quad (39)$$

Having obtained all three rotation quaternions, the quaternion estimate representing the orientation of the rigid body is finally given by:

$$\hat{q} = q_a \ q_e \ q_r. \quad (40)$$

E. Singularity Avoidance in Implementation

The factored quaternion algorithm presented above takes the normalized acceleration measurement vector and local magnetic field measurement vector as its input, and produces a quaternion as its output. It is a single-frame algorithm, that is, it takes measurements at a single instant of time, and produces an output. It does not require a history of measurements at multiple instants of time.

From the two measurement vectors, the half angle value of each rotation angle is first computed. Then the corresponding quaternion for each rotation is computed. Finally, the overall orientation quaternion is computed by

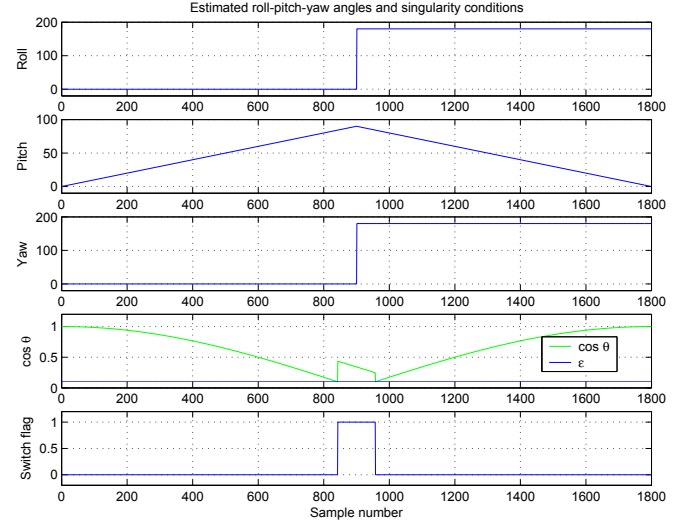


Fig. 1. Roll, pitch, yaw angles, singularity condition, and switch flag during a 180° rotation in pitch axis with ideal simulated data.

equation (40). It should be emphasized that the algorithm does not evaluate trigonometric functions at any step.

Although quaternions when used to represent the 3-dimensional orientation do not have singularities, the factored quaternion algorithm described above uses three angles to derive the quaternion estimate. It is known that any three-parameter representation of the 3-D orientation is inevitably singular at some point [17]. Without exception, the factored quaternion algorithm has a singularity, so does the QUEST algorithm. The QUEST algorithm uses the Gibbs vector

$$\rho = \frac{1}{q_0} \begin{bmatrix} q_1 \\ q_2 \\ q_3 \end{bmatrix} \quad (41)$$

in its derivation and is at a singular point if $q_0 = 0$. A method similar to the method of sequential rotations discussed in [18] is described below to avoid singularities in the numerical implementation. A singularity occurs in the factored quaternion algorithm if the elevation angle is $\pm 90^\circ$. This happens when $\cos \theta = 0$ or equivalently $\bar{a}_z = 0$ in equations (29) and (30). In implementation, the first step of the algorithm is to check the value of \bar{a}_z . If the absolute value of \bar{a}_z is smaller than a predefined constant ϵ (e.g., $\epsilon = 0.1$), the procedures described below are implemented to circumvent the numeric difficulty of having a small number in the denominator.

If $\bar{a}_z \leq \epsilon$, the elevation angle is close to $\pm 90^\circ$. The normalized acceleration measurement vector \bar{a} and magnetic field measurement vector ${}^b m$ in the body frame will be rotated about the body coordinate y_b -axis by an angle α to obtain the following offset (rotated) measurement vectors:

$$\bar{a}_{\text{offset}} = q_\alpha \bar{a} q_\alpha^{-1} \quad (42)$$

$${}^b m_{\text{offset}} = q_\alpha {}^b m q_\alpha^{-1} \quad (43)$$

where q_{offset} is the offset (rotation) quaternion given by

$$q_{\alpha} = \cos \frac{\alpha}{2} (1 \ 0 \ 0 \ 0) + \sin \frac{\alpha}{2} (0 \ 0 \ 1 \ 0). \quad (44)$$

Under the condition of $\bar{a}_z \leq \epsilon$, the offset measurement vectors will be used in place of the original measurement vectors to carry out the factored quaternion algorithm. The resultant orientation quaternion estimate from equation (40) in this case is called \hat{q}_{alt} .

The value of α can be chosen arbitrarily as long as it is sufficiently away from zero. It is chosen to be 20° in this discussion. Rotating measurement vectors about y_b -axis by 20° is equivalent to rotating the (original) body coordinate system $x_b y_b z_b$ to a temporarily offset body coordinate system $x'_b y'_b z'_b$ about y_b -axis by -20° . \hat{q}_{alt} represents the orientation of $x'_b y'_b z'_b$ in the Earth coordinate system. The quaternion estimate \hat{q} representing the orientation of the original body coordinate system $x_b y_b z_b$ is given by the following compound quaternion (i.e., rotating $x'_b y'_b z'_b$ back to $x_b y_b z_b$ about y'_b -axis by 20°):

$$\hat{q} = \hat{q}_{\text{alt}} q_{\alpha}. \quad (45)$$

To demonstrate how the singularity avoidance method described above works, ideal measurements as well as noisy measurements for a 180° rotation in pitch axis were synthetically generated. Figure 1 shows the results with ideal measurements. The top three plots are trajectories of roll, pitch, and yaw angles. The bottom two plots depict the value of $\cos \theta$ and the switch flag. The value of $\cos \theta$ is an indication of the singularity condition, and the switch flag indicates when the singularity avoidance method is invoked. As expected, the pitch angle increases from 0 to 90° while the roll and yaw angles remain at zero during the first half period. As the pitch angle approaches 90° , the value of $\cos \theta$ drops nearly to zero. When $\cos \theta$ is less than ϵ (whose value is chosen as 0.1 in this testing), the singularity avoidance method is activated during the

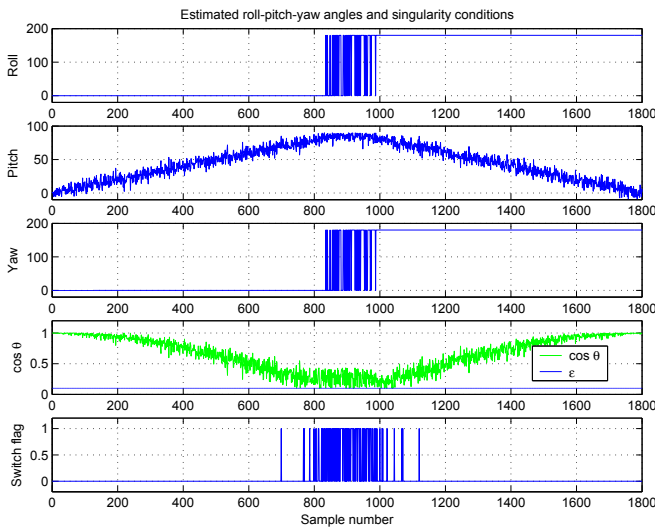


Fig. 2. Roll, pitch, yaw angles, singularity condition, and switch flag during a 180° rotation in pitch axis with noisy simulated data. The parameters used are: $\epsilon = 0.1$ and the offset angle $\alpha = 20^\circ$ degrees.

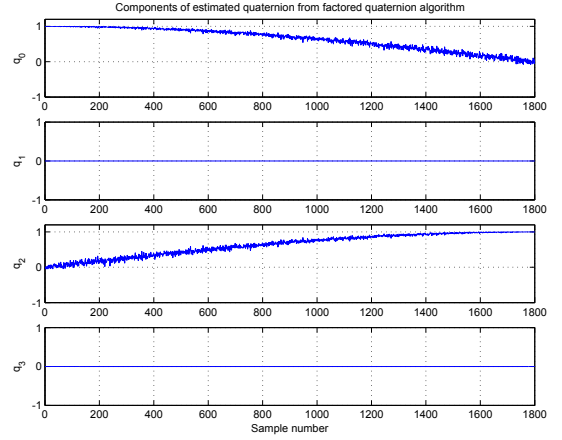


Fig. 3. Components of the estimated quaternion during a 180° rotation in pitch axis with noisy simulated data.

period of sample numbers from about 820 to 980 as seen in Figure 1. During this period, the value of $\cos \theta$ is lifted upwards to be away from zero. The value of the offset angle α is chosen to be 20° .

Owing to the conventional choice, the pitch angle is limited from -90° to 90° . As a result, the orientation of a 95° pitch, 0° roll, and 0° yaw is depicted as 85° pitch, 180° roll, and 180° yaw in Figure 1. This is the reason why the pitch angle increases from 0 to 90° and then decreases from 90° to 0 while the actual rotation increases from 0 to 180° .

Figure 2 shows the results with noisy measurements for the same rotational motion as in Figure 1. Noises were introduced using a random number generator. It is noted that the switch flag flipped many times, and the value of $\cos \theta$ was kept above $\epsilon = 0.1$ at all times. The trajectory of the pitch angle follows the same rise and fall pattern as in Figure 1 except with added noise. The roll and yaw angles flipped from 0 to 180° numerous times, signifying that the pitch angle jumped above and below 90° . Figure 1 and Figure 2 plot the trajectory of the roll, pitch, and yaw angles for visualization purposes. Although there are jumps in roll and yaw, there are no jumps in the trajectory of the estimated quaternion as seen from the corresponding plot of the estimated quaternion components shown in Figure 3.

III. Experimental Results

The experimental results described in this section compare the factored quaternion and QUEST algorithms. They also exhibit the unique properties of the factored quaternion algorithm. The first set of experiments constitutes a side-by-side comparison of the two algorithms for static and dynamic accuracy. In these experiments, an inertial/magnetic sensor module was subjected to a series of known rotations at several different rates. Both the factored quaternion and QUEST algorithms were tested first using raw accelerometer data and then low-pass filtered data. The second set of experiments demonstrate the effectiveness of the singularity avoid

method presented in the previous section. The third set of experimental results demonstrates the decoupling property of the factored quaternion algorithm. In these experiments a stationary inertial/magnetic sensor module was subjected to a magnetic field exhibiting a varying direction and magnitude by moving a ferrous object in the vicinity of the sensor module. Finally a rough comparison of the computational efficiency of the QUEST and factored quaternion algorithms is made.

Sensor data for the experiments was collected using a MARG III inertial/magnetic sensor module which was designed by the authors and fabricated by McKinney Technology [15]. Primary sensing components for this unit include a pair of two axis Analog Devices ADXL202E micromachined accelerometers, and Honeywell HMC1051Z and HMC1052 one and two-axis magnetometers. Overall, dimensions of the MARG III unit are approximately $0.7'' \times 1.2'' \times 1.0''$. Though the MARG III units contain angular rate sensors, no rate data was used in the experiments described in this paper.

A. Testing of Static and Dynamic Accuracy

Controlled rotations of the sensor modules were performed by placing an inertial/magnetic sensor module on a HAAS precision tilt table. The table has two degrees of freedom and is capable of positioning with an accuracy of 0.001 degrees at rates ranging from 0.001 to 80 degrees/second. In order to mitigate any possible magnetic effects generated by the steel construction of the tilt table, the sensor unit was mounted on a non-ferrous extension above the table. In each of these experiments, the sensor module was initially placed with its x_s, y_s, z_s axes respectively aligned with the North-East-Down directions. Following an initial still period, the sensor module was then subjected to a series of rotations.

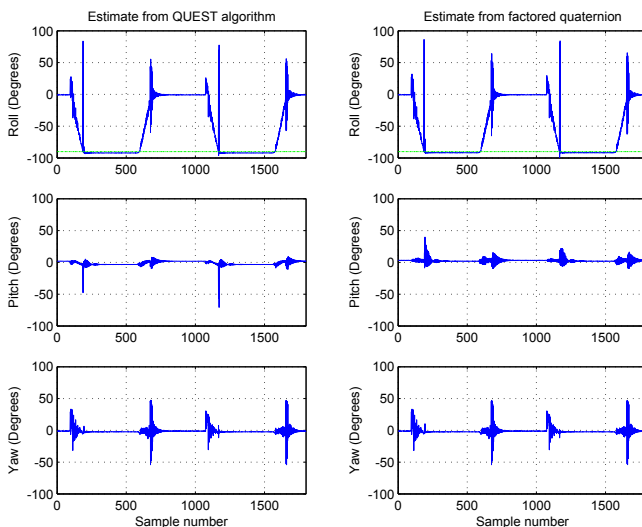


Fig. 4. Orientation estimate produced by the QUEST and factored quaternion algorithms with a 90° rotation in roll axis using raw accelerometer data.

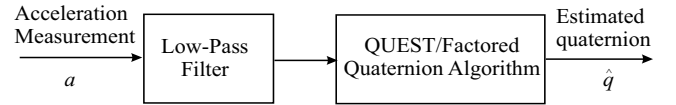


Fig. 5. Block diagram of the QUEST/factored quaternion algorithms with a low-pass filter.

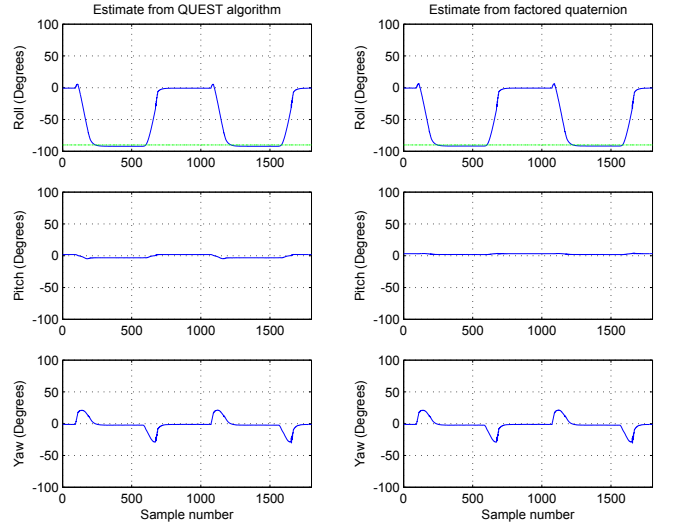


Fig. 6. Orientation estimate produced by the QUEST and factored quaternion algorithms with a 90° rotation in roll axis using low-pass filtered accelerometer data.

Figure 4 shows the performance of the each of the two algorithms using raw accelerometer and magnetometer data. The sensor was rotated -90° about the x-axis at a rate of $60^\circ/\text{s}$ and then rotated 90° at the same rate (in the reverse direction) for two cycles. The plots to the left show the orientation estimated by the QUEST algorithm, and the graphs to the right show the orientation estimated by the factored quaternion algorithm. The small pitch and yaw motions seen in the pitch and yaw sub-plots are due to misalignment of the sensor module with the motion axes of the tilt table. It can be seen that both algorithms were able to correctly estimate the roll angle before the first (negative) rotation, between the first and second (positive) rotations, and after the second rotation. Neither was able to correctly estimate orientation during rotational motion. Similar results were observed in experiments involving different angles of rotation at different rates.

During motion the accelerometers measure the sum of gravity and motion induced acceleration. In the case of the experiments described here, the motion induced acceleration is due to the motion of the tilt table and flexing of the non-ferrous extension on which the sensor module was mounted. Since both the QUEST and factored quaternion algorithms are single-frame algorithms, neither is able to filter out transient non-gravitational accelerations that occur during motion.

Figure 5 depicts a revised approach in which a low-pass filter for accelerometer data is combined with the factored quaternion or QUEST algorithm. To examine the performance of the QUEST and factored quaternion algo-

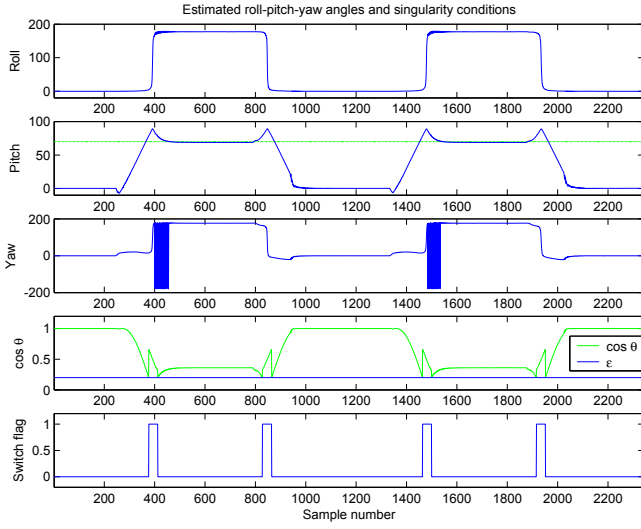


Fig. 7. Angles, singularity condition, and switch flag of the factored quaternion algorithm during 110° rotation in pitch axis.

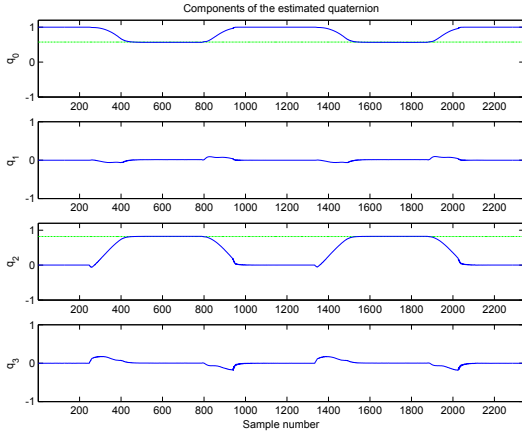


Fig. 8. Components of the estimated quaternion produced by the factored quaternion algorithm during 110° rotation in pitch axis.

ritms in conjunction with a low-pass filter, the rotation experiments were repeated. Figure 6 shows performance during 90° rolls at a rate of $60^\circ/\text{s}$. A comparison of Figure 6 to Figure 4 in which the sensor module was subjected to the same rotations shows that either algorithm can be used to track the orientation of a rigid-body in a dynamic environment when acceleration data is low-pass filtered. Again, similar results were observed in experiments involving different angles of rotation at different rates.

B. Avoidance of Singularity Conditions

Within the factored quaternion algorithm, three half angles are used to derive an orientation quaternion. Measurement vectors are rotated by an angle α when the pitch angle approaches $\pm 90^\circ$ and the $\cos \theta$ approaches zero. Figures 7 and 8 respectively depict the operation of the factored quaternion algorithm and its output during 110° pitch rotations. During this experiment, α was set to 45° and ϵ was 0.2. The bottom two subplots of Figure 7 trace the value the $\cos \theta$ and the value of the switch flag

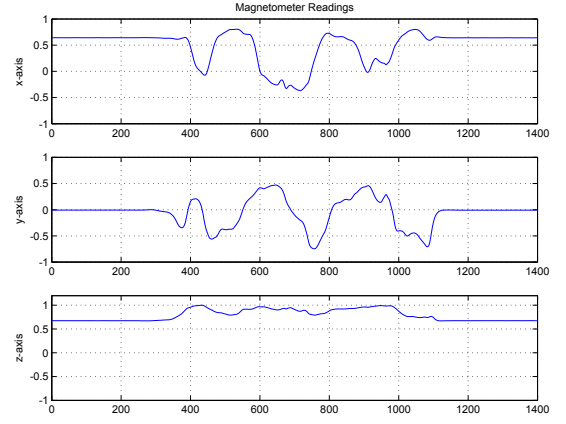


Fig. 9. Components of the normalized local magnetic field measurement vector under the influence of a moving magnetic field distortion.

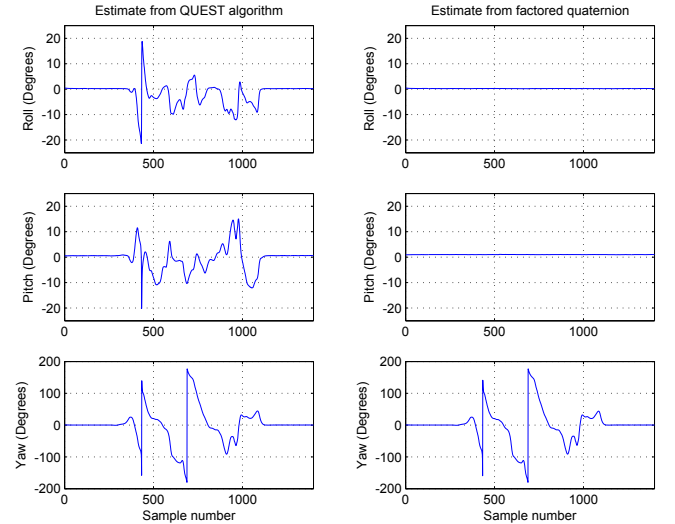


Fig. 10. Orientation estimate produced by the QUEST and factored quaternion algorithms with a static sensor module under the influence of a moving magnetic field distortion.

that triggers the singularity avoidance method and show the direct correspondence between the two in time. It can be observed that each time $\cos \theta$ was about to become less than ϵ , the switch flag was set to one. The top three subplots in Figure 7 depict the angles calculated from the quaternion estimate produced by the algorithm. The apparent rise of the pitch angle to 90° and then drop to 70° is a visualization artifact due to the use of the three angles for plotting purposes. 110° pitch is represented as 70° pitch together with a 180° roll and a $\pm 180^\circ$ yaw. At times the yaw angle flips between two alternate representations of the same rotation, namely -180° and 180° . The roll angle is stable at either 0° or 180° .

The quaternion elements depicted in Figure 8 are smooth and exhibit no flipping of orientation representations or singularity artifacts. The real part of the quaternion, q_0 , begins at 1.0 and changes to $\cos \frac{110^\circ}{2} = 0.5736$ during the 110° rotations. The element of the unit quaternion associated with rotations about the pitch axis,

q_2 , begins at zero and changes to $\sin \frac{110^\circ}{2} = 0.8192$ during the 110° rotations. The small changes in q_1 and q_3 are due to misalignment between the sensor module and the motion axes of the tilt table.

C. Testing of Static Accuracy When Subjected to Magnetic Field Variations

To test the decoupling property of the factored quaternion algorithm, an inertial/magnetic sensor module was mounted on a level non-ferrous stationary platform. The sensor module $x_s y_s z_s$ -axes were respectively aligned with the North-East-Down directions. Following an initialization period, the sensor module was exposed to a ferrous object. Movement of the ferrous object caused the direction of the measured magnetic field to change by as much as 360° . Changes in the measured magnetic field were observed in all measurement axes as illustrated by Figure 9. Figure 10 shows orientations calculated using the QUEST and factored quaternion algorithms. It can be observed that the orientations calculated using the QUEST algorithm (depicted by three subplots to the left) exhibited errors on all axes. On the other hand, the factored quaternion algorithm (depicted by three subplots to the right) showed no errors in either the pitch or roll axes.

D. Algorithm Efficiency

To make a rough comparison of the efficiency of the QUEST and factored quaternion algorithms, the time required for each to complete the computation of 5000 orientation quaternions was determined. This number represents 50 seconds of data at a sampling rate of 100 Hz. Both algorithms were able to complete the 5000 quaternion calculations in less than 10 seconds. The calculations were completed in 9.8 seconds by the QUEST algorithm and 7.8 seconds by the factored quaternion algorithm. In this experiment, the factored quaternion algorithm was approximately 25% faster than the QUEST algorithm.

IV. Conclusion

The paper has presented an intuitive algorithm for calculating orientation using accelerometer and magnetometer data. The algorithm produces estimates in quaternion form through a series of sequential rotations. In the algorithm, magnetometer data is not used to calculate orientation relative to the vertical, thus magnetic variations result in errors only in the horizontal plane. This property of the algorithm is demonstrated experimentally. Singularities in the numerical implementation are avoided through the use of a method that assigns an offset body coordinate system when a singularity occurs. The algorithm is efficient and does not require the evaluation of trigonometric functions. Experimental results indicate that when combined with a low-pass filter for accelerometer data, the algorithm is able to track orientation of a human limb segment. The algorithm has been successfully used in real-time human body motion tracking applications.

Acknowledgments

This research was supported in part by Army Research Office (ARO). Authors would like to thank James Calusdian for his technical support during the course of this project, Andreas Kavousanos-Kavousanakis for implementing the QUEST algorithm, and Conrado Aparicio for implementing the factored quaternion algorithm.

References

- [1] E. Foxlin, M. Harrington, and Y. Alshuler, "Miniature 6DOF inertial for track hmds," in SPIE vol. 3362, *Helmet and Head-Mounted Displays III*, AeroSense 98, Orlando, FL, Apr. 1998.
- [2] E. Foxlin, "Inertial head-tracker fusion by a complementary separate-bias Kalman filter," in *Virtual Reality Annual International Symposium (VRAIS 96)*, Santa Clara, CA, Mar. 1996, pp. 185–194.
- [3] E. R. Bachmann, "Inertial and magnetic tracking of limb segment orientation for inserting humans into synthetic environments," Ph.D. dissertation, Naval Postgraduate School, Monterey, CA, 2000.
- [4] E. R. Bachmann, R. B. McGhee, X. Yun, and M. J. Zyda, "Inertial and magnetic posture tracking for inserting humans into networked virtual environments," in *Proceedings of the ACM Symposium on Virtual Reality Software and Technology (VRST 2001)*, Banff, Alberta, Canada, Nov. 2001, pp. 9–16.
- [5] A. Gallagher, Y. Matsuoka, and A. Wei-Tech, "An efficient real-time human posture tracking algorithm using low-cost inertial and magnetic sensors," in *Proceedings of 2004 IEEE International Conference on Robotics and Automation*, Sendai, Japan, Sept. 2004, pp. 2967–2972.
- [6] H. J. Luinge, "Inertial sensing of human movement," Ph.D. dissertation, University of Twente, Dec. 2002.
- [7] R. Zhu and Z. Zhou, "A real-time articulated human motion tracking using tri-axis inertial/magnetic sensors package," *IEEE Transactions on Neural Systems and Rehabilitation Engineering*, vol. 12, no. 2, pp. 295–302, June 2004.
- [8] Z. Yan and K. Yuan, "An orientation tracking algorithm valid in a hemisphere space based on gravity field and earth magnetic field," in *Proceedings of the 2004 IEEE International Conference on Information Acquisition*, Hefei, China, June 2004, pp. 236–239.
- [9] D. Gebre-Egziabher, G. H. Kikaim, J. Powell, and B. W. Parkinson, "A gyro-free quaternion-based attitude determination system suitable for implementation using low cost sensors," in *Proceedings of IEEE 2000 Position Location and Navigation Symposium*, San Diego, CA, Mar. 2000, pp. 185–192.
- [10] G. Wahba, "Problem 65-1: A least squares estimate of satellite attitude," *SIAM Review*, vol. 7, no. 3, p. 409, July 1965.
- [11] M. D. Shuster and S. D. Oh, "Three-axis attitude determination for vector observations," *Journal of Guidance and Control*, vol. 4, no. 1, pp. 70–77, 1981.
- [12] J. Farrell and J. Stuelpnagel, "A least squares estimate of spacecraft attitude," *SIAM Review*, vol. 8, no. 3, pp. 384–386, 1966.
- [13] P. Davenport, "Attitude determination and sensor alignment via weighted least squares affine transformations," in *NASA X-514-71-312*, Goddard Space Flight Center, Greenbelt, Maryland, 1965.
- [14] R. B. McGhee, "The factored quaternion algorithm for orientation estimation from measured earth gravity and magnetic field," *MOVES Institute, Naval Postgraduate School, Monterey, CA, Technical Memorandum*, 2004. [Online]. Available: <http://www.users.muohio.edu/bachmaer/Papers/Factored%20Quaternion.pdf>
- [15] E. R. Bachmann, X. Yun, D. McKinney, R. B. McGhee, and M. J. Zyda, "Design and implementation of MARG sensors for 3-DOF orientation measurement of rigid bodies," in *Proceedings of 2003 IEEE International Conference on Robotics and Automation*, Taipei, Taiwan, May 2003.
- [16] J. B. Kuipers, *Quaternions and Rotation Sequences*. Princeton, NJ: Princeton University Press, 1999.

- [17] J. Stuelpnagel, "On the parameterization of the three-dimensional rotation group," *SIAM Review*, vol. 6, pp. 422–430, 1964.
- [18] M. D. Shuster and G. A. Natanson, "Quaternion computation from a geometric point of view," *Journal of the Astronautical Sciences*, vol. 41, no. 4, pp. 545–556, 1993.

Self-contained Position Tracking of Human Movement Using Small Inertial/Magnetic Sensor Modules

Xiaoping Yun, Eric R. Bachmann, Hyatt Moore IV, and James Calusdian

Abstract—Numerous applications require a self-contained personal navigation system that works in indoor and outdoor environments, does not require any infrastructure support, and is not susceptible to jamming. Posture tracking with an array of inertial/magnetic sensors attached to individual human limb segments has been successfully demonstrated. The "sourceless" nature of this technique makes possible full body posture tracking in an area of unlimited size with no supporting infrastructure. Such sensor modules contain three orthogonally mounted angular rate sensors, three orthogonal linear accelerometers and three orthogonal magnetometers. This paper describes a method for using accelerometer data combined with orientation estimates from the same modules to calculate position during walking and running. The periodic nature of these motions includes short periods of zero foot velocity when the foot is in contact with the ground. This pattern allows for precise drift error correction. Relative position is calculated through double integration of drift corrected accelerometer data. Preliminary experimental results for various types of motion including walking, side stepping, and running document accuracy of distance and position estimates.

I. INTRODUCTION

POSITION tracking of human movement commonly requires an unrestricted line of sight between one or more receivers and one of more transmitters. In inside-out systems a sensor attached to a person to be tracked, passively or actively receives information from multiple "sources" positioned around a tracking volume. In outside-in tracking systems, multiple sensors positioned around a tracking volume sense active or passive sources attached to the object to be tracked. The global positioning system (GPS) is a familiar example of a sourced inside-out tracking system. Optical tracking systems that use multiple cameras to view active or passive markers and calculate position through triangulation are an example of a sourced outside-in tracking system.

Inside-out or outside-in tracking systems require extensive set-up and calibration of the tracking volume. Line of sight and noise restrictions limit range as well as where these systems can be used. In some cases jamming or intentional interference makes their use impractical. "Sourceless"

systems are self-contained. Data that are produced by sensors attached to a person can be used to calculate position without reference to other devices or transmitters. In theory, a sourceless system with accuracy comparable to a sourced system is superior since it does not require extensive infrastructure positioned around or above a tracking environment of limited sized and is not susceptible to line of sight restrictions between a transmitter and source.

Sourceless orientation tracking using small inertial/magnetic sensor modules containing triads of orthogonally mounted accelerometers, angular rate sensors, and magnetometers has been successfully demonstrated. Several commercial posture tracking systems based on orientation tracking have resulted. The individual sensors used in inertial/magnetic sensor modules are low-cost Micro-Electro-Mechanical Systems (MEMS) sensors. Low cost MEMS accelerometers are susceptible to drift errors. Until recently, it was widely thought that position tracking using data from such accelerometers was not possible due to the quadratic growth of errors caused by sensor drift during double integration.

Most types of human movement including walking, side stepping, and running include repeated recognizable periods during which the velocity and acceleration of the foot are zero. These brief periods occur before entering the swing phase of the gait cycle each time the foot contacts the ground during the stance phase. Recognition of these periods allows determination of the drift error that occurred in between them. This allows precise corrections to be made to accelerometer data in either a forward or backward manner. The corrected accelerometer data combined with magnetic and angular rate data can then be used to calculate the direction and magnitude of displacement that occurs during each step. This allows accurate measurement of position relative to an initial starting point.

This paper describes a self-contained method for relative position tracking of a human engaged in various types of motion involving discrete steps. This method is based on the use of a single inertial/magnetic sensor module attached to the foot. The primary contributions of this work are:

- A method for tracking 2-D and 3-D position of human movement using a self-contained inertial/magnetic sensor module.
- Preliminary experimental results for various human motion including straight line walking, circular walking, side stepping, backward walking, running, and climbing stairs.

This remainder of this paper describes in detail how

Manuscript received September 15, 2006. This work was supported in part by the U.S. Army Research Office (ARO) and the Navy Modeling and Simulation Office (NMSO).

X. Yun, Hyatt Moore IV, and James Calusdian are with the Naval Postgraduate School, Monterey, CA 93943, USA (corresponding author phone: 831-656-2629; fax: 831-656-2760; e-mail: yun@ieee.org).

E. R. Bachmann, is with Miami University, Oxford, OH 45056 USA. e-mail: bachmaer@muohio.edu.

accelerometer data in conjunction with orientation estimates produced using data from inertial/magnetic sensor modules can be used to track human position in three dimensions without any supporting infrastructure. Section II presents related work and describes the foundation on which the work presented here is built. Section III is a detailed description on the sourceless position tracking method. Experimental results are presented in section IV. The final section is a summary and conclusions.

II. BACKGROUND

Much research has focused on using inertial and in a few cases magnetic sensors to measure distance walked and/or track position. Many methods have involved attempts to count steps and estimate distance based on an approximate step length. Other work has double integrated acceleration data recorded during the gait swing phase to estimate distance. Few have attempted to determine the direction of motion. In most cases, distance estimation errors when using more complex inertial sensor combinations have been only slightly better than those obtained using commercial pedometers.

Simple pedometers focus on counting steps. Based on this step count and a fixed step length, a pedometer unit can estimate distance traveled. In pedometers, step count is generally estimated by measuring vertical acceleration using a single axis piezo-electric accelerometer or by monitoring a spring suspended horizontal lever that moves up and down in response to vertical accelerations of the hips. The accuracies of pedometer produced step counts vary greatly depending on the type of technology used, walking speed, and physical aspects of individuals being tracked [1]. Pedometers do not have the ability to differentiate between different types of gait such as running, shuffling, and side stepping. In [2], Crouter et al. tested and compared several electronic pedometers in estimating step counts and distance traveled with subjects walking on a treadmill. Several models were able to count steps to within $\pm 1\%$ of the actual value during normal uniform walking. Estimates of distance traveled were less accurate with most units estimating mean distance to within $\pm 10\%$ at a walking speed of 80 meters per minute. Overshoots tend to occur at slower speeds. Undershoots tend to occur at higher speeds. In [3], Schneider et al. compared pedometer performance when subjects walked over a closed 400 meter course. Accuracy of step counts as well as distance estimates decreased in this more natural environment. Step count accuracy decreased to $\pm 3\%$. Since walking speed and stride length was no longer artificially controlled using a treadmill, the accuracy of distance estimates showed an greater decrease.

In [4], Pappas et al. describe a reliable gait phase detection system based on a single axis angular rate sensor and three force sensitive resistors. In this system, all motion is assumed to take place in the sagittal plane. The angular rate sensor is mounted to the heel with its sensing axis

perpendicular to the sagittal plane and is used to measure the rotational velocity of the foot. The force sensitive resistors are taped to the bottom of the same foot. Using a heuristic based algorithm designed to detect four different gait phases (stance, heel-off, swing, and heel-strike), the system was able to detect the phases with 99% reliability. Unlike simple pedometers, the described method worked well to detect gait phases during walking over level and unlevel surfaces as well as walking up and down stairs. In addition, the system demonstrated robustness in ignoring non-gait events such as standing up and sitting down, bending, and turning in place. The system did not have the ability to estimate distance or direction traveled.

Zijlstra and Hof use a single triaxial accelerometer, measured leg length, and an algorithm based on an inverted pendulum model [5] to predict the body center of mass trajectory during walking. The method determines foot contacts by monitoring for changes in sign of the forward acceleration of the lower trunk. Unlike pedometers which use a fixed step length, mean step length and walking speed are estimated based on up and down movement of the trunk. Experimental results in [6] include data from both treadmill and level ground walking trials. In most cases, the described method identified foot contacts with nearly 100% accuracy. In treadmill experiments, maximum observed differences between predicted speed and treadmill speed were no greater than 16%. In level ground walking experiments with presumably less uniform gait, differences between predicted mean speed and calculated mean speed did not exceed 20%. This method is able to detect gait event with great accuracy. However, due to the magnitude of the distance measurement errors and the inability to estimate direction of the travel, the navigation performance of this method shows little improvement over that of a simple pedometer.

Sagawa et al. [7], Sabatini et al. [8], and Cavallo et al. [9] use a combination of accelerometers and rate sensors attached to the foot to measure gait parameters and distance traveled. The Sagawa approach uses a tri-axial accelerometer and a single axis angular rate sensor attached to the toe (an atmospheric pressure sensor is used to measure change in altitude). The Sabatini and Cavallo approach uses a bi-axial accelerometer and a single axis angular rate sensor attached to the instep.

Sagawa et al. assumes that foot roll and yaw are zero during normal walking. Sabatini and Cavallo assume all motion takes place in a sagittal plane. In both cases, a rate sensor is mounted perpendicular to the sagittal plane. Gait events such as heel-off, heel-strike, and swing are detected using angular rate data. Instead of counting steps, walking speed and stride length are estimated by double integrating acceleration data during the swing phase. For best performance, the tracked subject is required to maintain a uniform walking speed and gait. Both research efforts were able to detect gait events with high levels of confidence. In limited experimental results, Sagawa et al. reports a

maximum distance estimation error of 5.3% over a 30 meter course. Reported experimental results obtained while walking over a 400 meter closed course in [9] characterize errors as being much smaller with an average measured distance of 401.2 ± 4.61 meters or just over a 1% error. Though GPS heading information was used in [9] to reconstruct the path of travel, neither of the systems described is able to determine the direction of displacement or position.

A great deal of research has focused on integrating inertial dead reckoning systems with positional information provided by GPS and DGPS. In [10], Jarawimut et al. implement a pedestrian navigation system. During periods of GPS availability, compass bias and average step length are updated to make dead reckoning results more closely match GPS estimates. When GPS information is unavailable, distance traveled is calculated by multiplying the number of steps times an average step length. A compass is used to estimate the direction of travel and the system is able to provide an estimate of position as long as the tracked subject is walking in a normal manner.

Other attempts to produce a personal navigation based on the integration of inertial/magnetic sensors are documented in [11] and [12]. In [11] Judd suggests that step length can be estimated based on a linear relationship with cadence. The described system consists of a GPS receiver, a three dimensional compass, and tri-axial accelerometer. The accelerometer is used as a tilt sensor to determine the horizontal component of the magnetic field and to detect foot falls. Average step length is estimated by a Kalman filter algorithm. Distance traveled is based on the product of the number of steps and the estimated step length. Again this approach is limited to level walking in open spaces. The personal navigation module described in [12] contains a tri-axial magnetometer, a tri-axial accelerometer, a barometric pressure sensor, and a GPS receiver. Distance traveled is still based on the step length/step count product. It is claimed that unlike other similar systems, a pattern recognition algorithm is used to identify acceleration signatures related to different types of movement such as forward and backward walking, lateral walking, and running. Performance claims for a commercial version of the system give a 2D positional accuracy of better than 5% of distance traveled for “forward walking under normal conditions [13].” No accuracy figures are given for other types of motion. However, in independent use of the product, the Sendero Groups reports typical errors on the order of 15% [14].

III. METHOD FOR TRACKING POSITION

In theory, the output of an accelerometer can be integrated twice to obtain displacement information. However, low-cost accelerometers are susceptible to drift errors. The position estimates based on double integration can diverge in a short time period lasting only a few seconds. Drift correction is thus essential for tracking position using low-cost accelerometers. In this section, a

drift correction method is first described. An application of this method to position tracking of a walking person is then detailed.

A. Correcting Accelerometer Drift

The drift correction method is best illustrated with the following experiment. An accelerometer is first placed on a level table top, and then is slid along a straight line for a distance of one meter. The initial and final velocities are zero. Figure 1 shows the accelerometer measurement data, as well as estimated velocity and position for such an experiment in which an Analog Devices ADXL210E accelerometer was used. The three plots on the left side show the results of the original data, and the plots on the right side show the results of the corrected data. The correction procedure is discussed below. The velocity is obtained by integrating accelerometer measurements once, and the position is obtained by integrating the velocity one more time. While the sensor actually moved a distance of one meter, the estimated distance obtained by double integration is 0.80m as seen in the lower-left plot. A close examination of the velocity in the middle-left plot indicates that the final estimated velocity is -0.23m/s at the end of the motion period, although the sensor stopped moving and the actual velocity was zero at this point. The error in the estimated velocity is due to drift in accelerometer

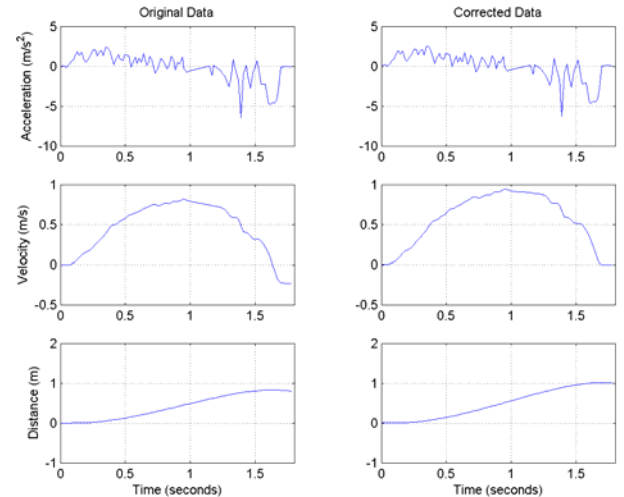


Figure 1. Results of a one-meter sliding motion experiment with original accelerometer data and integrated velocity and position on the left and the drift-corrected data and resulting velocity and position on the right side.

measurements. Because the final velocity is known to be zero in this case, a drift correction can be applied to the accelerometer measurements so that the final estimated velocity is zero. The three plots on the right side of Figure 1 are the corrected acceleration, velocity, and distance. It is seen that the final velocity is now zero. As a result of this drift correction, the estimated distance moved is 1.01m. Clearly, this drift correction method makes it possible to

obtain accurate position information through double integration. Many more experiments were conducted, and similar results were obtained. Figure 2 shows the results of an experiment where the sensor was moved a distance of three meters. With the uncorrected data, the final estimated distance is 2.01m, yielding an estimation error of 33%. After applying the drift correction, the final estimated

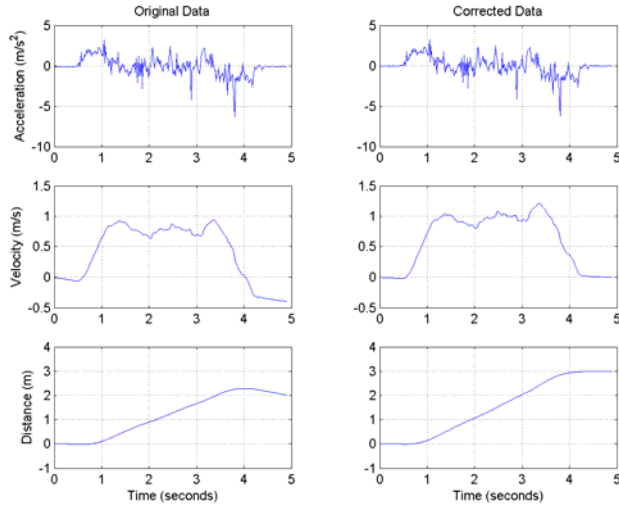


Figure 2. Original and drift-corrected data for a three-meter sliding motion experiment.

distance is 2.99m with an estimation error of only 0.3%.

B. Position Tracking of a Person

Human gait motion is cyclic in nature. During walking, each gait cycle consists of two phases: a stance phase and a swing phase. The stance phase is the portion of the cycle during which a foot is in contact with the ground. The swing phase is the portion of the cycle during which the same foot is not in contact with the ground. The stance phase takes approximately 60% of the gait cycle, and the swing phase takes the remaining 40%. During walking (rather than running or jumping), there are two periods of time in a single gait cycle when two feet are both in contact with the ground. This period of double support occupies about 20% of the gait cycle [15]. Based on the results of experiments presented in the previous subsection, it is possible to obtain accurate position information by double integrating accelerometer measurements as long as drift in accelerometer measurements can be corrected. During the stance phase, the foot is in contact with the ground, and foot velocity is zero. If an inertial/magnetic sensor module is attached to a foot, drift in accelerometer measurements can be corrected each time the foot is in the stance phase of the gait cycle [7]. If the estimated foot velocity is not zero, a drift correction can be applied to the accelerometer measurements as discussed in the previous subsection. Using this approach, Sagawa, etc. [7] and Gavallo, etc. [9] reported early efforts on estimating walking distance.

In this work, an inertial/magnetic sensor module is attached to the foot, and the 3-dimensional position (not just

walking distance) of a person is estimated and tracked. The inertial/magnetic sensor modules considered for this study contains triads of orthogonally mounted accelerometers, angular rate sensors, and magnetometers. Examples of such inertial/magnetic sensor modules include the MARG sensor [16], the 3DM-GX1 orientation sensor from MicroStrain [17], the nIMU from MEMSense [18], the MTx orientation tracker from Xsens [19], and the InertiaCube3 from InterSense [20]. These inertial/magnetic sensor modules are primarily designed for tracking 3-dimensional orientation. Algorithms used by these sensor modules for processing accelerometer, angular rate, and magnetometer measurements to produce orientation output typically use a Kalman filter [21]. In addition to providing orientation output in Euler angles and/or quaternions, some sensor modules including the MARG, 3DM-GX1 and nIMU also optionally provide scaled measurements of acceleration, angular rate, and magnetic field. 3DM-GX1 and nIMU are used in this study.

Acceleration measurements provided by the inertial/magnetic sensor module are in sensor or body coordinates. These measurements are first transformed into the earth coordinates. The transformation is accomplished by using the quaternion output of the sensor module. The three components of the acceleration measurements in the

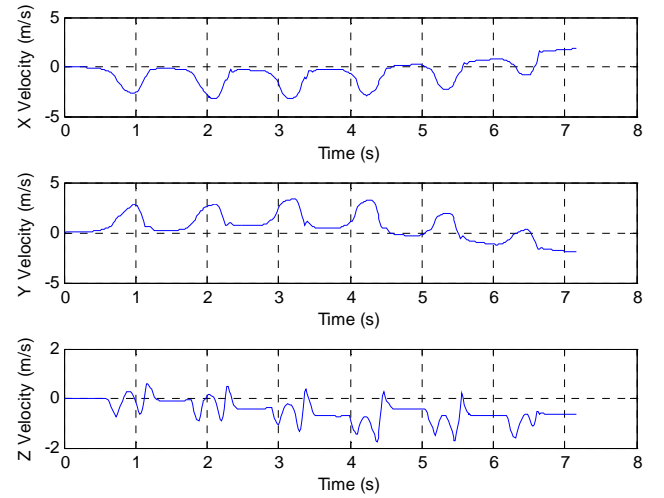


Figure 3. Three components of the velocity obtained by integrating the original acceleration measurement.

earth coordinates are then integrated to obtain velocity estimates. Figure 3 depicts the three components of the integrated velocity for an eight-meter walk. During the stance phase, each of the velocity components should be zero. However, it is seen that the estimated velocity tends to drift over the time. Applying the drift correction method discussed earlier each time the gait cycle enters the stance phase results in the corrected velocity profile shown in Figure 4. The corrected velocity is integrated once more to obtain 3-dimensional position information. The accuracy of the position information will be discussed in the next section which examines detection of gait events during various mobility modes including straight line walking,

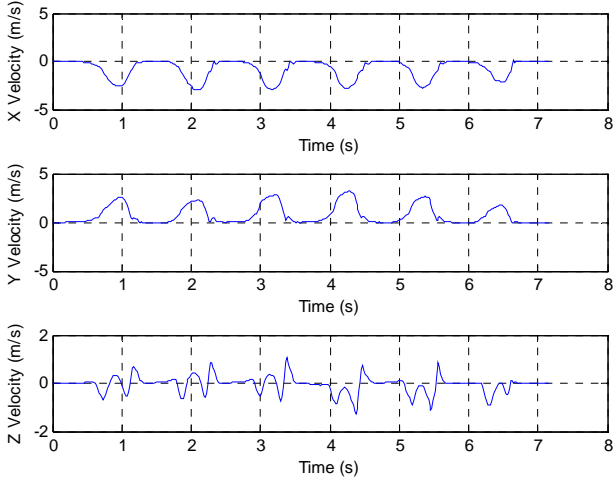


Figure 4. Velocity profile obtained from drift-corrected acceleration.

circular walking, running, side stepping, backward walking, and climbing stairs.

C. Detecting Gait Events

In order to apply the drift correction method for walking as discussed above, it is necessary to reliably detect gait events, particularly the stance phase, using only measurement data. Both accelerometer and angular rate data can be used for this purpose.

Figure 5 shows the three components of linear acceleration in the earth coordinates during walking. While all three acceleration components exhibit a cyclical pattern, it can be observed that z-axis acceleration data provide the strongest indication of gait events. During the stance phase, acceleration is near zero. Since there are a number of zero-crossings during the swing phase, a zero threshold and a time heuristic must be applied to the acceleration data to detect stance phases. The time heuristic is required to avoid classifying any zero crossing in the

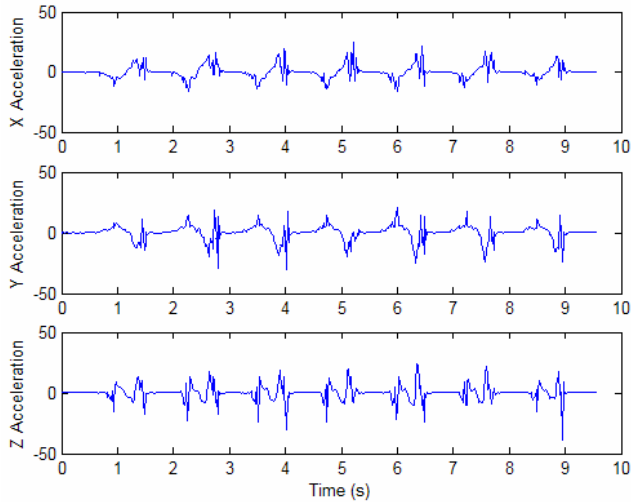


Figure 5. Three components of the foot acceleration in the earth coordinate system.

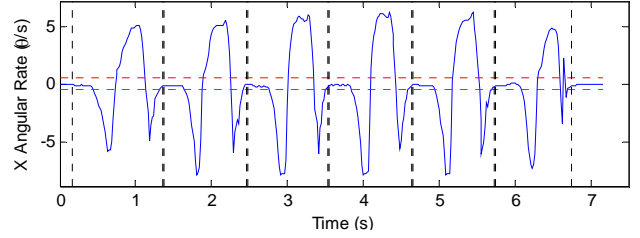


Figure 6. Foot angular rate in the ankle axis.

swing phase as a stance phase. If the acceleration is within the threshold for a specified period of time, the foot is determined to be in the stance phase.

Angular rate measurements also provide an indication of gait events. The angular rate in the sensor coordinates measuring ankle axis rotation is more prominent in differentiating the stance phase from the swing phase. Figure 6 shows the x-axis (or ankle axis) angular rate for a typical walk. The angular rate is near zero during the stance phase. A heuristic similar to the method discussed above can be applied to the angular rate data to detect the stance phase. In empirical studies involving several different people, the use of angular rate data was found to be more reliable than angular rate data.

IV. EXPERIMENTAL RESULTS

The following sub-sections describe preliminary experimental results demonstrating the accuracy of position estimation using inertial/magnetic sensor modules. These experiments include trials in which the tracked subject walked a specified distance in a straight line, walked around a closed circuit that was roughly circular in shape, ran a specified distance in a straight line, and finally followed a square pattern using three different types of motion. Preliminary results are also shown for walking up stairs. Data for each type of experiment was collected using several different individuals. These brief results are designed to demonstrate the robustness of position tracking using inertial/magnetic sensor modules and make apparent the wide applicability of this method to numerous applications. At the time of this writing, further experiments are under way as the position tracking method is further refined.

All experiments were conducted using a single sensor module attached to the foot as depicted in Figure 7. Distances walked were measured using a standard measuring tape. Data was collected in real-time and post-processed using a program written in Matlab. Sampling rate was approximately 70 Hz.

A. Straight Line Walking

Straight line walking experiments were conducted to validate the feasibility of estimating walking distance on a level surface. These experiments measure only displacement along a straight line. No attempt was made to estimate position. Table 1 shows experimental results for 24-meter straight line walk conducted in an indoor laboratory



Figure 7. MemSense nImu mounted on foot for position tracking during walking, side stepping, and running.

environment. Three different experimental subjects with varying stride lengths were used. The average distance estimation error for the indoor walking experiments is 5.5% with a standard deviation of 2.4%. Table 2 shows results for longer 120-meter straight line walks conducted in an outdoor environment. Two different subjects were used in these experiments. The distance estimation error for this small number of experiments was less than that observed during the indoor experiments with an average error of 1.3% and a standard deviation of 1.3%. Maximum error for the 120-meter walking experiments was 3.3%.

Table 1. Experimental results of 24-meter straight line walk.

Experiment #	Step Count	Estimated Distance (m)	Error
1	16	23.59	1.7%
2	16	21.95	8.5%
3	17	22.70	5.4%
4	17	25.61	6.7%
5	17	25.67	7.0%
6	17	23.07	3.9%

The marked difference in estimation accuracy between indoor and outdoor environments is attributed to errors in transforming measurement data from sensor coordinates to an Earth fixed coordinate system. Magnetometer measurements

along with accelerometer and angular rate measurements are used to compute an orientation quaternion, which is in turn used to transform data. In the presence of magnetic interference, orientation estimation algorithms designed for inertial/magnetic sensor modules exhibit errors in azimuth angle estimates [22]. In an indoor environment there is considerably more magnetic interference due to the presence of file cabinets, computers, monitors, and other laboratory equipment. This interference can cause estimated path of travel to appear to curve or wobble to the right and left when the true path of travel is a straight line. A correction method for these errors is currently under investigation.

Table 2. Experimental results of 120-meter straight line walk in an outdoor environment.

Walker	Experiment #	Step Count	Distance (m)	% Error
A	1	83	116.03	3.3%
A	2	82	119.42	0.5%
B	1	80	119.12	0.7%
B	2	79	119.05	0.8%

B. Straight Line Running

The described position estimation method is applicable to any context involving repeated short periods during which angular rate and velocity are zero. During running, as with walking, there are brief periods of time in the gait cycle during which the foot is in contact with the ground. Although these zero velocity periods are relatively short, the same method can be used to correct drift in accelerometer measurements. Relative to walking, it is more difficult to detect the stance phase from running data due to the short duration of these periods.

Straight line running experiments were conducted over the same 120-meter course used in the outdoor walking experiments. Again these experiments tested only the ability to measure displacement along a straight line. Table 3 shows the results of two running experiments over a 120-meter long course. The maximum error for these experiments was within 4.75% of the actual distance covered.

Table 3. Experimental results of 120-meter straight line running

Test #	Step Count	Actual Distance (m)	Estimated Distance (m)	Error
1	57	120.0	115.4	3.80%
2	54	120.0	114.3	4.75%

C. Circular Walking

Circular or curved walking experiments were the first to be conducted in order to validate the feasibility of tracking 2-D position. During these experiments the position of foot was simultaneously monitored by an optical tracking system. Figure 8 shows the position as estimated using inertial/magnetic sensor module data. Both axes are plotted in meters. The starting and ending point for the foot was the same point. This point is (0, 0) in the plot. Although truth reference data is not available as of the time of this writing, the accuracy of 2-D position tracking can be seen by observing that the estimated trajectory returns to the starting point following the period during which the walk occurred with high accuracy.

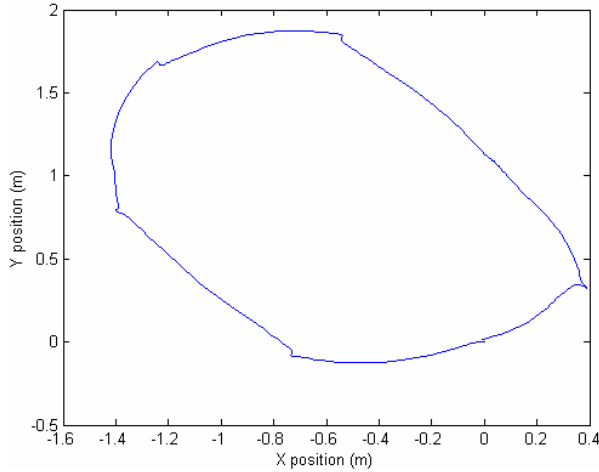


Figure 8. Position tracking of circular walking trajectory.

D. Combined Forward Walking, Side Stepping, and Backward Walking

To demonstrate that the position tracking method can be applied to mixed types of human movement, a 5.5 meter square pattern was measured and marked in an outdoor environment. The test subject followed this marked course by walking forward on the first leg of the square, side stepping to the right on the second leg of the square, walking backward on the third leg of the square, and side stepping to the left on the last leg of the square before the foot was returned to the starting point. Figure 9 shows the position tracking results for this mixed motion experiment. The x-axis is the north direction, and the y-axis is in the east direction. The starting and ending point is again (0, 0). It can be observed that the end point and starting point almost coincide, with a separating distance of 0.08 meters. The estimated total walking distance is 21.6 meters, while the actual total distance is 22.0 meters giving a distance estimation error of 1.8%.

E. Climbing Stairs

The inertial/magnetic sensor module provides

3-dimensional acceleration measurements in x-, y-, and z-axes. Thus, it is possible to track 3-dimensional position. The experiments described so far were primarily concerned with correcting and integrating x- and y-axis acceleration. Vertical axis acceleration can be corrected and integrated in the same manner in order to estimate relative height. Figure 10 depicts the 3-D estimated trajectory of a person who climbed stairs shown in Figure 11. It can be qualitatively observed that the estimated trajectory in Figure 10 closely resembles the actual profile of stairs.

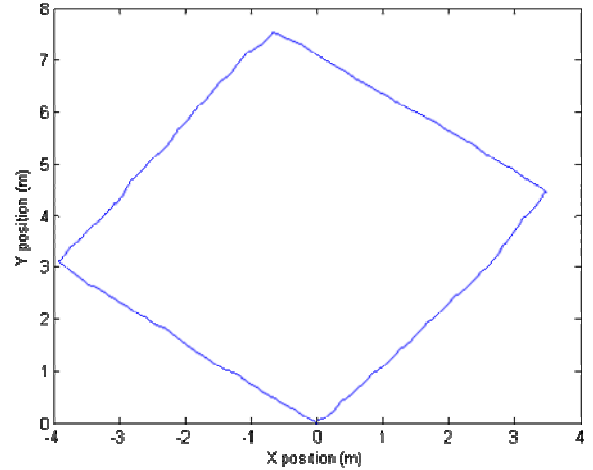


Figure 9. Position tracking results of combined forward walking, side stepping, and backward walking.

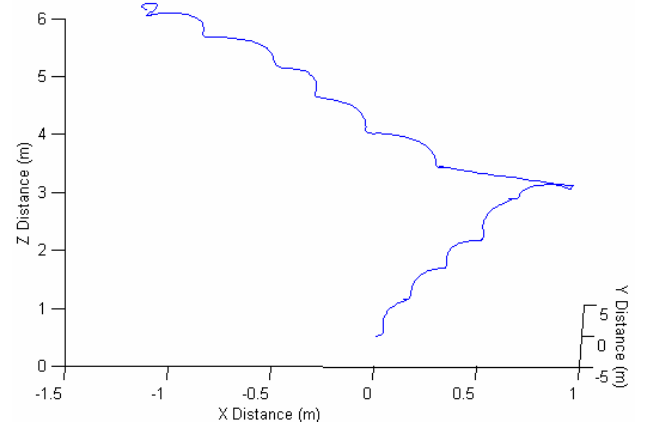


Figure 10. Estimated 3-D position of a person climbing stairs shown in the next figure.

V. WORK IN PROGRESS

At the time of this writing further experiments are being conducted to evaluate, improve, and document the accuracy of position estimation using inertial/magnetic sensor modules. These experiments include mixed motion types and additional tracking methods for the purpose of providing truth data.

The experimental results provided in this paper were obtained by post-processing the sensor data. Efforts are currently underway to implement a real-time system. This system will be integrated into an immersive virtual simulation.

As seen in the indoor walking experiments, orientation estimation errors caused by a non-uniform magnetic environment can cause errors in transforming data from sensor coordinates to Earth coordinates. A correction method has been devised and is currently being tested.



Figure 11. Photo of the stairs used in the experiment for estimating 3-D position.

VI. CONCLUSION

Self-contained position tracking using data from inertial/magnetic modules has applicability to a wide number of applications. Preliminary experimental results presented in this paper document that this technique can be used to track three dimensional position during a variety of motion types. Estimated errors from these experiments indicate that the method is accurate. Work is currently underway to further refine the method.

REFERENCES

- [1] Kong Y.Chen and David R. Bassett Jr., *The Technology of Accelerometry-Based Activity Monitors: Current and Future*, Medicine & Science in Sports & Exercise. 37(11) Supplement:S490-S500, November 2005.
- [2] Scott. E. Crouter, Patrick L. Schneider, Murat Karabulut, and David R. Bassett Jr., "Validity of 10 Electronic Pedometers for Measuring Steps, Distance, and Energy Cost," *Medicine and Science in Sports and Exercise*, 35(8):1455-1460, August 2003.
- [3] Patrick L. Schneider, Scott E. Crouter, Olivera Lukajic, and David R. Bassett Jr., "Accuracy and Reliability of 10 Pedometers for Measuring Steps over a 400-m Walk," *Medicine & Science in Sports & Exercise*. 35(10):1779-1784, October 2003.
- [4] Ion P. I Pappas, Milos R. Popovic, Thierry Kell, Volker Dietz, and Manfred Morari, "A Reliable Gait Phase Detection System," *IEEE Transactions on Neural Systems and Rehabilitation Engineering*, Volume: 9, Issue: 2, June 2001.
- [5] Wiebren Zijlstra and At L. Hof, "Displacement of the pelvis during human walking: experimental data and model predictions," *Gait and Posture*, Volume 6, Number 3, December 1997.
- [6] Wiebren Zijlstra and At L. Hof, "Assessment of spatio-temporal gait parameters from trunk accelerations during human walking," *Gait & Posture*, Volume 18, Issue 2, October 2003.
- [7] Koichi Sagawa, Yutaka Satoh, and Hikaru Inooka, "Non-restricted Measurement of Walking Distance," *Proceedings of IEEE International Conference on Systems, Man, and Cybernetics*, Volume 3, Nashville, TN., October 200.
- [8] Angelo M. Sabatini, Chiara Martelloni, Sergio Scapellato, and Filippo Cavallo, "Assessment of walking features from foot inertial sensing," *IEEE Transactions on Aerospace and Electronics Systems*, vol. 52, no. 3, pp. 486-494, Mar. 2005.
- [9] Filippo Cavallo, Angelo M. Sabatini, and Vincenzo Genovese, "A step toward GPS/INS personal navigation systems: real-time assessment of gait by foot inertial sensing," *Proceedings of IEEE/RSJ International Conference on Intelligent Robots and Systems*, 2005. (IROS 2005), Edmonton, Alberta, Canada, August 2005.
- [10] Rommanee Jirawimut, Piotr Ptansinski, Vanja Garaj, Franjo Cecelja, and Wamadeva Balachandran, "A Method for Dead Reckoning Parameter Correction in Pedestrian Navigation System," *IEEE Transactions on Instrumentation & Measurement*, Vol. 52 Issue 1, February 2003.
- [11] C. Tom Judd, "A Personal Dead Reckoning Module," *Proceeding of the Institute of Navigation (ION FPS-97)* Kansas City, MO., September, 1997.
- [12] Quentin Ladetto, Bertrand Merminod, "In Step With INS," *GPS World*, October 2002.
- [13] Vectronix (2005), "Position Yourself Anytime!", Vectronix AG, Max-Schmidheiny-Strasse 202, CH-9435 Heerbrugg, Switzerland, Available: www.vectronix.ch.
- [14] Michael May, "Seamless Outdoor/Indoor Navigation for Blind and Visually Impaired Individuals," *Technology and Persons with Disabilities Conference*, Los Angeles, CA., March 2006.
- [15] Pamela K. Kevangie and Cynthia C. Norkin, *Joint Structure and Function*, F.A. Davis Company, Philadelphia, PA, Third Edition, 2001.
- [16] Eric B. Bachmann, Xiaoping Yun, Doug McKinney, Robert B. McGhee, and Michael J. Zyda, "Design and Implementation of MARG Sensors for 3-DOF Orientation Measurement of Rigid Bodies," *Proceedings of 2003 IEEE International Conference on Robotics and Automation*, Taipei, Taiwan, September 2003.
- [17] MicroStrain Inc., <http://www.microstrain.com/>
- [18] MemSense LLC., <http://www.memsense.com/>
- [19] Xsens Technologies B.V., <http://www.xsens.com/>
- [20] InterSense Inc. <http://www.isense.com/>
- [21] X. Yun, C. Aparicio, E. Bachmann, and R. McGhee, "Implementation and Experimental Results of a Quaternion-Based Kalman Filter for Human Body Motion Tracking," *Proceedings of the 2005 IEEE International Conference on Robotics and Automation*, Barcelona, Spain, April 2005.
- [22] Eric R. Bachmann, Xiaoping Yun, and Christopher W. Peterson, C., "An Investigation of the Effects of Magnetic Variations On Inertial/Magnetic Orientation Sensors," *Proceedings of the 2004 IEEE International Conference on Robotics and Automation*, New Orleans, LA, April - May 2004.

Implementation and Experimental Results of a Quaternion-Based Kalman Filter for Human Body Motion Tracking

Xiaoping Yun, Conrado Aparicio, Eric R. Bachmann⁺, and Robert B. McGhee

Naval Postgraduate School, Monterey, CA 93943, USA

⁺*Miami University, Oxford, OH 45056, USA*

Abstract - A human body motion tracking system based on use of the MARG (Magnetic, Angular Rate, and Gravity) sensors has been under development at the Naval Postgraduate School and Miami University. The design of a quaternion-based Kalman filter for processing the MARG sensor data was described in [1]. This paper presents the real-time implementation and testing results of the quaternion-based Kalman filter. Experimental results validate the Kalman filter design, and show the feasibility of the MARG sensors for real-time human body motion tracking.

Index Terms – *Quaternion-based Kalman filter, human body motion tracking, MARG sensors, inertial/magnetic sensors.*

I. INTRODUCTION

Inertial/magnetic sensor modules can be used to estimate orientation of a rigid body relative to an Earth fixed reference frame without the need of an artificially generated reference. The estimates produced are based entirely on inertial quantities related to the motion and attitude of the module and the orientation of the ambient magnetic field relative to the module. If a single sensor module is placed on each of the segments of an articulated rigid body, the “posture” of the structure can be determined. Such “sourceless” orientation tracking has significant advantages over other methods owing to its low susceptibility to various sources of noise and lack of range limitations [8,9]. If the human body is modeled as articulated rigid bodies consisting of approximately fifteen segments, posture and gait could be accurately tracked and measured over an unlimited area. Thus, this methodology of body tracking could have important applications in virtual environments, robotic teleoperation, personal navigation, and human monitoring applications [10].

The Naval Postgraduate School and Miami University have teamed up to develop an inertial/magnetic sensor module called the MARG sensor for tracking human body motions in real time [2]. MARG (Magnetic, Angular Rate, and Gravity) sensor modules contain three magnetometers, three angular rate sensors, and three accelerometers. Each sensor type is orthogonally mounted in a triad. This paper presents the implementation and experimental testing results for a quaternion-based Kalman filter designed for the MARG sensors.

An earlier version of the Kalman filter implemented here was described in [1]. The overall filter design remains unchanged. However, some portions of the filter design

have been modified. In particular, the original design used a reduced-order Gauss-Newton method to compute an orientation quaternion from accelerometer and magnetometer measurements. This part of the filter was first modified to use the QUEST Algorithm [3] and later the Factored Quaternion Algorithm [4,5]. The QUEST algorithm [3,6] was created to determine the attitude of a rigid body in reference to a fixed coordinate system, using a set of measurement vectors. The algorithm computes a rotation (attitude) quaternion that rotates the measurement vectors to match the reference vectors. More recently, the Factored Quaternion Algorithm [4] was derived. It has the same goal as the QUEST algorithm but orientation estimate are derived through the measurement of sequential rotations about three orthogonal axes. It has been shown that the Factored Quaternion Algorithm has equal or better performance than the QUEST algorithm in estimating orientation quaternions with MARG sensor measurements [5]. Nevertheless, the Factored Quaternion Algorithm is computationally more efficient by about 25%, and is thus used as part of the filter design in the latest implementation [5].

This paper is organized as follows. Section II presents the process model of the Kalman filter for human body motion tracking. Section III describes implementation issues of the Kalman filter with a focus on how the nonlinear process model was first linearized and then discretized. Experimental modeling of the process noise covariance matrix and the measurement noise covariance matrix is also detailed. Section IV reports the MATLAB simulation and offline testing results of the Kalman filter. Section V describes the implementation and testing results, followed by conclusions in section VI.

II. KALMAN FILTER PROCESS MODEL

The process model of the quaternion-based Kalman filter presented in [1] will be briefly reviewed in this section. A diagram of the process model is shown in Figure 1. In this model, the angular rates ω in body coordinates are assumed to be generated by a first-order linear system with a white noise forcing function w . The time constant of the first-order linear system is τ . The orientation estimate produced by the filter is \hat{q} . The angular rates ω and the quaternion derivative \dot{q} are related by [7]:

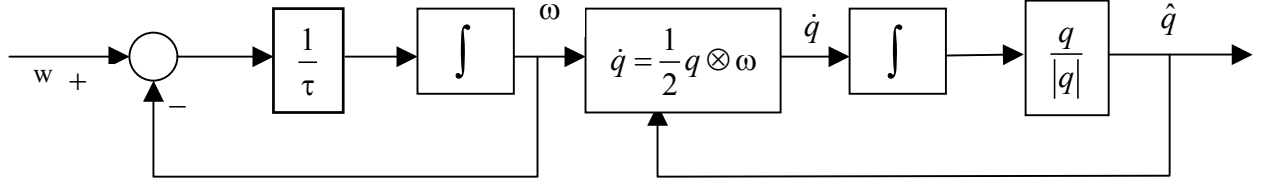


Figure 1. Kalman Filter Process Model.

$$\dot{q} = \frac{1}{2} q \otimes \omega \quad (1)$$

where q is the orientation quaternion in Earth coordinates, and \otimes represents quaternion multiplication. In order to take advantage of computational simplifications and efficiencies possible of unit quaternions, the quaternion is normalized to unit length in the last step of the process model. It is noted that quaternions are used to represent orientation in the filter design because quaternions do not have the singularity problem associated with Euler angles and eliminate the computational expenses related to approximation of transcendental functions.

The state vector is defined as a 7-dimensional vector with the first three components being the angular rates and the last four being the elements of the quaternion. The process model expressed in terms of state equations is characterized as follows:

$$\dot{x}_i = -\frac{1}{\tau_i} x_i + \frac{1}{\tau_i} w_i(t) \quad i = 1, 2, 3 \quad (2)$$

for the angular rates, and

$$\dot{x}_4 = -\frac{1}{2} [x_1 x_5 + x_2 x_6 + x_3 x_7], \quad (3)$$

$$\dot{x}_5 = \frac{1}{2} [x_1 x_4 - x_2 x_7 + x_3 x_6], \quad (4)$$

$$\dot{x}_6 = \frac{1}{2} [x_1 x_7 + x_2 x_4 - x_3 x_5], \quad (5)$$

$$\dot{x}_7 = \frac{1}{2} [-x_1 x_6 + x_2 x_5 + x_3 x_4] \quad (6)$$

for the quaternion components.

The MARG sensor provides a 9-dimensional measurement vector, consisting of three elements of the linear acceleration vector, three elements of the local magnetic field, and three elements of the angular rate vector. If this nine-dimensional measurement vector is provided directly to the Kalman filter as measurements, the measurement equations are nonlinear and the resulting Kalman filter becomes complex and computationally expensive. An alternative approach to the Kalman filter design was suggested in [1]. This approach uses the Newton method or a reduced-order Gauss-Newton method to find a quaternion corresponding to each set of accelerator and magnetometer measurements. These computed quaternion and angular rate measurements are then presented to the Kalman filter as measurements. As a result,

the measurement equation for the Kalman filter is linear and is given by:

$$z = Hx + v(t) \quad (7)$$

where z is the seven-dimensional measurement vector, H is a 7×7 identity matrix, and v is the vector of measurement noises.

Although the reduced-order Gauss-Newton method presented in [1] was considerably more efficient than the full-order Gauss-Newton method, it still is an iterative method that needs to be executed several times before convergence occurs. Following additional work, the reduced-order Gauss-Newton method was replaced by the QUEST Algorithm [3,6], and more recently by the Factored Quaternion Algorithm [4]. Both the QUEST Algorithm and Factored Quaternion Algorithm take a set of the accelerometer and magnetometer measurements and produce an orientation quaternion. They are appropriate for orientation estimation in static or slow moving applications where linear acceleration does not comprise a significant part of the total acceleration measurements. The Factored Quaternion Algorithm is computationally about 25% more efficient than the QUEST Algorithm.

III. KALMAN FILTER IMPLEMENTATION

In this section, the implementation of the Kalman filter based on the process model presented in the previous section will be described. It is noted that although Equation (2) is linear, Equations (3) to (6) are nonlinear. As a result, an extended Kalman filter must be used. Additionally, these continuous equations must be discretized for digital implementations.

A. Discrete Extended Kalman Filter

Equations (2) to (6) can be written in vector form as follows:

$$\dot{x} = f(x) + w(t). \quad (8)$$

This nonlinear state equation is linearized along the currently estimated trajectory \hat{x} :

$$\Delta \dot{x} = \left. \frac{\partial f}{\partial x} \right|_{x=\hat{x}} \Delta x + w(t), \quad (9)$$

where the actual trajectory, x , is the sum of estimated trajectory \hat{x} and the small increment Δx

$$x = \hat{x} + \Delta x. \quad (10)$$

Equation (9) is linear, but it is still in the continuous time domain. The next step is to discretize it to obtain a discrete

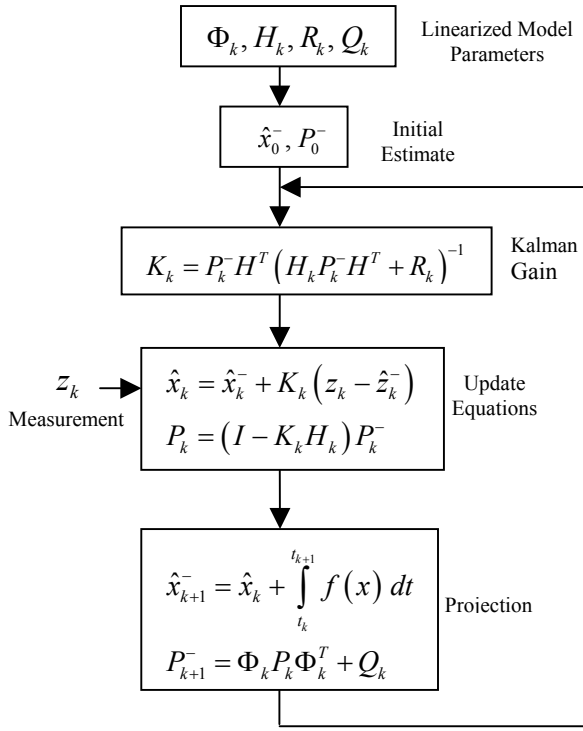


Figure 2. Diagram of the extended Kalman filter.

time process model. Let Δt be the sampling interval. Then the difference equation corresponding to the differential equation (9) is given by:

$$\Delta x(t_{k+1}) = \Phi_k \Delta x(t_k) + w(t_k) \quad (11)$$

where the discrete state transition matrix is:

$$\Phi_k = \begin{bmatrix} e^{\frac{\Delta t}{\tau_1}} & 0 & 0 & 0 & 0 & 0 & 0 \\ 0 & e^{\frac{\Delta t}{\tau_2}} & 0 & 0 & 0 & 0 & 0 \\ 0 & 0 & e^{\frac{\Delta t}{\tau_3}} & 0 & 0 & 0 & 0 \\ -\frac{\hat{x}_5 \Delta t}{2} & -\frac{\hat{x}_6 \Delta t}{2} & -\frac{\hat{x}_7 \Delta t}{2} & 1 & -\frac{\hat{x}_1 \Delta t}{2} & -\frac{\hat{x}_2 \Delta t}{2} & -\frac{\hat{x}_3 \Delta t}{2} \\ \frac{\hat{x}_4 \Delta t}{2} & \frac{\hat{x}_7 \Delta t}{2} & \frac{\hat{x}_6 \Delta t}{2} & \frac{\hat{x}_1 \Delta t}{2} & 1 & \frac{\hat{x}_3 \Delta t}{2} & -\frac{\hat{x}_2 \Delta t}{2} \\ \frac{\hat{x}_7 \Delta t}{2} & \frac{\hat{x}_4 \Delta t}{2} & -\frac{\hat{x}_5 \Delta t}{2} & \frac{\hat{x}_2 \Delta t}{2} & -\frac{\hat{x}_3 \Delta t}{2} & 1 & \frac{\hat{x}_1 \Delta t}{2} \\ -\frac{\hat{x}_6 \Delta t}{2} & \frac{\hat{x}_5 \Delta t}{2} & \frac{\hat{x}_4 \Delta t}{2} & \frac{\hat{x}_3 \Delta t}{2} & \frac{\hat{x}_2 \Delta t}{2} & -\frac{\hat{x}_1 \Delta t}{2} & 1 \end{bmatrix}$$

and the elements of discrete white noises are given by:

$$w_i(t_k) = \begin{cases} \int_{t_k}^{t_{k+1}} e^{-\frac{(t_{k+1}-\gamma)}{\tau_i}} w_i(\gamma) d\gamma & i = 1, 2, 3 \\ 0 & i = 4, 5, 6, 7 \end{cases} \quad (12)$$

Equation (7) is linear. Thus, linearization is not needed. The corresponding discrete process model equation is simply given as:

$$z_k = H_k x_k + v_k \quad (13)$$

A standard discrete Kalman filter may now be designed for the discrete process equation (11) and the discrete

measurement equation (13). A complete diagram of the extended Kalman filter is depicted in Figure 2.

B. Modeling of Process and Measurement Noises

In order to implement the Kalman filter described above, it is necessary to determine values of the process noise covariance matrix Q_k and the measurement noise covariance matrix R_k . These matrices represent the confidence in the system model and the measurement data, respectively.

The process noise matrix Q_k is given by:

$$Q_k = E[w(t_k)w(t_k)^T] \quad (14)$$

where E is the expectation operator, and $w(t_k)$ is the discrete white noise of Equation (12).

It is noted that $w_i(\gamma)$ in Equation (12) is the continuous, independent white noise process of Equations (2) to (6), with zero mean and variance D_i . Therefore,

$$E[w_i(t)w_j(\tau)] = \begin{cases} D_i \delta(t - \tau) & i = j \\ 0 & i \neq j \end{cases} \quad (15)$$

This implies that the process noise matrix is a diagonal matrix with non-zero elements only in the first three positions of the main diagonal, and can be computed using Equations (14) to (15) as

$$Q_k = \begin{bmatrix} q_{11} & 0 & 0 & 0 & 0 & 0 & 0 \\ 0 & q_{22} & 0 & 0 & 0 & 0 & 0 \\ 0 & 0 & q_{33} & 0 & 0 & 0 & 0 \\ 0 & 0 & 0 & 0 & 0 & 0 & 0 \\ 0 & 0 & 0 & 0 & 0 & 0 & 0 \\ 0 & 0 & 0 & 0 & 0 & 0 & 0 \\ 0 & 0 & 0 & 0 & 0 & 0 & 0 \end{bmatrix} \quad (16)$$

where q_{11} , q_{22} , and q_{33} are given by:

$$q_{11} = E[w_1(t_k)w_1(t_k)] = \frac{D_1}{2\tau_1} \left(1 - e^{-\frac{2\Delta t}{\tau_1}} \right), \quad (17)$$

$$q_{22} = E[w_2(t_k)w_2(t_k)] = \frac{D_2}{2\tau_2} \left(1 - e^{-\frac{2\Delta t}{\tau_2}} \right), \quad (18)$$

and

$$q_{33} = E[w_3(t_k)w_3(t_k)] = \frac{D_3}{2\tau_3} \left(1 - e^{-\frac{2\Delta t}{\tau_3}} \right). \quad (18)$$

Up to this point, the variance of the white noise processes D_i and the time constants of the process model τ_i have been assumed known. To implement the Kalman filter, these parameters must be determined.

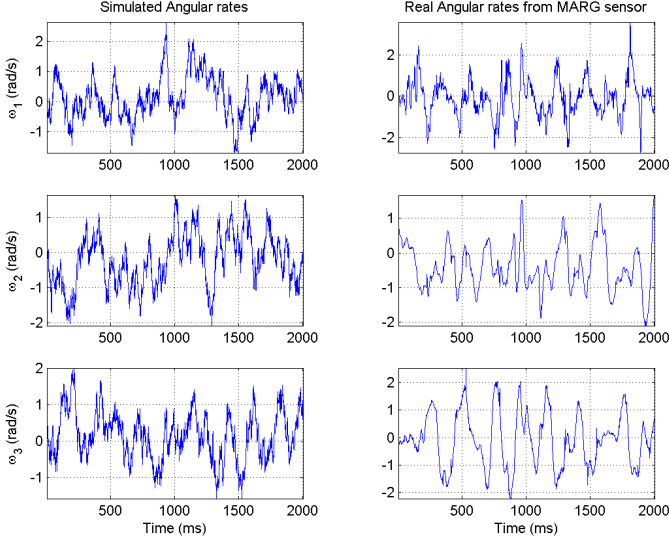


Figure 3. Simulated angular rate (left) and actual angular rate measurements (right).

Using measurement data available from the MARG sensors, the variances and time constants can be found using a simulated process model for the angular rates, where the variance and time constants are adjusted until the output of the simulated model closely matched the real data collected from the MARG sensors. For this purpose, a sensor was attached to the arm of a person and typical arm motion data was collected.

The resultant variances and time constants are shown in Table 1, where ω_1 , ω_2 and ω_3 are respectively the angular rates about the x , y , and z body coordinate axes.

Table 1. White noise variance and the time constant of the linear system.

Angular rate	Variance D_i (rad^2/s^2)	Time constant τ_i (s)
ω_1	50	0.5
ω_2	50	0.5
ω_3	50	0.5

Figure 3 shows a comparison between the simulated angular rates and the actual angular rates obtained from a MARG III sensor for typical arm motions. The graphs to the left represent the angular rates generated by the simulation model. The graphs to the right are the angular rates measured by a MARG sensor. It can be observed that the two sets of data exhibit similar characteristics.

The measurement noise covariance matrix R_k represents the level of confidence placed in the accuracy of the measurements, and is given by:

$$R_k = E[v(t_k)v(t_k)^T]. \quad (19)$$

Assuming that measurements are uncorrelated, Equation (19) leads to the following expression for the measurement noise covariance matrix:

$$R_k = \begin{bmatrix} r_{11} & 0 & 0 & 0 & 0 & 0 & 0 \\ 0 & r_{22} & 0 & 0 & 0 & 0 & 0 \\ 0 & 0 & r_{33} & 0 & 0 & 0 & 0 \\ 0 & 0 & 0 & r_{44} & 0 & 0 & 0 \\ 0 & 0 & 0 & 0 & r_{55} & 0 & 0 \\ 0 & 0 & 0 & 0 & 0 & r_{66} & 0 \\ 0 & 0 & 0 & 0 & 0 & 0 & r_{77} \end{bmatrix}. \quad (20)$$

The diagonal elements are the variances of the individual measurements, which can be determined experimentally using measurement data from the MARG sensors. For this purpose, the measurements from a static MARG sensor were collected. Table 2 summarizes the values derived from experimental measurements.

Table 2. Elements of the measurement noise covariance matrix.

r_{11}	r_{22}	r_{33}	r_{44}	r_{55}	r_{66}	r_{77}
0.01	0.01	0.01	0.0001	0.0001	0.0001	0.0001

Table 3. Convergence of the quaternion estimate.

Sample	\hat{q}_0	\hat{q}_1	\hat{q}_2	\hat{q}_3
1	0.99985	0.0082135	0.0066032	0.01357
2	0.99991	0.0057585	0.0049037	0.011901
3	0.9999	0.0055983	0.0048826	0.011882
4	0.9999	0.005288	0.0046884	0.011784
5	0.9999	0.0052297	0.0046353	0.011506

IV. MATLAB IMPLEMENTATION AND TESTING

After deriving all the required parameters to initialize the Kalman filter, it was implemented using MATLAB to test the performance and accuracy of the quaternion orientation estimates produced by the extended Kalman filter. Real world data recorded using a MARG sensor was used in these tests.

Since the Kalman gain was determined such that the sum of squared errors is minimized, one way to measure the performance of the Kalman filter is through examination of

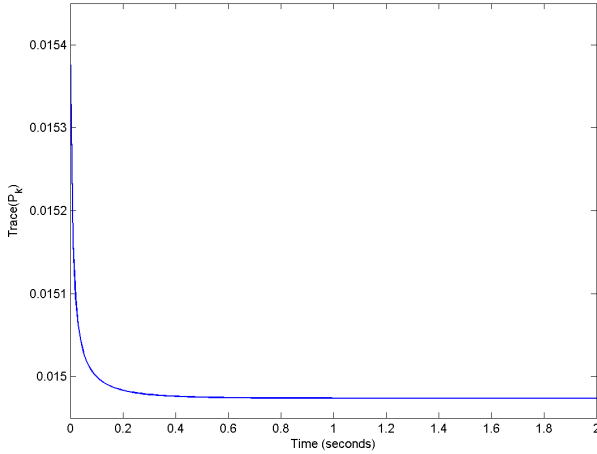


Figure 4. Trace of the error covariance matrix.

the trace of the error covariance matrix P_k . Figure 4 shows the trace of P_k for the first 200 samples of data obtained with the sensor in its reference position (x axis pointing north, y axis pointing East, and z axis point down). It is noted, that the sum of squared errors reaches a steady state after approximately 60 iterations.

Table 3 shows the elements of the quaternion for the first five samples. The initial estimate was chosen to be the unit quaternion $(0.5, 0.5, 0.5, 0.5)$. The actual position of the sensor in the reference position is represented by the quaternion $(1, 0, 0, 0)$. The data shown in Table 3 indicates that the Kalman filter estimate converged to the actual position in a single iteration.

While both the QUEST Algorithm and the Factored Quaternion Algorithm worked well for static orientation and slow movements, the objective of the Kalman filter is to blend angular rate measurements with the estimates produced using magnetometer and accelerometer data during periods in which the sensor module is subjected to motions involving high angular rates and large linear accelerations. To verify the estimation accuracy during such periods, the orientation estimates of the Kalman filter were compared to the estimates produced using only the Factored Quaternion Algorithm with no rate measurement. Two kinds of experiments were conducted for this test. The first used controlled rotations produced by a HAAS precision tilt table. The second used a random motion pattern produced while the sensor was attached to the arm of a person.

In the first set of experiments, the sensor was initially placed at the end of a 1-meter pole attached to the rotating table with its xyz axes aligned with West-North-Down directions. The sensor was rotated 90° about the y -axis at a rate of $60^\circ/\text{s}$ and then rotated -90° at the same rate (in the reverse direction). Figure 5 shows the performance of the Kalman filter in estimating the orientation of the sensor. The graphs to the left show the orientation estimated by the Factored Quaternion Algorithm, and the graphs to the right show the orientation estimated by the Kalman filter. It can be seen that the Factored Quaternion Algorithm was able to

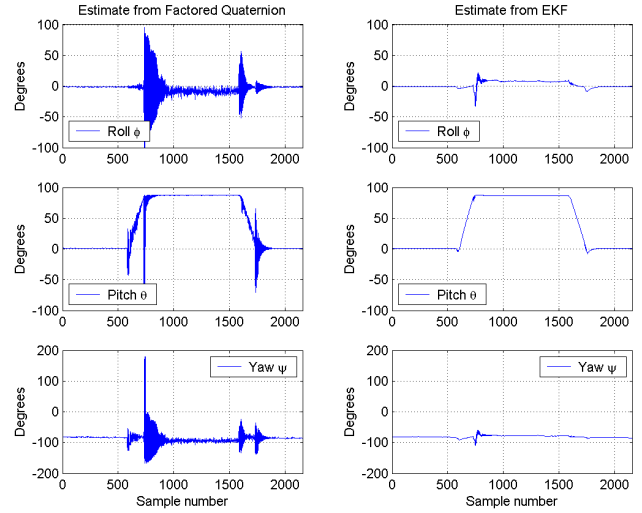


Figure 5. Quaternion estimates produced by the Factored Quaternion Algorithm (left) and Kalman filter (right) with a 90° -degree rotation in pitch axis.

correctly estimate the pitch angle before the first (positive) rotation, between the first and second rotations, and after the second (negative) rotation, but it is not able to correctly estimate orientation during the rotational motions. Large errors in roll and yaw were also produced by the Factored Quaternion Algorithm. On the other hand, it can be seen from the right-center plot that the Kalman filter was able to correctly estimate the pitch angle throughout the duration of the experiment. The small roll and yaw motions seen in the top-right and bottom-right plots are due to misalignment of the individual sensor components within the MARG sensor module.

Figure 6 shows the results of an experiment in which the sensor was rotated randomly while attached to the arm of a person. Although there is no true reference in this case, it can be seen that the Kalman filter eliminated the jittering and spiking contained in the orientation estimates produced by using the Factored Quaternion Algorithm alone.

V. REAL-TIME TESTING RESULTS

After initial testing of the extended Kalman filter with the MATLAB implementation, the Factored Quaternion Algorithm and extended Kalman filter algorithm were implemented in Java for real-time testing and evaluation. The real-time quaternion produced by the Kalman filter was visualized by a human-like avatar called “Andy” as seen in Figure 7. Two MARG sensors were used to track the motion of a human arm, one sensor being attached to the upper arm and the other attached to the lower arm.

The Factored Quaternion Algorithm was able to track the motion of the human arm under slow moving conditions where linear acceleration was not significant. However, when the arm motion became faster, the algorithm was not able to follow the arm motion resulting in observable lag as well as overshoots.

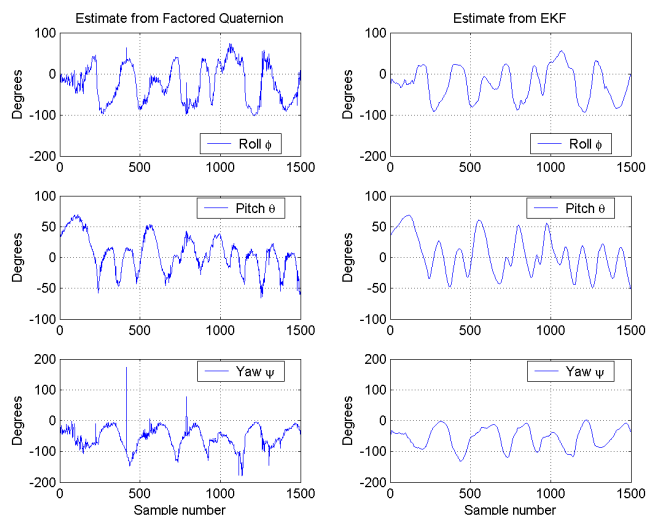


Figure 6. Quaternion estimates produced by the Factored Quaternion Algorithm (left) and Kalman filter (right) with random arm movements.

When the extended Kalman filter was integrated with the Factored Quaternion Algorithm, the avatar was able to successfully track the human arm motion in real time under all conditions. Furthermore, the filtering process did not produce any noticeable lag. Movement of the human arm and the avatar was synchronized.

V. CONCLUSIONS

The paper presents implementation and experimental results for a quaternion-based Kalman filter designed for real-time human body motion tracking using the MARG sensors. A simple process model designed for human body motion tracking was first introduced. The model was then linearized and discretized. Experimental determination of error covariance matrices was described. An extended Kalman filter was implemented, first in MATLAB for offline evaluation and finally in Java for real-time testing and evaluation. The estimated orientation quaternion was visualized using a human avatar. Testing results indicated that the Kalman filter performed satisfactorily for tracking motions of a human arm in real time under all conditions.

ACKNOWLEDGMENT

This research was supported in part by Army Research Office (ARO), Navy Modeling and Simulation Management Office (N6M). Authors would like to thank James Calusdian for his technical support during the course of this project, and to thank Doug McKinney for collaboration on the MARG sensors and Control Interface Unit (CIU).

DISCLAIMER

The views expressed in this paper are solely those of the authors, and do not reflect the opinions of the Naval Postgraduate School, Department of Navy, Department of Defense, or U.S. Government.

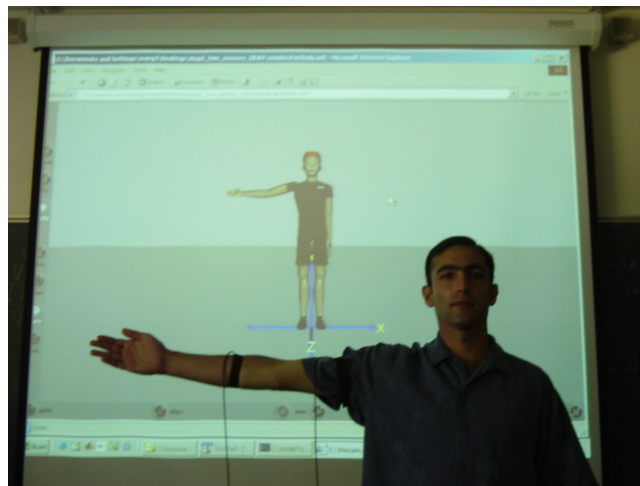


Figure 7. A snapshot of real-time testing.

REFERENCES

- [1] Xiaoping Yun, Mariano Lizarraaga, Eric R. Bachmann, and Robert B. McGhee, "An Improved Quaternion-Based Kalman Filter for Real-Time Tracking of Rigid Body Orientation," Proceedings of the 2003 IEEE/RSJ International Conference on Intelligent Robots and Systems, pp. 1074-1079, Las Vegas, Nevada, October 2003.
- [2] E.R. Bachmann, Xiaoping Yun, D. McKinney, R.B. McGhee, M.J. Zyda, "Design and Implementation of MARG Sensors for 3-DOF Orientation Measurements of Rigid Bodies," Proceedings of 2003 IEEE International Conference on Robotics and Automation, pp. 1171-1178, Taipei, Taiwan, September 14-19, 2003.
- [3] M.D. Shuster and S.D. Oh, "Three-Axis Attitude Determination from Vector Observations," Journal of Guidance and Control, Vol. 4, No. 1, pp. 70-77, January-February 1981.
- [4] Robert B. McGhee, "The Factored Quaternion Algorithm for Orientation Estimation from Measured Earth Gravity and Magnetic Field," Technical Memorandum, MOVES Institute, Naval Postgraduate School, Monterey, CA, June 2004. <http://www.users.muohio.edu/bachmaer/Papers/Factored%20Quaternion.pdf>
- [5] Conrado Aparicio, "Implementation of a Quaternion-Based Kalman Filter for Human Body Motion Tracking Using MARG Sensors," Master's Thesis, Naval Postgraduate School, Monterey, CA, September 2004.
- [6] F. Landis Markley and Daniele Mortari, "Quaternion Attitude Estimation Using Vector Observations," The Journal of the Astronautical Sciences, Vol. 48, No. 2-3, pp. 359-380, 2000.
- [7] Jack B. Kuipers, Quaternions and Rotation Sequences, Princeton University Press, Princeton, NJ, 1999.
- [8] K. Meyer, H. Applewhite, and F. Biocca, "A Survey of Position Trackers," Presence: Teleoperators and Virtual Environments, Vol. 1, No. 2, pp. 173-200, 1992.
- [9] D.M. Gavrilu, "The Visual Analysis of Human Movement: A Survey," Computer Vision and Image Understanding, Vol. 73, No. 1, January 1999, pp. 82-98.
- [10] Michael Macedonia, "Games Soldiers Play," IEEE Spectrum, March 2003, pp. 32-37.

Design and Implementation of the MARG Human Body Motion Tracking System

Xiaoping Yun, Eric R. Bachmann⁺, Andreas Kavousanos-Kavousanakis, Faruk Yildiz, Robert B. McGhee

Naval Postgraduate School, Monterey, CA 93943, USA

⁺Miami University, Oxford, OH 45056, USA

Abstract—Real-time tracking of human body motion has applications in tele-operation, synthetic reality and others. A motion tracking system based on use of the MARG sensors has been under development at Naval Postgraduate School and Miami University. The Magnetic, Angular Rate, and Gravity (MARG) sensor modules use a combination of three orthogonal magnetometers, three orthogonal angular rate sensors, and three orthogonal accelerometers to measure 3-D orientation of individual limb segments in order to determine posture. This paper presents the latest results of the MARG human body motion tracking system. The design and implementation of a Control Interface Unit (CIU), a real-time 3-D human avatar called “Andy,” and a concurrent client-server program are discussed. Experimental testing and evaluation of the overall MARG system is also presented. The system is able to track multiple human limbs in real time. The captured human motion data can be visualized over the Internet by multiple clients using the 3-D avatar.

Keywords - Human body motion tracking; MARG sensors; avatar; wireless communication.

I. INTRODUCTION

Accurate real-time tracking of human body motion is important for many applications that involve human-machine interactions. One such application is in virtual training [1]. Real-time motion tracking makes it possible to create immersive virtual environments in which trainees will act and react as if the environments were real. Captured human motion data can also be used to control humanoid robots [1] [3]. Measurements of human body movements can be used to estimate physical and mental conditions of patients in clinical applications [4]. Motion tracking of human movements is widely used in sports training and production of animated movies.

There are a number of technologies for tracking human body motion, including mechanical trackers, active magnetic trackers, optical tracking systems, acoustic tracking systems, and inertial tracking systems [5][6][7]. Among the inertial tracking systems, Sakaguchi et al. [8] describes a gyroscope and accelerometer-based motion tracking system for tracking human arm motion. Lee and Ha [9] reports a study of human motion tracking using only accelerometers. There are broadly two kinds of image-based motion tracking methods. One method requires markers on the tracked human body, and other method does not use markers.

OPTOTRAK from Northern Digital Inc. is a typical example of a marker-based system [10]. Another is the motion tracking method developed for the CAVE system [11]. Marker-free methods are in general preferred because they are less cumbersome [12][13]. In most cases, multiple cameras are used to overcome occlusion problems and to construct 3-D motion data from 2-D images [14][15].

This paper presents a MARG sensor-based motion tracking system. The Magnetic, Angular Rate, and Gravity (MARG) sensor modules use a combination of magnetometers, angular rate sensors, and accelerometers to measure 3-D angular motion of rigid bodies. MARG sensors are self-contained, and do not require any artificially generated sources. They are constructed using MEMS sensors. As a result, they are small and are power-efficient. MARG sensor module design and implementation details were presented in [16]. A quaternion-based Kalman filter used to process MARG data was discussed in [17].

This paper presents other components of the MARG human motion tracking system, and experimental testing results of the overall system. These presented components include the Control Interface Unit (CIU), the 3-D human avatar, “Andy,” and a client-server protocol for transmitting MARG animation data. The CIU is designed to provide control signals to and multiplex measurement data from multiple MARG sensor modules. It packages measurement data from up to 16 MARG sensors for wireless transmission using the 802.11b wireless LAN standard. “Andy,” the human avatar is a cartoon-type avatar developed using X3D [18] and follows the H-Anim specification [19]. It is specialized to allow animation using orientation data expressed relative to an Earth fixed reference frame such as that provided by MARG sensor modules. The MARG human motion tracking system allows multiple clients to visualize the captured human motion over the Internet using the avatar Andy, supported by the client-server program.

II. MARG SENSORS

MARG sensor modules are designed to provide data for measuring 3-DOF orientation in real time without singularities [17]. A more detailed description of the

design and implementation of the third generation prototype can be found in [16]. The dimensions of the MARG III are 28 x 30.5 x 17.3 mm. It weighs approximately 8.5 grams (0.3 oz). Power consumption is 144 mW (20 mA) when powered with 7.2 Volts. Sampling rate is 100 Hz. The MARG III is fabricated by McKinney Technology [20].

The MARG III contains three major sensing components. A pair of the two-axis (HMC1052) and one-axis (HMC1051Z) magnetic sensors are used for low frequency, three dimensional measurement of the direction of the local magnetic field vector. A pair of two-axis Analog Devices ADXL202E acceleration sensors is used for low frequency, three dimensional measurement of the gravity vector relative to the coordinate frame of the sensor module. A triad of orthogonally mounted NEC/TOKIN CG-L43 ceramic angular rate sensors are used for high frequency measurement of sensor module body rates. Two of the three sensing components of the MARG III (the magnetometers and the rate sensors) produce analog data. The Texas Instruments MSP-430F149 microcontroller is a fourth major component in the sensor module. It performs the analog-to-digital conversion of data and transmits digital data to the CIU. After collection and retransmission by the CIU, MARG sensor data is processed by a filter that takes advantage of the complementary characteristics of the installed sensor components [17].

III. CONTROL INTERFACE UNIT (CIU)

A. Role of the Control Interface Unit

When completed, the MARG human motion tracking system will deploy 15 MARG sensors to track motion of 15 limb segments. There is a need to multiplex measurement data from all 15 MARG sensors and transmit them to a network-based computer for processing. For this and other purposes, the concept of the Control Interface Unit (CIU) was introduced. It is a component of the motion tracking system that is designed to be worn by the user at the waist or on the back. All 15 MARG sensors are connected to the CIU by a custom-made cable. Through this cable, the CIU delivers the power and the clock signal to each of the MARG sensors. The MARG sensors transmit measurement data to the CIU. The CIU then multiplexes the measurement data from multiple MARG sensors, and wirelessly transmits the data to a networked PC (server) for processing. The wireless transmission is achieved using the IEEE 802.11b standard.

The MARG sensor communicates with the CIU through a Universal Synchronous Asynchronous Receiver Transmitter (USART) operating in the Synchronous Peripheral Interface (SPI) mode. In this

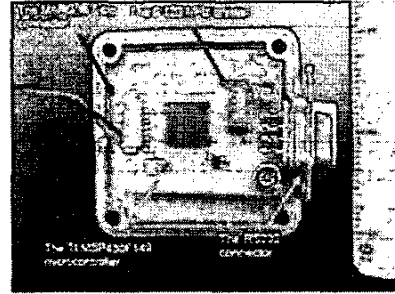


Figure 1. The One-Channel Control Interface Unit (One-Channel-CIU).

configuration, the MARG sensor operates as a slave device whereas the CIU is the master device. The clock signal needed for synchronizing the data transmission is delivered to the MARG sensor by the CIU.

B. The One-channel CIU

The CIU was designed and implemented in stages. A one-channel CIU was designed and implemented first. It connects to one MARG sensor, and delivers the output data by a standard RS232 port. An 802.11b wireless serial adaptor named WiSER2400.IP from OTC Wireless Inc. [21] was utilized for wireless transmission of the output data to the networked PC. A picture of the one-channel CIU is shown in Figure 1. The main component of the one-channel CIU is a TI MSP430F149 microcontroller identical to the one onboard the MARG III sensor.

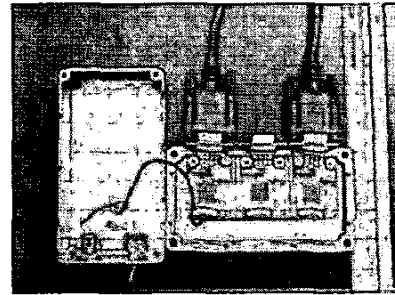


Figure 2. The Three-channel Control Interface Unit (Three-channel CIU).

C. The Three-channel CIU

After the one-channel CIU was designed, implemented, and successfully tested, a three-channel CIU was built. The purpose of the three-channel CIU was to test motion tracking of multiple limb segments with multiple MARG sensors, and to test the operation of

the human avatar Andy and the client-server program (discussed later). The three-channel CIU is shown in Figure 2. It is constructed from three one-channel CIUs in a parallel configuration.

D. The Sixteen-channel CIU

The MARG motion tracking system is designed to simultaneously track 15 limb segments. For this purpose, a sixteen-channel CIU was designed. Sixteen rather than fifteen was chosen because input/output number of multiplexers usually is in power of two. This CIU is to multiplex all measurement data from 16 MARG sensors, packages them in a proper format, and transmit them using a single wireless communication channel. The selected multiplex method was to use a XILINX® Spartan™-II XC2S100 Field Programmable Gate Array (FPGA) [22]. The prototype board of the sixteen-channel CIU is shown in Figure 3.

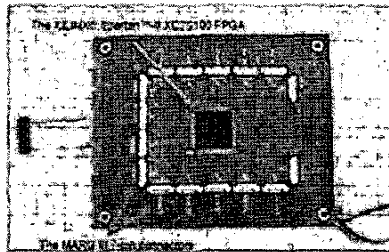


Figure 3. Top View of the Sixteen-channel Control Interface Unit (Sixteen-channel CIU).

TABLE I. THE SIXTEEN-CHANNEL CIU OUTPUT FORMAT

Number of Bytes	Content
2	Communication Synchronization
2	MARG III "Alive" Identification Bits
2	Payload "Health" Status
1	Timing
1	Sample Number
(13.5 + 0.5) x 16 MARG III sensors (Total of 224 bytes)	Payload and MARG III Identification Number
Total: 232 Bytes	

The data format used by the CIU shown in Table 1 consists of 232-byte words, which include the data from all sixteen MARG III sensors and the necessary communication overhead. In the event that one or more MARG III sensors are not connected or that they transmit incorrect data, the FPGA replaces the respective bits with zeros in order to keep a constant transmission rate.

The data for each of the sixteen MARG III sensors consists of the measurements from the three magnetic (Mx, My, Mz), the three angular rate (Rx, Ry, Rz), and the three acceleration sensors (Ax, Ay, Az) onboard the MARG III sensor (nine channels for each sensor). Each channel (transmitted in the order of Rx, Ry, Rz, Ax, Ay,

Az, Mx, My, Mz) occupies one and a half byte, giving a total of 13.5 bytes of data for each MARG III sensor. An identification number of a half a byte is added to associate the data received with the corresponding MARG III sensor. This ID number leads to a total payload of 14 bytes for each MARG III sensor.

An 802.11b wireless LAN OEM module Airborne from DPAC Technologies [23] was used for wireless transmission. The Airborne unit is interfaced to the TI microprocessor onboard the CIU using UART. The data transmission rate is 232 kbps.

IV. HUMAN AVATAR ANDY

Avatar Andy was developed to allow networked viewing of human body motion using a web browser. It is a cartoon-type avatar created using the Extended 3D (X3D) language [18]. It is a modification of the low-resolution avatar named AndyLow, developed by Seamless Solutions, Inc. [24]. AndyLow was originally implemented using the Virtual Reality Modeling Language (VRML) and follows the H-Anim specification [19]. It was converted to X3D, an extended version of VRML [25]. Modification of AndyLow was required due to the characteristics of orientation estimates produced from MARG data [25].

The geometries of all limb segments in the AndyLow avatar are described relative to a single unique reference frame, located at the center point between the feet. Limb segments are arranged in a hierarchy radiating from this reference point with the segments that are closer to the reference being termed "inboard" of those that are further away. Joint rotations for each limb segment must be set using an orientation that is relative to the reference frames of each of the more inboard joints. Limb segment orientation estimates derived from MARG sensor data are given relative to an Earth fixed reference frame. This requires that each limb segment be oriented independently of all other segments. For this reason, AndyLow was incompatible with the system described here. To overcome this drawback, each segment's geometry was redefined using its own local reference position with only a connection point to the parent or next most inboard segment.

The H-Anim specification [19] defines several levels of articulation. Highly detailed levels allow for the individual animation of minor limb segments such as finger joints. Coarser levels only allow individual animation of major limb segments such as the upper leg or lower arm. Level one articulation (LOA-1) is preferred for AndyLow. This level offers 18 joints arranged in a hierarchical human skeleton structure. The MARG system was designed to track up to 15 individual limb segments. Avatar Andy fixes the *sacroiliac*, *l_midtarsal* and *r_midtarsal* joints in order to reduce the total number limb segments to 15. Figure 4 shows the skeleton

structure of the avatar Andy with numbering used to represent the joints. Figure 5 shows Andy in a standing position.

HumanoidRoot : sacrum/pelvis	[0]
l_hip : l_thigh	[1]
l_knee : l_calf	[2]
l_ankle : l_hindfoot	[3]
r_hip : r_thigh	[4]
r_knee : r_calf	[5]
r_ankle : r_hindfoot	[6]
v15 : 15	[7]
skullbase : skull	[8]
l_shoulder : l_upperarm	[9]
l_elbow : l_forearm	[10]
l_wrist : l_hand	[11]
r_shoulder : r_upperarm	[12]
r_elbow : r_forearm	[13]
r_wrist : r_hand	[14]

Figure 4. Hierarchical Skeleton Structure of the Avatar Andy.

Real-time orientation data is supplied to avatar Andy through a Java Script node. The node contains a TCP socket for handling control information and commands. Orientation data is received via a separate UDP socket. The avatar is thus capable of controlling all its 15 joints in networked virtual environments (NVEs).

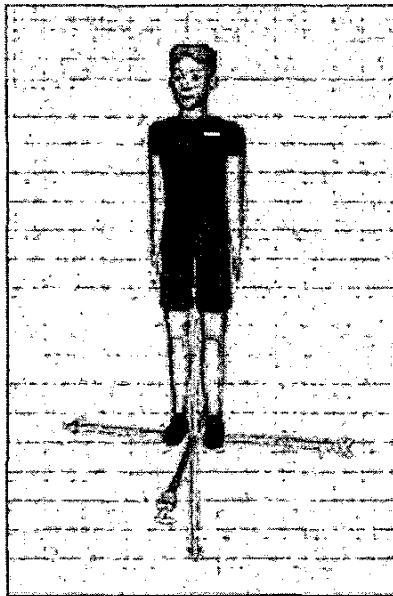


Figure 5. Avatar Andy.

V. CONCURRENT CLIENT-SERVER PROTOCOL

Networking capability was added to the MARG system in order to produce a flexible system with real-time data streaming. Therefore, a concurrent client-server

program is developed to provide a network interface to the system. The concurrent client-server program receives MARG sensor data through a UDP socket and delivers the data to the clients on the wide area network (WAN) simultaneously. Delivering the same motion data to multiple clients simultaneously is implemented by a method called Multicasting Using TCP and UDP Protocol (MUTUP) [25].

Multicasting is the most efficient way of transmitting information among a large number of group members spread out over different networks. Reduced network bandwidth use is the major advantage of using multicasting protocols. Unfortunately, most routers on the Internet are not configured for multicasting. A technique called tunneling is used to overcome this problem. Tunneling is a software solution that runs on the end point routers/computers and allows multicast packets to traverse the network by putting them into unicast packets. MUTUP overcomes the tunneling problem using shared memory in the server and a unicast TCP and UDP messages between the server and each client. The major disadvantage of MUTUP is a limitation on the number of clients that can be handled by the server at any time. This limitation is caused by an increase in load on the CPU and additional memory consumption for each client. Low performance or out-of-memory problems may occur if the server must handle too many clients. MUTUP also uses greater network bandwidth than multicasting because separate update messages must be sent to each client. Since a relatively small number of clients are expected in the MARG project, MUTUP was chosen as an alternative method to the multicasting protocol despite its drawbacks.

MUTUP uses shared memory in the server program for storing the latest motion data. Clients request TCP connections from the server. The server accepts the requests and creates a separate thread for handling each of the connections. The TCP connection is used for general-purpose communication. The TCP protocol is not appropriate for data streaming due to increased latency and overhead. Therefore, a second connection based on UDP sockets is established between the client and the server. The server program asks the client to create a UDP socket and send the IP address and the UDP port number of this socket back to the server. The server adds the IP address and the UDP port number of the client as a destination for the packets sent by the server program. To provide the same motion data for all connected clients simultaneously, a shared memory array that always stores the latest update is created on the server program. An updater thread updates this array. All client handler threads access this array at any time they want. A diagram of MUTUP is provided in Figure 6.

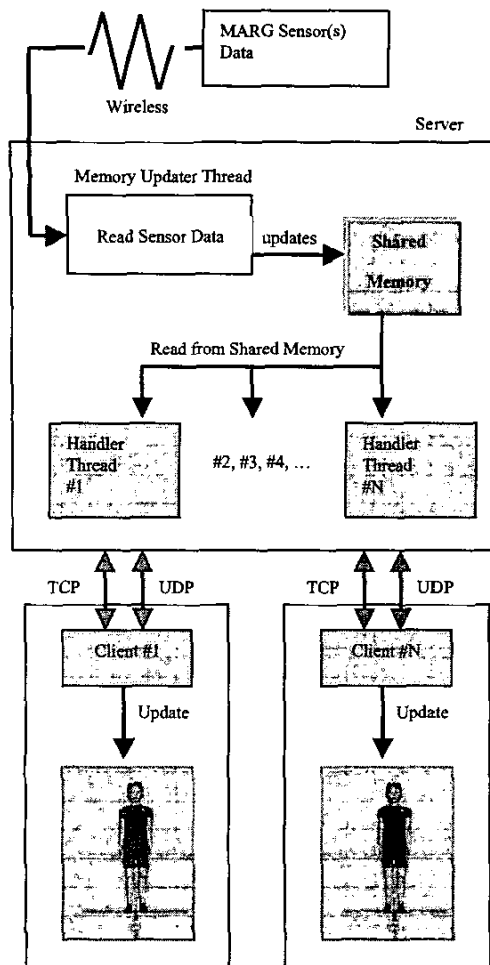


Figure 6. Concurrent Client Server Communication.

VI. TESTING AND EVALUATION

The performance of the individual MARG sensors was tested first. Each MARG sensor produces nine components of raw measurement data at the rate of 100 Hz. The raw measurement data are processed by the filter algorithm [17] to produce a quaternion representation of orientation. For plotting purposes, quaternions are converted to Euler angles (roll ϕ , pitch θ and yaw ψ). Figure 7 shows the output of the MARG sensor as it performs a 720° rotation (roll ϕ) about its longitudinal axis. It is seen that the sensor starts from a zero roll. When the motion starts, the sensor responds with a linear rotation toward negative 180°. The plot displays angles within the range of negative 180° and positive 180°. Therefore, a sudden transition from negative 180° to positive 180° appears. In reality, the

sensor continues to rotate with a constant angular rate until it reaches a full 720° rotation and then stops. A slight pitch deviation and an even smaller yaw deviation are also observed.

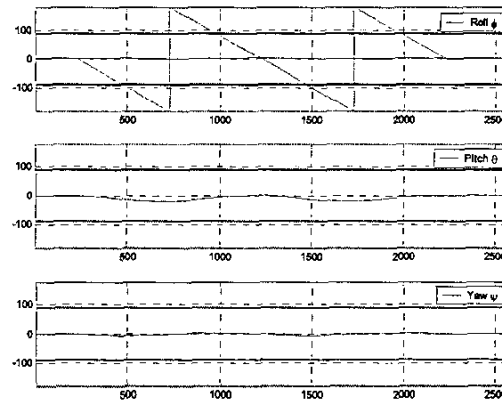


Figure 7. Response of MARG Sensor to 720° Roll Motion.

The real-time performance of the overall tracking system was evaluated in connection with the human avatar Andy. Two MARG sensors were attached to an arm of a user, and connected to the three-channel CIU. The CIU then wirelessly transmitted the sensor data to a network-based server computer. The sensor data were filtered, and the resulting orientation quaternions were transformed into axis-angle pairs. This transformation was necessary since the avatar was created using the X3D language, which has been standardized to use axis-angle pairs to represent rotations.

Testing results with the full-body avatar were very successful. With the use of two MARG III sensors, the avatar followed the motion of the human right arm exactly. Figure 8 and Figure 9 show two snapshots of the testing scene. The user moves his arm, and the motion is followed in real time by the avatar.

VII. CONCLUSION

The paper presents the system components of a body motion tracking system based on MARG sensor modules and testing and evaluation results for a prototype three-sensor system. The components presented include a Control Interface Unit, a human avatar, and a Client/Server protocol for transmitting animation data. The CIU packages data from up to 16 MARG sensors for wireless transmission. The Client/Server program receives MARG sensor data and delivers that data to multiple clients simultaneously. The avatar allows networked viewing of animations produced using MARG data in real time. Tests of a prototype three sensor system indicate that these components provide the necessary infrastructure to support a 16 sensor system for full body tracking.

ACKNOWLEDGMENT

This research was supported in part by Army Research Office (ARO), and Navy Modeling and Simulation Management Office (N6M). Authors would like to thank James Calusdian for his technical support during the course of this project, and to thank Doug McKinney for collaboration on the MARG sensors and CIU.

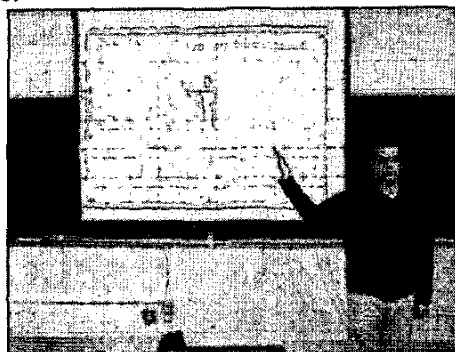


Figure 8. Avatar Andy and the User in Real-Time Testing.

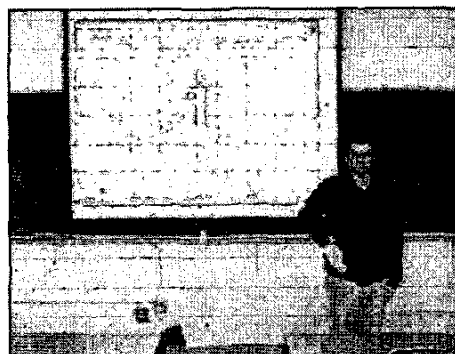


Figure 9. Another View of Avatar Andy and the User in Real-Time Testing.

REFERENCES

- [1] Michael Macedonia, "Games Soldiers Play," *IEEE Spectrum*, March 2003, pp. 32-37.
- [2] Nancy S. Pollard, Jessica K. Hodgins, Marcia J. Riley, and Christopher G. Atkeson, "Adapting Human Motion for the Control of a Humanoid Robot," *Proceedings of the 2002 IEEE International Conference on Robotics and Automation*, Washington DC, May 2002, pp. 1390-1397.
- [3] Anirvan Dasgupta and Yoshikiko Nakamura, "Making Feasible Walking Motion of Humanoid Robots from Human Motion Capture Data," *Proceedings of the 1999 IEEE International Conference on Robotics and Automation*, Detroit, MI, May 1999, pp. 1044-1049.
- [4] Tatsuya Harada, Tomomasa Sato, and Taketoshi Mori, "Human Motion Tracking System Based on Skeleton and Surface Integration Model Using Pressure Sensors Distribution Bed," *Proceedings of Workshop on Human Motion*, Las Alamitos, CA, December 2000, pp. 99-106.
- [5] K. Meyer, H. Applewhite, and F. Biocca, "A Survey of Position Trackers," *Presence: Teleoperators and Virtual Environments*, Vol. 1, No. 2, pp. 173-200, 1992.
- [6] W. Frey, M. Zyda, R. McGhee, and W. Cockayne, "Off-the-Shelf, Real-time, Human Body Motion Capture Synthetic Environments," Technical Report NPSCS-96-03, Naval Postgraduate School, Monterey, CA, June 1996.
- [7] D.M. Gavrilu, "The Visual Analysis of Human Movement: A Survey," *Computer Vision and Image Understanding*, Vol. 73, No. 1, January 1999, pp. 82-98.
- [8] Takashi Sakaguchi, Tsutomu Kanamori, and Haruhiro Katayose, "Human Motion Capture by Integrating Gyroscopes and Accelerometers," *Proceedings of the 1996 IEEE/SICE/RSJ International Conference on Multisensor Fusion and Integration for Intelligent Systems*, Washington DC, December 1996, pp. 470-475.
- [9] J. Lee and I. Ha, "Sensor Fusion and Calibration for Motion Captures Using Accelerometers," *Proceedings of the 1999 IEEE International Conference on Robotics and Automation*, Detroit, MI, May 1999, pp. 1954-1959.
- [10] Northern Digital Inc., <http://www.ndigital.com/>.
- [11] Kenichi Kida, Masayuki Ihara, Shinichi Shiwa, and Satoshi Ishibashi, "Motion Tracking Method for the CAVE System," *Proceedings of International Conference on Signal Processing*, Beijing, China, August 2000, pp. 859-862, Vol. 2.
- [12] Ioannis Kakadiaris and Dimitris Metaxas, "Model-Based Estimation of 3D Human Motion," *IEEE Transactions on Pattern Analysis and Machine Intelligence*, Vol. 22, No. 12, December 2000, pp. 1453-1459.
- [13] Carlo Colombo, Alberto Del Bimbo, and Alessandro Valli, "Real-Time Tracking and Reproduction of 3D Human Body Motion," *Proceedings of International Conference on Image Analysis and Processing*, Palermo, Italy, September 2001, pp. 108-112.
- [14] Q. Cai and J.K. Aggarwal, "Tracking Human Motion in Structured Environments Using a Distributed-Camera System," *IEEE Transactions on Pattern Analysis and Machine Intelligence*, Vol. 21, No. 12, November 1999, pp. 1241-1247.
- [15] Jason P. Luck, Christian Debrunner, William Hoff, Qiang He, and Daniel E. Small, "Development and Analysis of a Real-Time Human Motion Tracking System," *Proceedings of the sixth IEEE Workshop on Applications of Computer Vision*, Orlando, FL, December 2002, pp. 196-202.
- [16] Eric B. Bachmann, Xiaoping Yun, Doug McKinney, Robert B. McGhee, and Michael J. Zyda, "Design and Implementation of MARG Sensors for 3-DOF Orientation Measurement of Rigid Bodies," *Proceedings of 2003 IEEE International Conference on Robotics and Automation*, Taipei, Taiwan, September 2003, pp. 1171-1178.
- [17] Xiaoping Yun, Mariano Lizarraga, Eric R. Bachmann, Robert B. McGhee, "An Improved Quaternion-Based Kalman Filter for Real-Time Tracking of Rigid Body Orientation," *Proceedings of 2003 IEEE/RSJ International Conference on Intelligent Robots and Systems*, Las Vegas, NV, October 2003, pp. 1074-1079.
- [18] <http://www.web3d.org/>.
- [19] <http://www.h-anim.org/>.
- [20] McKinney Technologies, Chandler, AZ.
- [21] OTC Wireless Inc., <http://www.otcwireless.com/>.
- [22] XILINK Inc. *Spartan-II 2.5V FPGA Family: Complete Data Sheet*, 3 September 2003, <http://www.xilinx.com/>.
- [23] DPAC Technologies, Garden Grove, CA 92841, <http://www.dpactech.com>.
- [24] Vcom 3d, Inc., <http://www.vcom3d.com/Viewer.html>.
- [25] Faruk Yildiz, *Implementation of a Human Avatar for the MARG Project in Networked Virtual Environments*, Master's Thesis, Naval Postgraduate School, 2004.
- [26] Andreas Kavousanos-Kavousanakis, *Design and Implementation of a DSP-based Control Interface Unit (CIU)*, Master's Thesis, Naval Postgraduate School, 2004.